Université de Montréal

Detecting Uterine Cervical Cancer Cells Using Molecular Biomarkers

par
Ahmed Mousa

Département de Sciences biomédicales
Faculté de médecine

Mémoire présenté à la Faculté de médecine
en vue de l'obtention du grade de Maître en Sciences biomédicales
Option générale

Novembre, 2014

Université de Montréal

Faculté des études supérieures

Ce mémoire intitulé:

Detecting Uterine Cervical Cancer Cells Using Molecular Biomarkers

Présenté par:

Ahmed Mousa

a été évalué par un jury composé des personnes suivantes:

Dr Suzanne Fortin, président-rapporteur

Dr Francis Rodier, directeur de recherche

Dre Vanessa Samouëlian, codirectrice de recherche

Dr Susie Lau, membre du jury

RÉSUMÉ

Arrière-plan: les cellules tumorales circulantes (CTC) sont détectables dans de nombreux cancers et peuvent être utiles cliniquement pour le pronostic de la maladie, pour mesurer la récidive et pour prédire la sensibilité aux medicaments chimiothérapeutiques. Au cours des dernières années, l'études des CTC dans de nombreux cancers tels que le cancer du sein, du poumon, du côlon et de la prostate a grandement évolué. Alternativement, il y peu d'études à ce sujet concernant le cancer du col de l'utérus (CCU). **Objectifs:** Notre objectif est d'optimiser le processus d'enrichissement des CTC dans le CCU et la détection moléculaire des biomarqueurs E6 et E7. **Matériel et Méthodes:** Dans l'optique de mimer la présence de CTC dans le sang, nous avons dilué des cellules cancéreuses CaSki VPH16-positif provenant d'un CCU dans du sang humain prélevé sur des volontaires sains. Les CaSki ont été collectées suite à une centrifugation par densité avec le Ficoll, la lyse des globules rouges (RBC) et la lyse des RBC combinée avec un enrichissement positif et négatif à l'aide de marqueurs de surface cellulaire. Les CTC ont été détectées par la mesure d'expression des oncogènes E6 et E7 du virus du papillome humain (VPH), de la cytokératine 19 (CK19) et de la cycline $p16^{INK4}$ en utilisant la technique quantitative en temps réel de Reverse Transcriptase-Polymerase Chain Reaction (qRT-PCR). Pour valider notre méthode de détection des CTC *in vivo*, nous avons recruté dix patientes atteintes d'un CCU VPH16 positif et six contrôles sains. **Résultats:** Dans le modèle de dilutions de cellules CaSki, la lyse des RBC seule ou combinée avec l'enrichissement négatif ou positif suggèrent des limites de détection de 1 CTC par mL de sang pour tous les biomarqueurs moléculaires utilisés. La sensibilité de détection est accrue lors de l'utilisation de l'enrichissement positif et négatif en réduisant le bruit de fond causé par les monocytes sanguins. Contrairement aux oncogènes E6 et E7, les marqueurs CK19 et $p16^{INK4A}$ ont été détectés chez des individus sains, les niveaux d'expression de base appropriés doivent donc être déterminés avec précision par rapport aux patientes CCU. Le gradient de densité par Ficoll a une limite de détection de seulement environ 1000 cellules par mL de sang. Enfin, les CTC ont été détectées dans 2/10 patientes en utilisant le marqueur CK19. Cependant, ces patientes étaient négatives pour les oncogènes E6/E7. Le marqueur $p16^{INK4A}$ était exprimé au même niveau dans tous les échantillons (CCU et normaux). **Conclusion:** Notre étude suggère que les oncogènes E6 et E7 du VPH16 sont les marqueurs biologiques les plus sensibles et spécifiques en qRT-PCR pour

détecter les CTC dans le modèle de dilution de cellules de CCU dans le sang. Chez les patientes atteintes d'un CCU de stade précoce, seulement CK19 a révélé la présence potentielle de CTC, ce qui suggère que ces cellules sont rares à ce stade de la maladie.

Mots clés: cancer du col de l'utérus, cellules tumorales circulantes, RT-qPCR, E6 et E7, CK19, $p16^{INK4A}$, enrichissement immunomagnétique, détection moléculaire.

ABSTRACT

Background: Circulating tumor cells (CTCs) have been detected in many cancers and are used in multiple clinical applications including disease prognosis, tumor recurrence prediction and prediction of tumor sensitivity to chemotherapeutic drugs. Studies in most major solid cancer(s) (breast, lung, colon and prostate) are progressing rapidly, but there has been very little progress concerning uterine cervical cancer (UCC).**Objective:** our aim is to optimize enrichment processes and the molecular biomarker-based detection of human circulating tumor cells (CTCs) in uterine cervical cancer (UCC). **Material & Methods:** To mimic CTCs in patients, we designed an experimental spiking model where the CaSki HPV16-positive UCC cell line was serially diluted and spiked into human blood collected from healthy volunteers. CaSki CTCs were enriched using either Ficoll density centrifugation, red blood cell (RBC) lysis or RBC lysis combined with cell surface markers negative or positive enrichment. CTCs were detected using real-time quantitative reverse-transcription polymerase chain reaction (qRT-PCR) to measure the gene expression of human papillomavirus (HPV) viral oncogenes (E6 and E7), cytokeratin 19 (CK19), or the cyclin dependent kinase inhibitor $p16^{INK4A}$. Finally, ten HPV16- positive UCC patients and six healthy controls were recruited to validate CTCs detection in vivo. **Result:** In the spiking model, RBC lysis alone or combined with negative or positive enrichment suggests detection limits close to 1 CTC per mL of blood for all molecular biomarkers used. The sensitivity of detection increased when using positive and negative enrichment probably by reducing the peripheral blood mononuclear cell-derived RNA background. Unlike HPV oncogenes, CK19 and $p16^{INK4A}$ were detected in normal individuals, thus appropriate basal expression levels need to be accurately determined compared to cancer patients. Alternatively, Ficoll density gradient had a detection limit of only about 1000 cells per mL of blood. Finally CTCs were detected in 2/10 patients using CK19. None of the patients had E6/E7 transcripts and $p16^{INK4A}$ was expressed at similar level across all samples (cancer and healthy). **Conclusion:** qRT-PCR of HPV16 E6 and E7 is the most sensitive and specific biomarker used to detect CTCs in the spiking model. In early disease UCC patients, only CK19 revealed the presence of CTCs suggesting that these cells are rare at that stage of the disease.

Keywords: uterine cervical cancer, circulating tumor cells, qRT-PCR, E6 and E7 oncoprotein, CK19, $p16^{INK4A}$, immune-magnetic enrichment, molecular detection.

CONTENTS

TABLE LIST

FIGURE LIST

ABBREVIATION LIST

A

A260/280: The ratio of absorbance at 260 nm and 280 nm.

ACK lysing buffer: Ammonium-Chloride-Potassium lysing buffer

ADM: Automated digital microscopy

AKT: Protein Kinase B

Ang-2: Angiopoietin-2

B

BAK: Bcl-2-homologous antagonist/killer

C

CDK: Cyclin-dependent kinase

cDNA: Complementary deoxyribonucleic acid

CEA: Carcinoembryonic antigen

CEE: Cell Enrichment and Extraction™ channel

CHUM: Centre Hospitalier de l'Université de Montréal

CK: Cytokeratin

CO2: Carbon dioxide

CT: Cycle threshold

CTCs: Circulating tumor cells

D

DAPI: 4',6-diamidino-2-phenylindole

ddH2O: Double distilled water

DD-RT-PCR: Digital-Direct-RT-PCR

DEP: Dielectrophoresis

depFFF: Dielectrophoretic field-flow fractionation

DMEM: Dulbecco's Modified Eagle Medium

DMSO: Dimethyl sulfoxide

DNA: Deoxyribonucleic acid

E

EDTA: Ethylenediaminetetraacetic acid

EGFR: Epidermal growth factor receptor

EGR: Epidermal growth factor

EMT: Epithelial-mesenchymal transition

EpCAM: Epithelial cell adhesion molecule

EPISPOT: Epithelial immuonSPOT

ERK: Extracellular-signal-regulated kinases

ETOH: Ethanol

F

FACS: Florescence-activating cell sorting

FAST: Fiber-optic array scanning technology

FBS: Fetal bovine serum

FFPE: Formalin-Fixed Paraffin-Embedded

FGF: Fibroblast growth factor

FIGO: The International Federation of Gynecology and Obstetrics

FSC: Forward scatter

G

GEDI: Geometrically-enhanced differential immunocapture chip

GFP: Green fluorescent protein

GSK3β: Glycogen synthase 3 beta

H

H&E: Haematoxylin and Eosin

HGF: Hepatocyte growth factor

HIF: Hypoxia-inducible factor

HPV: Human papillomavirus

hTERt: Human telomerase reverse transcriptase

HER-2: Human epidermal growth factor receptor 2

I

IGF-1: Insulin-like growth factor 1

IHC: Immunohistochemistry

IL-6: Interleukin-6

ISET: Isolation by size of epithelial tumor cells

ITC: Isolated tumor cells

J

JAK: Janus kinase

JNK: C-Jun N-terminal kinases

L

LEF: Lymphoid enhancer-binding factor

LN: Lymph node

LVSI: Lymphovascular space invasion

M

MEK: Mitogen-activated protein kinase pathway

MET: Mesenchymal-epithelial transition

miRNA: microRNA

MNC: Mononucleated cells

MOFF: Multi-orifice flow fractionation

MPAK: Mitogen-activated protein kinases

mRNA: Messenger RNA

mTOR: Mammalian target of rapamycin

N

NSCLC: Non-small-cell lung carcinoma

NTC: No template control

O

ORF: Open reading frames

OSNA: One-step nucleic acid amplification assay

P

$p16^{INK4A}$: Cyclin-dependent kinase inhibitor inhibiting CDK4

p53: Tumor suppressor protein p53

PBMC: Peripheral blood mononucleated cell

PBS: Phosphate buffered solutions

PCR: Polymerase chain reaction

PDMS: Polydimethylsiloxane

PI3: Phosphatidylinositol-4,5-bisphosphate 3-kinase

Q

qPCR: Quantitative real time polymerase chain reaction

R

RAF: Proto-oncogene serine/threonine-protein kinase

RAS: Rat sarcoma

Rb: Retinoblastoma tumor suppressor protein

RBC: Red blood cell

RNA: Ribonucleic acid

RPM: Revolutions per minute

RT-PCR: Reverse transcription polymerase chain reaction

qRT-PCR: Real-time quantitative reverse-transcription polymerase chain reaction

S

SARMS: Scorpion Amplification Refractory Mutation System

SLN: Sentinel lymph node

SNAIL: Snail family zinc finger

SSC: Sideward scatter

T

TBP: TATA-binding protein

TCF: T cell factor

TGF: Tumor growth factor

TJP: Tight junction protein

TWIST: Twist basic helix-loop-helix proteins

U

UCC: Uterine cervical cancer

UV: Ultraviolet

V

VEGR-A: Vascular endothelial growth factor-A

W

WBC: White blood cell

Z

ZEB: Zinc finger E-box binding homeobox

CHAPTER I : INTRODUCTION

1.1 Circulating tumor cells and the induction of metastasis

Metastasis is a complex process that involves interplay between tumor cells and the hosting organs. The invasion-metastasis cascade consists of multiple steps as shown in Figure I-1. Tumor cells found within the blood stream are defined as circulating tumor cells (CTCs) [1, 2]. At the primary tumor site, multiple signaling pathways function to promote cellular proliferation, growth inhibition, survival, and invasion, as well as induce tumor angiogenesis, all of which facilitate the metastatic process [3]. Tumor cells proliferate in response to various growth factors; such as transforming growth factor-beta (TGF-β), insulin-like growth factor-1 (IGF-1), and epidermal growth factor (EGF) that activate the RAS, mTOR, and PI3K-AKT signaling pathways [4, 5]. Once tumors reach a critical size where the local blood supply does not meet cellular metabolic demands, hypoxia-inducible factor (HIF) is released to promote the expression of the angiogenic proteins vascular endothelial growth factor-A (VEGF-A) and angiopoietin-2 (Ang-2) [6]. This event results in the formation of neovasculature characterized by high permeability, abnormal structure, and variable blood flow [7-9]. In addition, the co-influence of TGF-β and HIF promotes a process termed epithelial-mesenchymal transition, where epithelial tumor cells acquire a mesenchymal phenotype that allows them to invade, migrate, and gain cancer stem cell-like traits [10-12]. Once through the basement membrane, tumor cells can reach the blood and lymphatic vessels and travel to distant organ sites where they can then move out. Cells within this founder population undergo mesenchymal-epithelial transition (MET) and begin to form metastatic tumor colonies.

Studies suggested that hematogenous spread is an early event that can occur prior to diagnosis of the primary tumor [13]. Multiple studies have reported that the detection of CTCs in early-stage cancer is associated with poor prognosis [14]. CTCs have been identified in many epithelial cancers, including breast, colon, lung, and prostate, and have recently demonstrated prognostic value [15-18]. Other applications of CTC detection include assessing treatment response, genetic mutations, drug resistance screening and selection of patients for adjuvant systemic treatments [19].

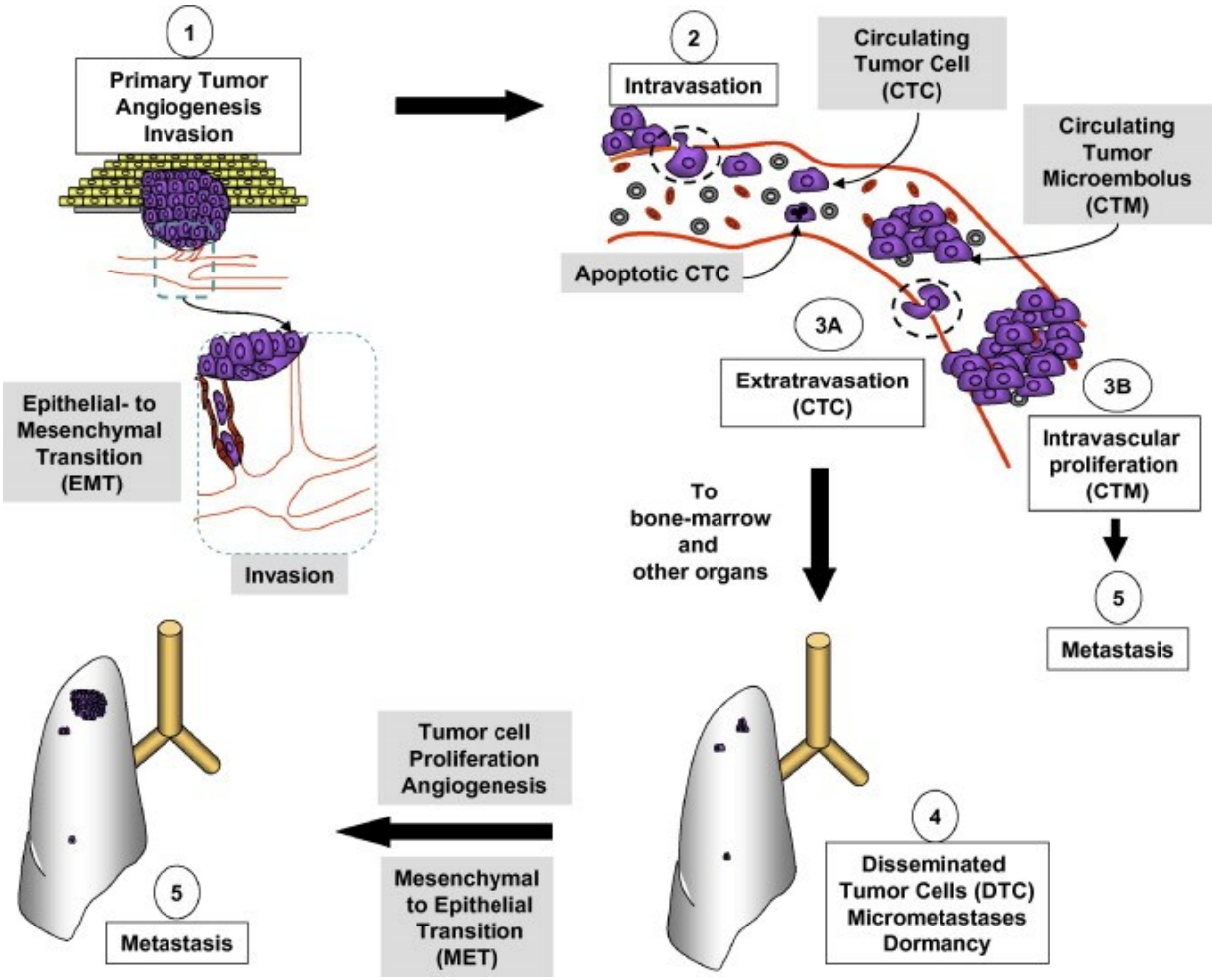

Figure I.1. Invasion-metastasis cascade. Angiogenesis initiates to meet the metabolic demand of rapidly proliferating tumor cells, and subsequently promotes EMT. Cells then gain invasive and migratory properties, and intravasate into blood vessels. Within the blood, CTC travel to distant organ sites and extravasate to form dormant foci. Cells can remain dormant or undergo MET to form metastatic microtumors. Most CTCs undergo apoptotic death and are phagocytosed by macrophages; however, the minority can proliferate within the vasculature to form CTM, and eventually metastasis. Reprinted from reference [20]. © 2007, with permission from Elsevier.

1.1.1 Epithelial-Mesenchymal transition

Epithelial-mesenchymal transition (EMT) is a process by which cells that bear epithelial characteristics transform into mesenchymal phenotype, and can be classified into three types

based on biological context: type I occurs during embryogenesis and organogenesis; type II during fibrosis, tissue regeneration, and wound healing; and type III during tumorigenesis [21].

EMT results in a spectrum of cells exhibiting partial to full mesenchymal phenotypes and stem cell properties. This is a complex process that involves cross-talk between several molecular pathways [22]. The increased expression of HIF within the tumor results in upregulation of TGF-β and integrins, as well as transcriptional mediators with known roles in mediating EMT, such as TWIST, SNAIL, and ZEB. These factors repress epithelial genes and activate mesenchymal genes leading to a loss of apicobasal polarity and spindle shape morphology and increases in cell motility and invasiveness (Table I-I).

Cancer stem cells are cancer cells that have acquired characteristics of normal stem cells, including self-renewal and differentiation. They are responsible for tumor heterogeneity and the formation of metastatic foci [23]. They have been identified in multiple solid and hematological malignancies by the expression of population-specific markers, and account for tumor drug resistance and progression [24].

Table I-I. Comparison between epithelial and mesenchymal phenotype.

	Epithelial cells	Mesenchymal cells
Cell shape	Apical-basolateral polarization	Spindle
Cell-Surface Proteins	E-Cadherin ZO-1 Claudins Mucin 1 Desmoplakin	N-Cadherin Downregulation / Attenuation E-Cadherin ZO-1(TJP) Integrin
Cytoskeletal Markers	CK 8 ,9 and 19	Vimentin β-Catenin FSP1 Downregulation / Attenuation Cytokeratin
Growth pattern	Remain within epithelial layer and closely adjoined Form organized cell layer Presence of basal lamina	Can migrate, highly motile & loosely adjoined Don't form organized cell layer Focally present
Transcription Factors		SNAIL 1 SNAIL 2 TWIST ZEB-1 SMAD SIP1
[21, 25]		

1.1.2 Metastatic inefficiency

It is important to note that the presence of CTCs does not imply the development of metastasis. Evidence from animal models has demonstrated that only a subset of tumor cells, of the millions injected, survive to successfully graft and form tumors [26]. For instance, a study using murine melanoma cells tagged with a fluorescent marker demonstrated that 87.3% of cells remained within the vasculature at 90 minutes post-injection into the superior mesenteric vein of mice. By day three, 82% had extravasated into tissue, and 63% were lost by day 13. The majority of

extravasated cells remained as dormant, solitary cancer cells, with only 0.07% and 0.01% of injected cells forming micrometastases and macroscopic tumors, respectively [27]. Notably, most CTCs either undergo anoikis (programmed cell death as result of cell detachment from the extracellular matrix), immunogenic cell death, or apoptosis after extravasation and formation of dormant micrometastatic foci [27-30].

1.2 CTC Detection

CTCs are often detected by isolating the exceedingly small CTC population from billions of RBC and millions of WBC within the blood through a process termed enrichment. There are many methods used to enrich and identify CTCs. The following section will discuss the techniques currently available and their advantages and disadvantages.

1.2.1 Density gradient separation of mononucleated cells

Density gradient separation is a classical method to separate cells based on their buoyant density [31]. Ficoll-Paque-Hypaque (GE Healthcare) is the most used separation reagent (Figure I-2). Blood is layered over the Ficoll-Paque in a conical tube and then centrifuged to form layers. Cells are arranged from bottom to top as red blood cells, granulocytes, density gradient, peripheral blood mononuclear cells (PBMCs), and plasma, where CTCs co-separate with the PBMC population. Collection of the PBMC must be performed immediately, otherwise cells begin to mix. This enriched population is then subjected to immuno-labeling, cytological analysis or molecular analysis in order to detect CTCs.

OncoQuick is a modified density-based method that uses a porous barrier to prevent the PBMC from mixing with granulocytes and RBC after centrifugation. In direct comparison, both found to have similar performance in CTC recovery, although OncoQuick provides a slightly higher purity of PBMCs that facilitates immunocytological analysis and limits false positives in real-time quantitative reverse-transcription polymerase chain reaction (qRT-PCR) screening. However, the increased purity comes at the expense of recovery, as OncoQuick has a recovery rate ranging between 70-90% due to the loss of normal and tumor cells to other phases [32].

Another alternative is RosetteSep™, which uses tetrameric antibody against glycoprotein A opposite of various leukocyte-specific antibodies, depending on your population of interest. The RosetteSep reagent is added to the isolated blood product. This results in the crosslinking of unwanted cells to RBC, forming rosette-like aggregates with high density, which

can then be pelleted with centrifugation. Importantly, this method has been found to minimize variability between operators and facilitate the processing of larger blood volumes [33].

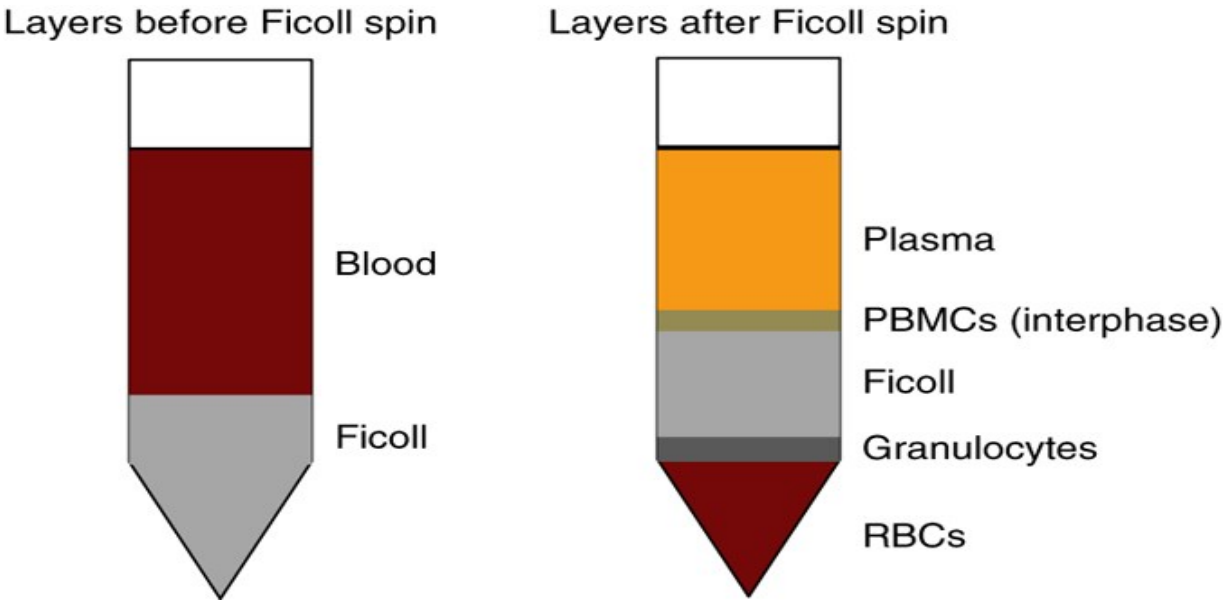

Figure I.2. Ficoll density separation of PBMC and tumor cells. Blood is layered on top of Ficoll density gradient and is followed by centrifugation. Cells are arranged from the bottom to the top based on their buoyant density: RBC, granulocytes, PBMC and tumor cells, and plasma. The PBMC interphase can then be collected and used to detect and/or characterize tumor cells by cytological examination, immuno-labeling, or molecular analysis. Reprinted from reference [34]. © 2014, with permission from Nature Publishing Group.

1.2.2 Size-based approach to CTC enrichment

Average CTCs are reported to be larger than normal blood cells with an average size of 20-25 μm compared to ~8 μm for normal leukocytes [35]. The isolation by size of epithelial tumor cells method, or ISET, uses a polycarbonate membrane with 8 μm pores. Whole blood is diluted with a buffer to fix cells, which are then filtered through the membrane. Cells larger than 8 μm trapped by the membrane are harvested, and then subjected to immunostaining and molecular analysis to detect and characterize the CTC population. This method has a reported detection sensitivity of one cell per mL of blood [36]. The main advantages of ISET include the enrichment of cells with intact morphology, as well as simplicity and reproducibility. However, its recovery rate ranges between 50-60% and tumor cells less than 8 μm are lost in the filtering

process [35], In addition, the membrane is fabricated by track etching to randomly distribute the pores, which might result fuse to create larger pores, and the clogging of pores can occur.

Although, optimized filter construction with microfabrication has led to the production of membrane pores with precise size, geometry, and density in order to overcome the major limitations associated with track etching, and has improved the recovery rate to 90% (Figure I-3) [37]. More recently, a 3D microfilter device has shown the ability to detect viable CTCs with a 90% capture efficiency from whole blood in 10 minutes [38].

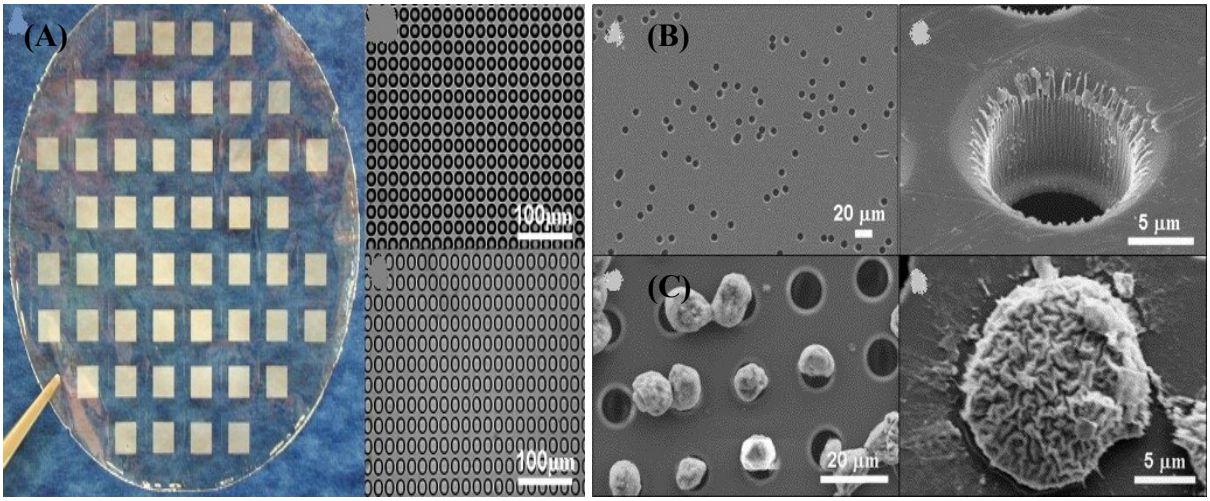

Figure I.3. Comparison of microfabrication and track-etched membranes. Scanning electron microscopy (SEM) imagining demonstrating **(A)** microfabrication with precise size and geometry compared to **(B)** track etching that can result in randomly placed and/or fused pores. **(C)** SEM showing captured cells on microfabricated membrane. Reprinted from reference [37], © 2007 with permission from Elsevier.

1.2.3 Magnetic immunolabeling isolation

Epithelial cell adhesion molecule (EpCAM) is a transmembrane glycoprotein that mediates homotypic cell-cell adhesions on epithelial cells [39]. Antibodies targeting EpCAM have been used to isolate CTCs directly through a process called positive enrichment. In contrast, negative enrichment is used to deplete leukocytes from a heterogeneous population with antibodies targeting CD45, a cell surface antigen expressed by both leukocytes and lymphocytes.

The CellSearch® system (Veridex) is the only system approved by the FDA for the detection of CTCs, and uses ferrofluid nanoparticles conjugated to anti-EpCAM antibodies to magnetically isolate epithelial cells. Enriched cells are then stained with DAPI (4′,6-diamidino-2-phenylindole) and for CD45 and/or cytokeratin 8, 18, or 19, and then analyzed with a CellTracks Analyzer. Cells positive for DAPI and cytokeratin, but negative for CD45, are considered CTCs. The system is semi-automated, fast, and has a detection sensitivity of 1 CTC/mL. This method is capable of detecting CTCs in 36% of tested patients, with 85% recovery and 0.1% purity [35, 40], however, it is subject to false positives as result of non-specific binding to Fc-receptor bearing cells, extraneous expression of epithelial antigens, inability to analyze cells, and false negatives for cancers that lack epithelial antigen expression due to EMT [35, 41-46]. Cells that are CD45 and CK positive are excluded from analysis and their prognostic value has not yet been evaluated; although, these cells can represent cancer stem cells or CTCs phagocytosed by leukocytes [47].

The AdnaTest is another platform to positively enrich CTCs using multiple markers immunomagnetically. RNA is then isolated from the enriched cells and used for a multiplex qRT-PCR to detect CTC based on the expression of tumor genes. AdnaTest has a sensitivity of 0.4 CTCs/mL of blood [48, 49].

Negative enrichment can be used to detect CTCs regardless of their surface antigen expression. Yang et al. recently evaluated multiple products to negatively enrich CTCs and found that an anti-CD45 tetrameric antibody complex manufactured by StemCell® provided better enrichment than other products with average detection of 2.32 CTCs/mL of blood [50]. The variation in performance between different reagents can be explained by antibody binding capacity, as well as the size and composition of the magnetic particle [51]. Magnetic particles are bound to the antibody directly or indirectly through a secondary antibody. Indirect labeling by two-step binding was found to be more efficient and yields a higher affinity to cells [52]. The

loss of tumor cells due to leukocyte binding and their rarity within high background of leukocytes precludes the isolation of pure CTCs are disadvantages of negative enrichment-based analyses [53].

1.2.4 Microfludic systems for CTC isolation

Microfluidics is a system used to manipulate and process micro-volumetric fluids using microchannels. The advantages of microfluidic cell isolation include its high throughput, sensitivity, and resolution that facilitate CTC detection and separation at a low-cost with high efficiency. This process also provides for gene expression analysis at single cell level and integration with other technologies [54]. These features make it ideal for the detection and enrichment of CTCs with minimal cell loss. As such, multiple microfluidics-based platforms have been developed to isolate CTCs based on both physical and immunological characteristics.

1.2.4.1 *Immunoaffinity based enrichment*

Nagrath et al. developed a CTC-chip microfluidic device consisting of an array of 78,000 microposts coated with anti-EpCAM antibody embedded on silicon chip to capture CTCs [55]. Whole blood is passed through the chip at flow rate of 1-2 mL/h. CTCs were detected in 99% of cancer patients tested with an average purity of 55%, 80% recovery rate, and high experimental reproducibility. Enriched cells are 99% viable (Figure I-4) [55]. The same group reported on the detection and identification of CTCs with epidermal growth factor receptor (EGFR) genetic mutations in non-small-cell lung cancer using the Scorpion Amplification Refractory Mutation System (SARMS) technology designed to detect mutations involved in drug susceptibility or resistance. The CTC-chip detected CTCs in all tested patients with a median of 74 cells/mL of blood. Furthermore, EGFR mutations were identified from enriched CTCs in 95% of patients compared to 39% of patients from plasma examination [56]. The efficiency of the CTC-chip to enrich CTC is hindered with increasing the flow rate and shear force, and thus relies on laminar flow that reduce surface area of interaction.

Stott et al. developed the Herringbone (HB)-Chip that consists of a glass slide bonded to a polydimethylsiloxane (PDMS) structure, containing eight microchannels with patterned herringbones on their upper surface with their internal walls coated with anti-EpCAM antibody [57]. The herringbone structure generates passive microvortices that disrupt the laminar flow

streamlines that carries the cells to increase the number of cell-surface interactions (Figure I-5). This improves the capture efficiency by 40%, which can be maintained at flow rates up to 4.8 mL/h, compared to the 1-2 mL/h for CTC-chips.

Dickson et al. developed the Cell Enrichment and Extraction™ (CEE) channel composed of 9000 randomly sized and positioned posts that are derivatized with streptavidin. Enriched cells are labeled with biotin-conjugated antibodies, which can then interact with streptavidin to capture CTCs. This allows for multiple surface markers to be targeted simultaneously with biotinylated antibodies to increase capture efficiency [58]. The capture efficiency of CEE is dependent on both antigen density and flow rate, and processing 8 to 10 mL of whole blood requires 7 to 9 hours.

Gleghorn et al. developed the geometrically enhanced differential immunocapture (GEDI) chip optimized to maximize interactions with large cells (15 to 25 μm) and reduce wall shear force to enhance the capture of CTCs in prostate cancer cells using prostate-specific membrane antigen-antibody [59]. This optimization resulted in a 40% increase in efficiency and CTC capture from whole blood.

Myung et al. further demonstrated the ability to capture CTCs through a functionalized epoxy glass immobilized with E-selectin and EpCAM antibodies [60].

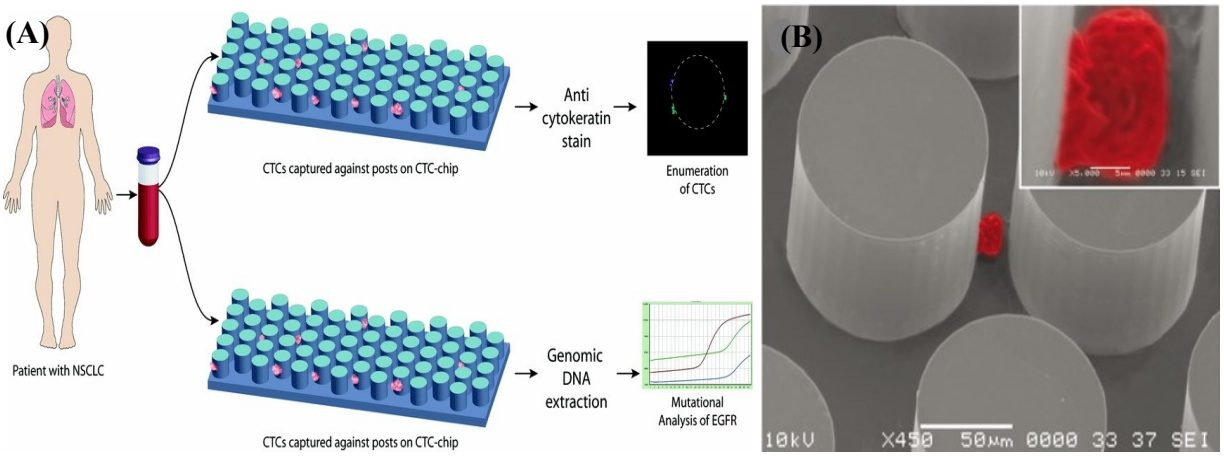

Figure I.4. CTC-chip. **(A)** Whole blood is passed through the chip using pressure regulated pump in laminar flow fashion. CTCs are captured against posts coated with anti-EpCAM antibody and can then be enumerated and characterized. Reprinted [61], © 2009 with permission from Wolters Kluwer Health . **(B)** SEM image demonstrating captured CTCs from a lung cancer patient. Reprinted from reference [55]. © 2007, with permission from Nature Publishing Group.

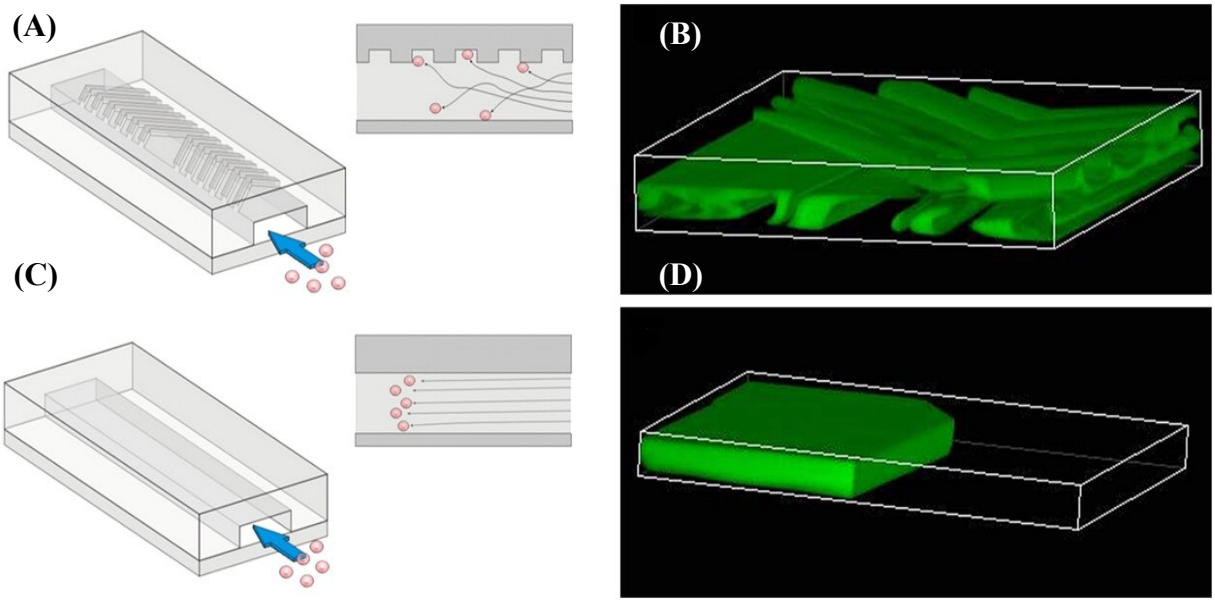

Figure I.5. HB-chip. **(A-B)** Microvorticies generated by the HB-chip that increases cell-surface interactions compared to the CTC-chip **(C-D)** with laminar flow streamlines. Reprinted from reference [57]. © 2010, with permission from the National Academy of Sciences of the United States of America.

1.2.4.2 *Immunomagnetic affinity*

Kang et al. developed an integrated micromagnetic-microfluidic device to capture and culture CTCs from animal cancer models [62]. CTCs captured with Anti-EpCAM microbeads are directed toward a culture plate after enrichment with RBC lysis buffer. This method has 87% capture efficiency and enriched CTCs are >90% viable (Figure I-6).

Hoshino et al. later reported on a micromagnetic chip that captured CTCs with anti-EpCAM-conjugated ferrous nanoparticles from whole blood with average capture rate of 86% at 10 mL/h flow rate and sensitivity of 5 CTCs/mL of blood (Figure I-7) [63].

Chen et al. also described a negative enrichment of blood spiked with Jurkat T-cells into mononucleated cells (MNC) using a multistage magnetic-microfluidic disk [64]. Labeled cells are trapped and target cells collected in reservoir with successive increases in rotational speed. The average recovery of the device is 60%.

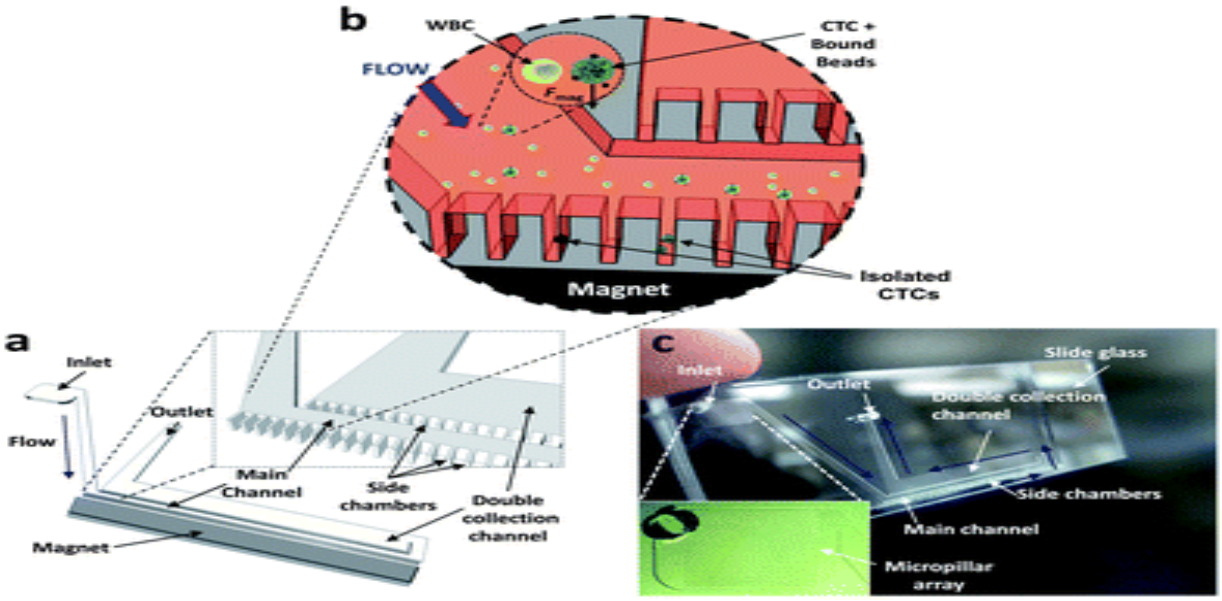

Figure I.6. Schematic presentation of the integrated micomagnetic-microfluidic device. The devise is composed of a main channel and double collection channel lined by rows of dead-end side chambers. Magnetically labeled cells are collected when magnetic field is applied. Reproduced from reference [62]. © 2012, with permission from the Royal Society of Chemistry.

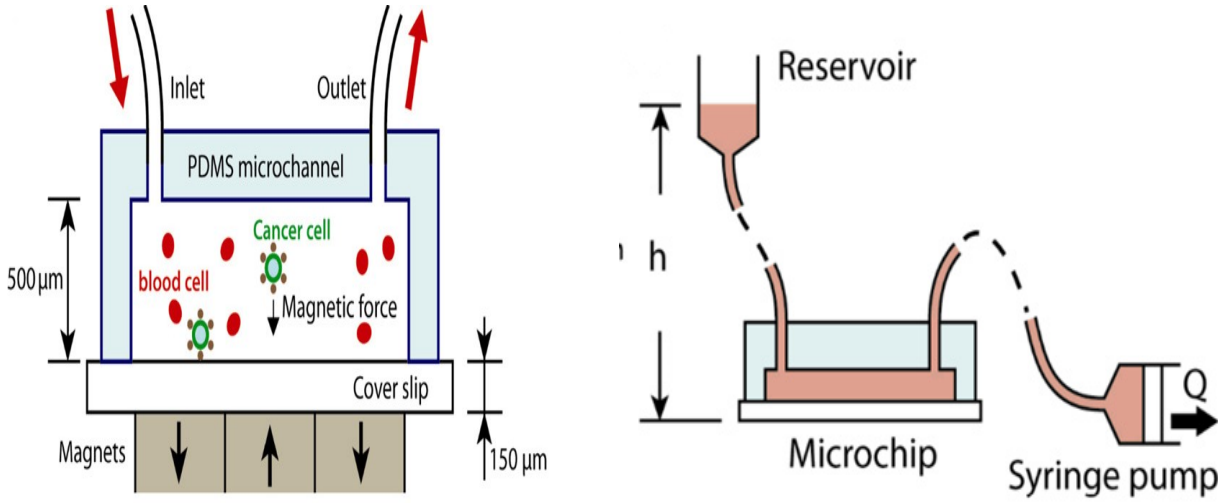

Figure I.7. Microchip design for immunomagnetic detection of cancer cells. Whole blood is admixed with anti-EpCAM antibody functionalized Fe_3O_4 nanoparticles to label CTCs. The blood then withdrawn using a regulated syringe pump through the chip where magnetic field collects labeled cells. Reproduced from reference [63]. © 2011, with permission from the Royal Society of Chemistry.

1.2.4.3 *Sized based*

Kuo et al. reported on a microchip optimized to detect spiked cancer cells based on size and deformability. The chip consists of a serpentine channel lined with rectangular apertures. This device captures CTCs with 90% or 50% recovery for fixed and unfixed cells from whole blood, respectively [65].

1.2.5 Flow cytometry

Advances in flow cytometry have allowed for the analysis of thousands of particles in a short amount of time and is currently used for cell sorting, counting, and biomarker detection. Fluorescence-activating cell sorting (FACS) separates cells based on their fluorescence following immunofluorescent labeling. Multi-parameter immunofluorescent labeling has demonstrated the ability to detect CTC [66], with Hu et al. reporting a sensitivity of one CTC for every 100,000 normal cells [67]. However, this platform lacks the sensitivity to isolate exceedingly rare cells, lengthy protocols to remove red blood cells and to stain the enriched population, as well as the high cost of the equipment [68].

Fiber-optic array scanning technology (FAST) combined with laser-printing optics can be used to excite 300,000 cells/second to achieve higher detection and sensitivity, and enables the processing of 100 million cells in 5 minutes [69]. Fixed cells are immunolabeled against cell surface markers and then read and analyzed with software to differentiate CTCs. However, this method lacks the capability to verify true positive cells. The author later improved the system by scanning isolated cells with automated digital microscopy (ADM). Despite these improvements, FAST/ADM only provides for the identification of viable CTCs, and not their enrichment, making it less conducive for clinical use necessitating the further characterization of CTCs [19].

Epithelial immuonSPOT (EPISPOT) is a technique to detect viable CTCs based on protein secretion. Negatively enriched cells are cultured for one to two days on plates coated with antibody-specific protein markers on a nitrocellulose membrane. Cells are then washed off and a secondary fluorochrome-tagged antibody is used to detect the captured protein [70]. CTCs are identified based on the immunospots. This technique allows for multiple markers to be evaluated simultaneously and provides for CTC quantification. It has also been used to detect CTCs in breast cancer patients [71, 72]. However, the process is lengthy and the protein markers must be actively secreted by the tumor in order for detection [70].

1.2.6 Dielectrophoresis

Dielectrophoresis (DEP) technology enables the detection of unlabeled cells based on their dielectric properties. As the cells are exposed to a non-uniform electrical field, they differentially migrate toward the electric-field maximum based on their membrane properties, size, morphology, density, metabolic activity [73].

Multiple DEP devices have been developed and optimized for the detection of CTCs [74]. Early technologies demonstrated a high recovery rate, purity, and viability [75-77], but was limited by its low throughput. Later, Gascoyne et al. developed dielectrophoretic field-flow fractionation (depFFF) to overcome these limitations, enabling the processing of up to 4.5 mL of blood with decreased time. [78]. However, the recovery efficiency ranged from 10-90% and was inversely related to PBMC concentration and chamber volume loading. Moreover, cell viability was dependent on immersion time, and most of the fractions collected first were non-viable; and could be the result of low voltage tolerance.

An integrated microfluidic-DEP device using multi-orifice flow fractionation (MOFF) and dielectrophoresis (DEP) was also developed by Moon et al [79]. MOFF is first used to enrich cancer cells based on size by hydrodynamic inertial force, and are then further sorted by DEP. The system enables continuous flow-through separation in contrast to other platforms based on non-continuous batch separation. The MOFF/DEP method has 78.81% recovery rate with high purity.

Gupta et al. introduced the ApoStream™ device comprised an integrated microfluidic flow chamber-modified depFFF that isolates cells based on the crossover frequency in continuous flow mode (Fig. I-8) [80]. DEP exerts a force on levitating blood cells, leading to a transition from negative to positive force to pull cancer cells toward the chamber floor while other blood cells are repelled and exit the chamber. The device can process 1.2×10^7 PBMCs/hour with an average recovery of 74.9%, high purity, and leaves 97.6% of the cells viable.

The major limitations of DEP in CTC enrichment are that whole blood cannot be processed, buffers must be optimized, purity issues resulting from some shared characteristics of CTCs and PBMC, and cells must be processed immediately to prevent early apoptotic changes that affect their dielectric properties [81, 82].

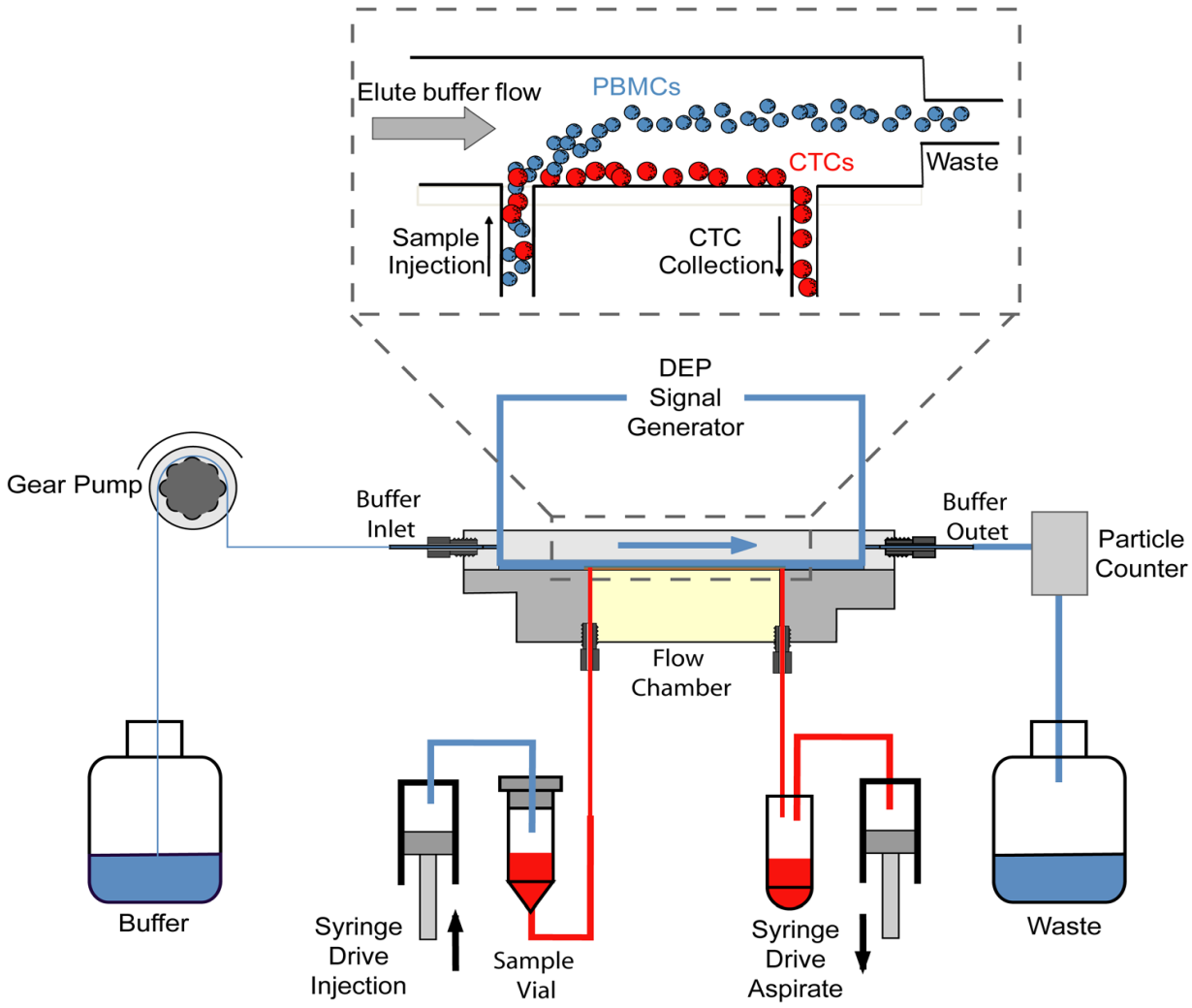

Figure I.8. Schematic diagram of the ApoStream device. Levitating PBMC are exposed to DEP at a crossover frequency that separates PBMCs into waste chamber and CTCs into collection chamber. This crossover frequency ranges between 30-40 kHz for CTCs compared to 90-140 kHz for PBMCs. Reprinted from reference [80], © 2012, with permission from AIP Publishing LLC.

1.3 Detection and clinical applications in selected cancers

1.3.1 Breast

A prospective multi-center study reported that metastatic breast cancer patients with a detection of ≥0.67 CTCs/mL of blood using the CellSearch system had lower progression-free and overall survivals [83, 84]. Using the AdnaTest to detect and genetically profile CTCs, Tewes et al. was

able to predict treatment responses in 78% of cases [85]. Furthermore, the persistence of CTCs after treatment is associated with poor prognosis [14].

Multiple ongoing interventional trials evaluating the utility of CTCs in treatment selection [86]. STIC CTC METABREAST (NCT01710605) is designed to assess progression free survival and medico-economics in metastatic hormone-dependent breast cancer based on the baseline of CTCs count before treatment initiation. Following randomization, the CTC-driven decision cohort is treated with either hormonal therapy or chemotherapy based on cutoff of 5 CTCs/7.5 mL and compared to clinician choice cohort. In phase III trial, the SWOG 0500 (NCT00382018) randomizes metastatic breast cancer patients with persistent elevated CTCs at the first follow-up assessment to changing therapy versus maintaining therapy. The overall survival, progression-free survival and toxicity are the primary outcome measures of this trial. In innovative approach, The DETECT III study (EudraCT 2010-024238-46) is randomizing HER2-negative metastatic breast cancer to standard therapy versus standard therapy combined with anti-HER2 targeted therapy based on HER-2 status of detectable CTC to assess progression-free survival.

1.3.2 Colon

CTC persistence at 4 weeks post-surgical intervention in patients with stage II-III colorectal cancer is associated with earlier cancer recurrence, as determined by membrane-array and qRT-PCR analysis [87]. In a multi-institutional study, the qRT-PCR of multiple markers (CK/CEA/CD133) were used to detect CTCs in Dukes' stage B and C found that CTC positivity was associated with lower disease-free and overall survival [88].

1.3.3 Lung

CTCs identified in NSCLC decreased in quantity with treatment when measured with the CTC-chip [55]. Maheswaran et al. described the detection of EGFR mutations in CTCs, which subsequently predicted drug response to EGFR tyrosine kinase inhibitor [56]. More interestingly, EGFR mutations were detected in 94% of patients with CTC analysis, compared to 34% by plasma testing.

1.3.4 Prostate

CTCs identified in 93% of castration-resistant prostate cancer patients with the CellSearch® system [89]. Baseline CTCs count more than 5 CTCs/7.5mL of blood was associated with poor

survival. Moreover, CTCs serial follow during treatment in castration-resistant prostate cancer served as surrogate marker to predict response to treatment and survival [90, 91]. In a randomized, double-blind, placebo-controlled, phase III trial assessing abiraterone acetate following docetaxel, CTCs enumeration was evaluated prospectively as surrogate efficacy response biomarker of overall survival in metastatic castration-resistant prostate cancer [92]. CTC conversion from unfavorable counts, defined as CTC ≥ 5/7.5 mL of blood, to favorable counts was predictive of overall survival.

CTCs have been detected in ovarian, hepatocellular carcinoma, bladder transitional carcinoma and many other types [93-95]. The field of CTCs detection and their clinical applications are evolving rapidly and provide insights into personalized medicine approach [96]. Isolating CTCs and successfully culturing them in ex-vivo enabled genomic profiling and assessing molecular pathways involved in tumorigenesis to predict sensitivity of targeted cancer therapy [97, 98]. In HER-2 negative breast cancer, 40% of patients with detectable CTC had HER-2 expression [99]. This finding has led to the initiation of The DETECT III study (EudraCT 2010-024238-46) that's primary objective to evaluate treatment response targeting anti-HER-2 based on molecular characterization of detectable CTCs.

In summary, CTCs detection and characterization have a wide range of clinical applications; predict disease prognosis; evaluate response to treatment; genomic profiling; predict drug sensitivity and selection of patients for adjuvant systemic/targeted treatments.

1.4 Human papillomavirus

HPV is a non-enveloped, circular double-stranded DNA, epitheliotropic virus (Figure I-9). It belongs to the *Papillomaviridae* family and more than 100 types have been reported [100, 101]. HPV are classified into high and low risk types based on their oncogenic characteristics [102-104].

The genome is organized into the early, late, and long control regions (LCR) (Figure 1-10). The LCR has no protein coding function. The early region contains E1, E2, E4, E5, E6, E7 and E8 open reading frames (ORF). The late region encodes L1 and L2 capsid proteins [105-107]. The L1 ORF has the most conserved DNA sequence of the HPV genome, because of that it is widely used for viral typing. Differences of >10%, between 2% and 10%, and <2% constitutes new papillomaviruses isolates, subtypes, and variants respectively [101].

E6 and E7 oncogenes encode for the oncoproteins with the same name, E6 and E7 [108-110]. Together, the E6 and E7 expression are necessary and sufficient to induce cellular transformation and immortalization [111, 112]. Importantly, the oncoprotein E6 can bind p53 resulting in the p53 ubiquitin-mediated degradation, and can also induce BAK (Bcl-2-homologous antagonist/killer) degradation and telomerase activation. The oncoprotein E7 binds and inactivates retinoblastoma tumor suppressor (Rb) that leads to the release of the E2F transcriptional activator, which inhibits cyclin-dependent kinases (CDK) and indirectly induces $p16^{INK4A}$.

During the progression of oncogenic HPV-infected lesion, the viral genome integrates into to the host genome [113]. The net effect is induction of genomic instability, cellular immortalization, and malignant transformation (Figure I-11) [109, 110, 114-117]. Abolishing E6 and E7 expression in cervical cancer cell lines leads to growth arrest, cellular senescence, and apoptosis [118-123].

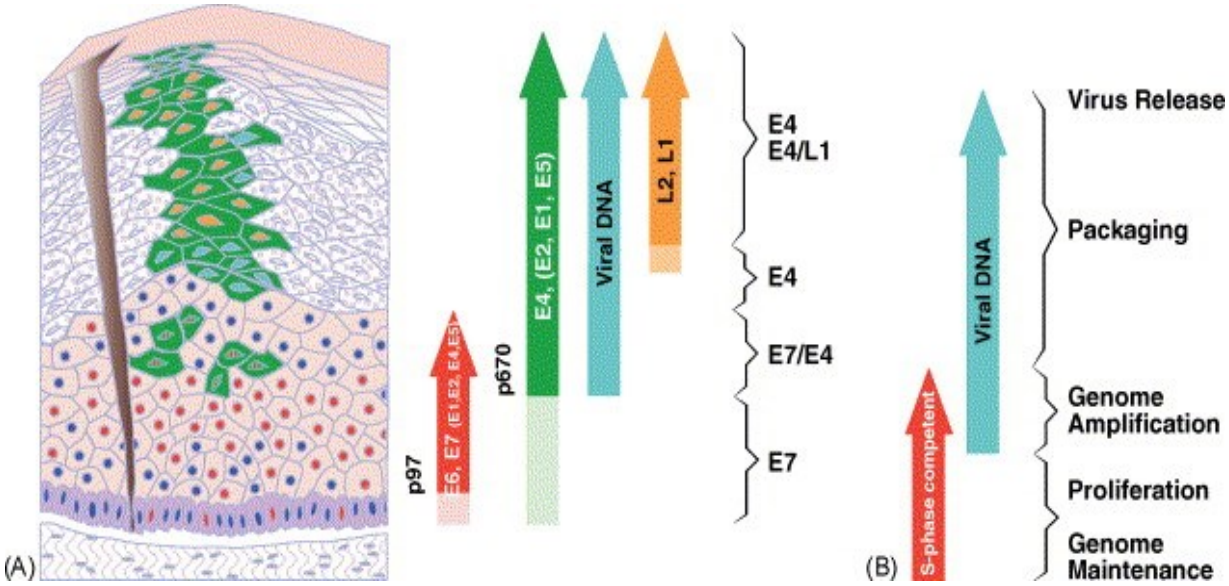

Figure I.9. HPV life cycle. HPV infection is confined to epithelial cells. Following access to the basal cell layer, the viral promoter induces E6 and E7 expression to initiate S-phase entry, viral genome amplification, and protein expression during epithelial cell differentiation. Viral capsid proteins are formed at the uppermost layer leading to viral particle assembly and release. The viral genome is maintained at low copy number at the basal layers by the E1, E2, E6 and E7 proteins. E4 and E5 are necessary to aid E6 and E7 expression. Reprinted from reference [124]. © 2005, with permission from Elsevier.

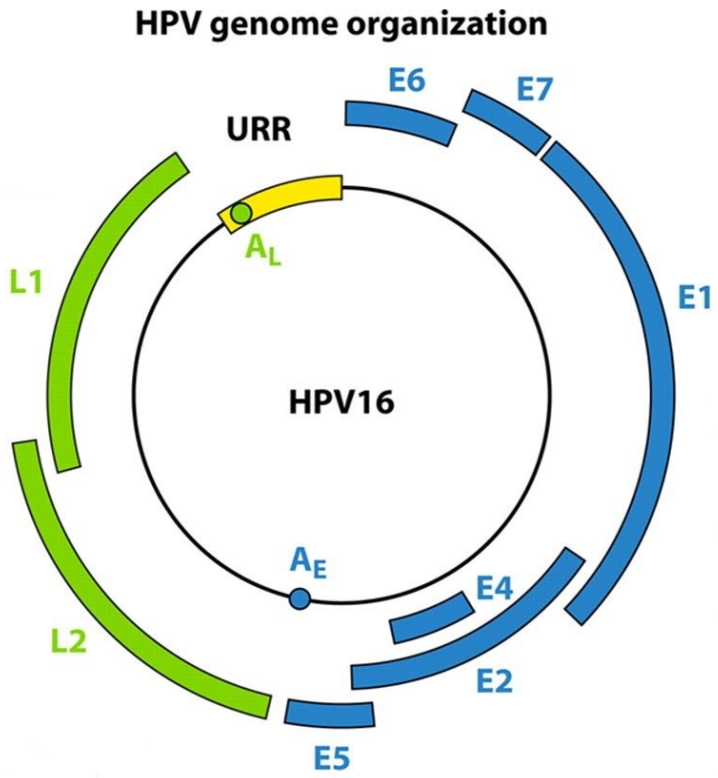

Figure I.10. The HPV genome and ORF function. E1 and E2: viral DNA replication. E4: viral release and packaging. E5: immune evasion, proliferation, and enhances E6 and E7. E6 and E7: oncoproteins. L1: major capsid protein. L2: minor capsid protein. The Upstream Regulatory Region (URR) that harbors the viral promoter and enhancer. Reprinted from Reference [125]**.** © 2012, with permission from the American society for Microbiology.

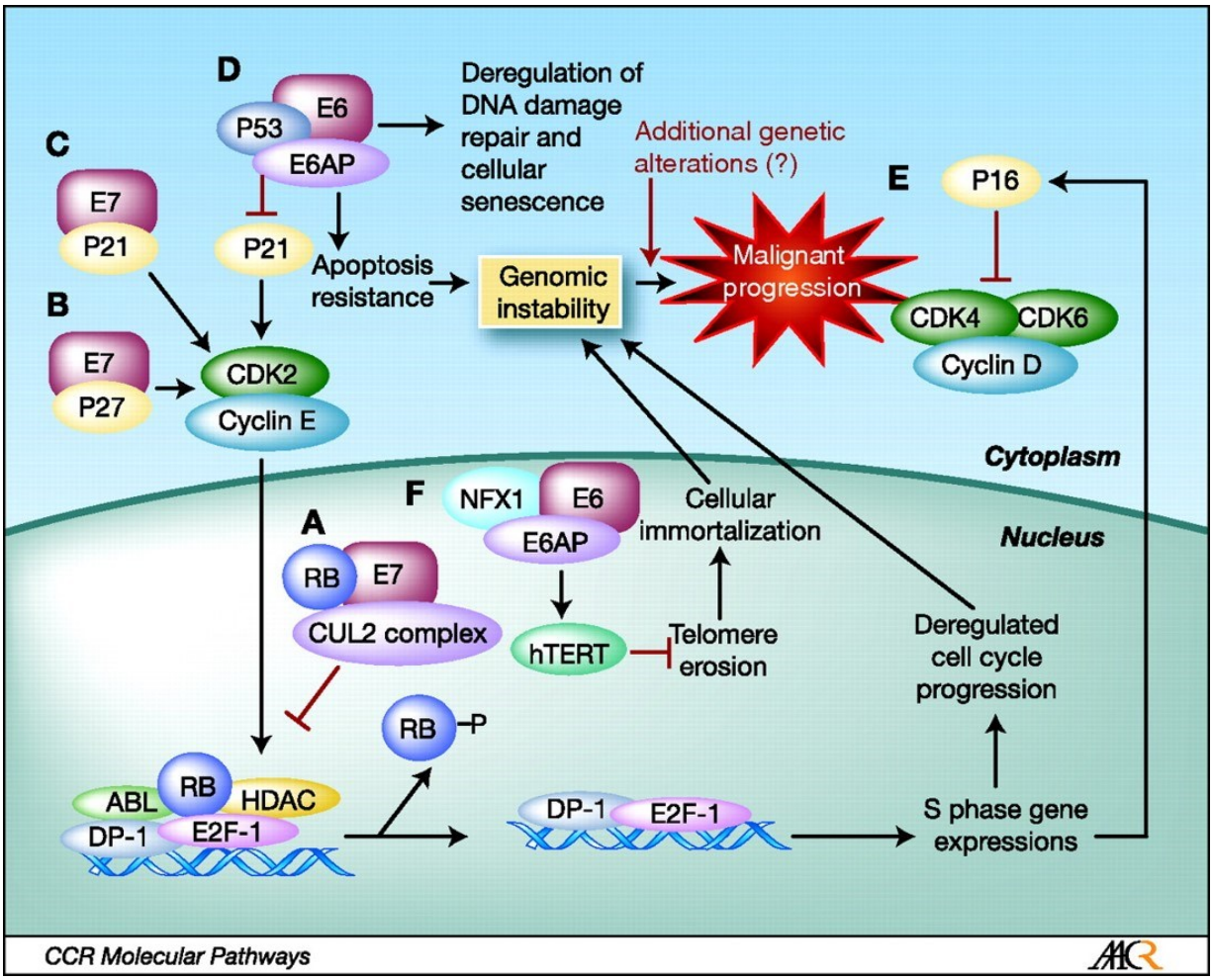

Figure I.11. E6 and E7 molecular mechanisms of inducing malignant transformation. E6 forms a complex with E6AP that functions as p53-specifc ubiquitin-protein ligase, leading to its degradation and the subsequent inhibition of the CDK inhibitor p21. The sequestration and/or degradation of p53 leads to cell cycle deregulation, DNA damage repair, and cellular senescence. The E6/E6AP complex additionally degrades NFX1, a transcriptional repressor of hTERT, resulting in cellular immortalization. E7 induces Rb degradation leading to liberation of the E2F-1 transcriptional factor. Furthermore, the p16 CDK inhibitor, which inhibits Rb phosphorylation, is indirectly induced through activation of E2F-1. E7 rescues the functional activity of E6 by inhibiting p21 and p27 CDK inhibitors, leading to activation of cyclin A and E. The net effect is induction of genomic instability, cellular immortalization, and proliferation. Reprinted from reference [126]. © 2009, with permission from AACR.

1.5 Uterine cervical Cancer

Uterine cervical cancer (UCC) is the fourth most common cancer affecting women worldwide, and the fourth leading cause cancer related deaths in women. There were 528,000 estimated new cases of UCC in 2012, with 85% occurring in developing countries [127].

HPV is an etiological risk factor for the development of cervical cancer and HPV DNA is detected in 99.7% of cervical carcinomas [128]. HPV is the most common sexually transmitted disease with a 79% estimated lifetime risk of cervical infection [129, 130]. Two high-risk HPV types, HPV16 and 18, account for 73% of cervical cancer cases; whereas HPV31, 33, 35, 39, 45, 51, 52, 56, 58, and 59 account for the remaining cases [131].

The International Federation of Gynecology and Obstetrics staging system (FIGO 2009) used to stage cervical cancer relies on clinical and basic radiological assessment [132, 133]. In developed countries, surgical staging and advanced radiological techniques are used to guide treatment [134-136]. The treatment of early stage cancer usually consists of surgery or primary radiotherapy with comparable outcomes [137]. Despite primary surgical treatment, approximately 50% of patients require adjuvant radiotherapy following the identification of further risk factors at final surgicopathological examination. This combined treatment is associated with increased morbidity [137]. In addition, risk factors that are detrimental for prognosis include pelvic lymph node metastasis, parametrial involvement, and positive resected margins [138, 139].

Pelvic lymph node metastasis is an independent prognostic factor associated with a decrease in disease-free and overall survival. Although the risk of nodal metastasis is about 21% in early stages [140], radiological assessment lacks the sensitivity to detect lymph node metastases [141]. The sensitivity of PET/CT scan, MRI, and CT to detect lymph node metastases is 75%, 56%, and 58%, respectively. Additionally, metastatic size <5 mm are below the detection limit of these technologies [142]. Approximately 15% of stage IB patients relapse, despite the absence of lymph node metastasis by routine histopathological examination and clear surgical margins [138]. Horn et al. retrospectively re-examined surgically resected pelvic lymph nodes and detected micrometastasis in 22.2% of patients and found a range between 3.8-23.9% in previously published literature [143]. In breast cancer, the reexamination of lymph nodes previously reported as negative with current methods of serial sectioning and

immunohistochemistry (IHC) detected occult metastasis in 20% of patients compared to 7% by haematoxylin and eosin (H&E), which correlated with poor prognosis [144].

Micrometastases are defined as tumor cell clusters more than 0.2 mm to and including 2 mm in size, whereas isolated tumor cells (ITC) are 0.2 mm or less. Using IHC and serial cuts, they are found in 10-90% of lymph nodes determined to be negative by routine histological examination [145, 146]. In cervical carcinoma, micrometastasis is an independent risk factor associated with reduced overall survival [147, 148]. Ultrastaging has improved the detection rate of lymph node metastasis [149, 150]; however, the technique is cumbersome and requires the examination of several histological slides.

Sentinel lymph node (SLN) mapping has emerged to improve detection rates and reduce the complications associated with complete pelvic lymphadenectomy [150-152]. The SLN is the first lymph node in the lymphatic pathway draining from a tumor and, if that lymph node is negative, then all others are also assumed to be negative. However, the performance of SLN depends on multiple factors including the technique used to detect the SLN [147, 153], surgical experience [154], tumor volume [155, 156], and pathological examination [147, 157]. In a large multicenter retrospective study, SLN and ultra-staging was able to identify micrometastases at a sensitivity of 91% with a false negative rate of 2.8% [158].

1.6 CTCs in UCC

Studies addressing CTC in UCC are scarce. Pao et al. used a Ficoll-Paque density gradient medium to enrich CTCs, which were then subjected to qRT-PCR analysis to detect HPV16 E6 expression. Notably, the E6 transcript was detected in 92% of stage IV-B UCC [159]. In follow-up publication by the same group, HPV16 and/or 18 E6 oncogenes expression was detected in 51.4% of locally advanced UCC cases, and positivity was associated with higher recurrence risk, the presence of distant metastasis, and lower overall survival [160]. In addition, Weismann et al. was able to detect ≥25 spiked cells in 7.5 mL of blood after enrichment using Ficoll-Paque followed by a secondary positive enrichment with αEpCAM antibody; however, the average recovery was 50% and CTCs were undetectable if present at <25 cells/mL of blood. Nevertheless, the technique could detect CTCs in 23% of patients with early-state UCC [161].

Digital-Direct-RT-PCR of HPV16/18 E6 expression demonstrated a sensitivity of 1 CTC for every 500,000 normal cells, and a sensitivity of 5 CTCs/mL of blood, which was inversely related to the background number of PBMCs [162].

In contrast, nested RT-PCR for the cytokeratin-19 (CK19) transcript was sufficient to detect CTCs in 21.4% of stage IB-IIB patients; although, its expression did not correlate with any clinicopathological parameters [163].

Finally, Mitsuhashi et al. comparatively assessed the use of EGFR and CK19 qRT-PCR for the detection of CTCs. Notably, EGFR was expressed in 98% of primary tumors and was detected in the blood of 26.7% cancer patients, with no detectable levels in normal controls; whereas, CK19 was detected in 77.8% and 65% of patients and normal controls, respectively [164].

1.7 Hypothesis and Objective

Tumor markers expressed by cancer cells that can be used to detect them and to monitor their progression [165]. These markers can be organ-specific, tumor-specific, or tumor non-specific. The ideal marker should be exclusively expressed in tumor cells and be organ-specific. For instance, prostate cancer expresses prostate-specific antigen (organ-specific). Alfa-fetoprotein is expressed by hepatocellular carcinoma and yolk sac tumor (tumor-specific). Cytokeratin are variably expressed in epithelial cells and the most prevalent in tumor cells of epithelial origin (tissue-specific and tumor non-specific). CA-125 a common tumor marker that is expressed by epithelial ovarian cancer is also expressed by other tumors such as the breast, lung and gastrointestinal (organ non-specific and tumor non-specific) [166]. However, tumor markers are not entirely specific as they can be expressed in many benign conditions and by multiple tumors [165].

The current method used to detect RNA expression in tumor cells and has a wide range of clinical applications is the qRT-PCR, which indirectly assess genes expression [167, 168]. The qRT-PCR sensitivity is one target cell per 10 million, corresponding to approximately to one cell per 0.1-1 mL of blood [26]. Multiple studies have reported on the detection of CTCs using cytokeratin, prostate-specific antigen, and other tumor-specific markers using qRT-PCR [169-172].

Cytokeratin are a family of intermediate filament proteins that participate in the formation of the cellular cytoskeleton. The two types of CK proteins, acidic type I and neutral/basic type II, both of which are variably expressed in epithelial cells and are usually maintained during malignant transformation [173]. CK8, CK18, and CK19 are the most prevalent in tumor cells of epithelial origin [174]. A previous study assessing the use of CK19 qRT-PCR analysis for the detection of lymph node micrometastasis in cervical cancer found CK19 expression in ~50% of lymph nodes. Moreover, 44% of lymph nodes deemed negative by histological analysis were found positive for CK19 expression, a result that correlated with clinicopathological features [175]. In breast carcinomas, a one-step nucleic acid amplification assay (OSNA) for CK19 used for the rapid intraoperative detection of lymph node metastasis has a sensitivity of 93.3% [176]. In comparison, frozen section has 58% sensitivity for detecting nodal micrometastasis [177]. Similar findings have been reported for the analysis of frozen sections in cervical cancer with a sensitivity range of 20.7-56.2% [178-180]. This suggests that CK19 OSNAs may be of potential value in the management of UCC to avoid further unnecessary surgical procedures and quickly identify the proper standard of care.

HPV DNA can be detected in 99.7% of UCCs [128]. The E6 and E7 oncoproteins encoded by HPV are constitutively expressed and facilitate the development and maintenance of a malignant phenotype. Thus, they are ideal molecular markers to detect CTCs in UCC patients [118-123]. Notably, a previous study identified CTCs in 92% of stage IV-B UCC patients by analyzing HPV16 E6 oncogene expression [159]. In follow up study, the HPV16 and/or 18 E6 oncogenes expression were detected in 51.4% of locally advanced UCC cases, which was associated with a higher risk of recurrence, distant metastasis, and lower overall survival [160].

The cyclin dependent kinase (CDK) inhibitor $p16^{INK4A}$ functions as tumor suppressor and regulates the G1/S cell cycle transition by binding CDKs to inhibit the phosphorylation of Rb. This prevents the release of E2F transcription factors and aberrant transition into S-phase [181, 182]. $p16^{INK4A}$ is indirectly overexpressed in cervical cancer as result of the functional inactivation of Rb by E7 and can be used as biomarker for diagnosis [183].

Despite the numerous studies addressing CTCs in many other cancers, only a limited amount of information is available for the use of CTCs in UCC diagnostics. Due to their known roles in UCC etiology and lack of expression in normal cells, we hypothesize that HPV

oncogene expression will allow for the detection of CTCs and lymph node metastases with high sensitivity. These findings have the potential to improve current CTC detection methods for UCC and to determine the potential clinical impact of these cells in UCC management. Thus, we propose to use these markers to detect CTCs.

Objective #1:

Optimize, establish protocols and validate for the use of E6/E7, CK19 and $p16^{INK4A}$ genes expression to detect CTCs and lymph node metastases in UCC.

Objective #2:

Develop a tumor bank consisting of tumor tissue biopsies, plasma, and PBMCs accompanied with HPV DNA genotyping and clinical data for UCC patients treated at the Centre Hospitalier de l'Université de Montréal (CHUM).

Objective #3:

Determine the capacity of CK19, $p16^{INK4A}$, E6, and E7 expression analysis by qRT-PCR to detect CTCs in patients with UCC.

CHAPTER II : MATERIALS AND METHODS

2.1 Cell Culture

The HeLa, HCA2-hTERT, U2OS, and AT3-OVA cell lines were cultured in Dulbecco's Modified Eagle Medium (DMEM). The CaSki cell line was cultured in RPMI media. TOV-1946, TOV-112D, and TOV-21G were cultured in OSE medium (Table II-I). All culture media were supplemented with 8% Fetal Bovine Serum (FBS), 100 IU/mL penicillin, and 100 μg/mL streptomycin, and grown at 37°C in a humidified atmosphere of 5% CO2. Cells were passaged every two to three days prior to confluency with 0.05% trypsin supplemented with 0.53 mM EDTA.

Table II-I. Cell line

Cell Line	Origin
HeLa	Uterine cervical adenocarcinoma (HPV18 DNA-positive, about 10-50 copies per cell). Obtained from the American Type Culture Collection (Manassas, VA).
HCA2-hTERT	Immortalized human fibroblast [184].
U2OS	Human osteosarcoma [185].
AT3-OVA	Mice breast carcinoma [186].
CaSki	Uterine cervical squamous cell carcinoma (HPV16/18 DNA positive, about 60-600 copies per cell). However, HPV16 RNA is solely expressed [187]. Obtained from the American Type Culture Collection (Manassas, VA).
TOV-1946	High grade ovarian serous carcinoma [188].
TOV-112D	High grade endometroid ovarian carcinoma [189].
TOV-21G	Clear cell ovarian carcinoma [189].

2.2 Ficoll-Paque Density gradient enrichment

2.2.1 Validation

A solution containing 15 mL of each FBS and PBS was prepared and spiked with a pre-determined number of cells. It was then layered over 15 mL Ficoll-Paque in a 50 mL conical

tube. After centrifugation at 400*g* at 20°C for 30 minutes without breaking, the cell layer above the Ficoll-Paque was collected and transferred to a separate tube. In addition, the cell-free phases above the cell layer and below the Ficoll-Paque were collected and transferred into new tubes. Cells were washed twice with PBS and counted with a hemocytometer and TC20™ automated cell counter.

2.2.2 Enrichment of spiked cancer cells

Blood from healthy volunteers were collected in EDTA tubes. HPV16-positive CaSki-GFP cells were serially diluted and spiked into blood. The spiked blood was further diluted 2-4-fold with cold PBS containing 2 mM EDTA. After centrifugation at 400*g* at 20°C for 30 minutes without breaking, the following layer phases were formed from the bottom to the top: erythrocyte, granulocytes, Ficoll-Paque, PBMC, and plasma. The PBMC layer was collected and transferred to a separate tube and washed twice with cold PBS, and equally divided for RNA extraction and formalin fixation for flow cytometry.

2.3 Enrichment by RBC lysis

CaSki-GFP cells was serially diluted and spiked into blood collected from healthy donors. CTCs were then enriched by adding 10 mL of ACK RBC lysis buffer per mL of blood and incubating for 5 minutes at room temperature kept in gentle agitation. Incubations were extended for an additional 5 minutes if the RBC lysis was not complete [113]. Cells then were collected by centrifugation at 400*g* at 4°C for 5 minutes, washed once with cold PBS, and then split equally for RNA extraction and formalin fixation for flow cytometry.

2.4 Flow cytometry strategy for sorting and counting CTCs

GFP-tagged CaSki cells were used to differentiate target cells from normal PBMCs. Following enrichment, cells were fixed with 1% cold formalin for 10 minutes at 4°C and washed once with cold PBS. Fixed cells were preserved in 75% ethanol at −20°C. CountBright™ Absolute Counting Beads were used to determine the absolute number of recovered cells. Briefly, previously enriched fixed cells were washed once with PBS, resuspended in 1000 µL PBS, and 50 µL bead slurry (50,000 Beads in 50 µL) was then added to each suspension. The following formula was used to calculate cell concentration:

$$(\text{Number of cell events}/\text{Number of bead events}) \times (\text{Assigned bead count}/\text{Volume of sample}) = \text{Cells}/\mu\text{L}$$

Where the number of cell and bead events represent cells and beads detected following excitation.

Flow cytometry data was collected on a BD LSRFortessa™ cell analyzer and analyzed with FlowJo software (Figure II-1). Enriched cells were not stained with DAPI whereas the beads are positive when exited with the DAPI channel.

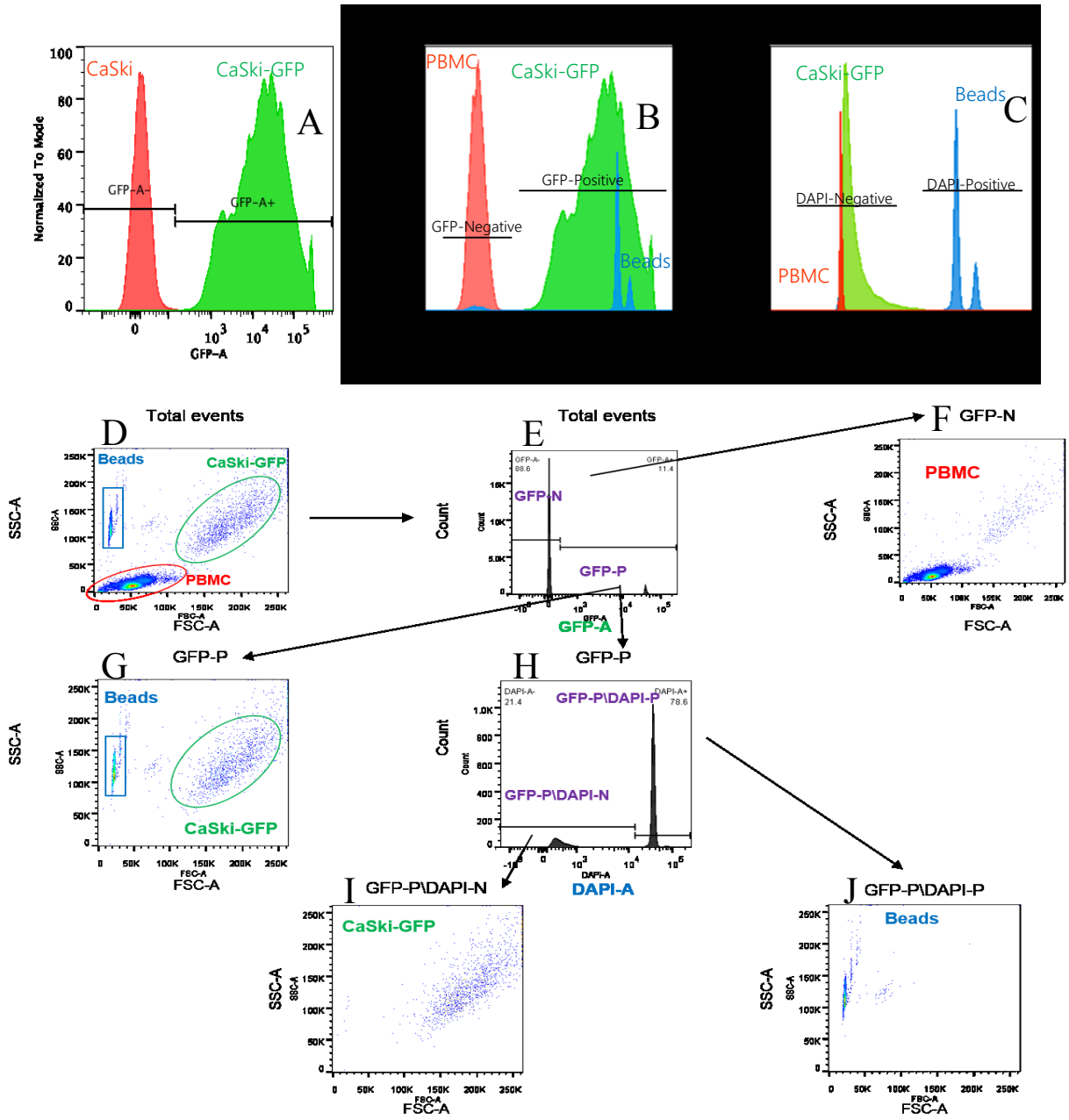

Figure II.1. Flow cytometry gating strategy to isolate GFP-positive spiked cancer cells. **(A-C)** Fluorescence intensity histogram with indicated gate setting. GFP intensity and counts are plotted on the x- and y-axes, respectively. **(A)** CaSki (red) vs CaSki-GFP (green) vs CaSki cells based on GFP fluorescence. **(B)** PBMC (red), CaSki-GFP (green), and counting beads (blue) based on GFP fluorescence. **(C)** PBMC (red), CaSki-GFP (green), and counting beads (blue) based on DAPI fluorescence. **(D)** Forward scatter versus side scatter plot (FSC vs. SSC) on total, ungated events demonstrating the three populations as indicated. **(E)** Total events on GFP

intensity histogram. **(F)** FSC vs. SSC on GFP-negative PBMCs **(G)** FSC vs. SSC on GFP-positive gating for CaSki-GFP cells and counting beads. **(H)** GFP-positive gating based on DAPI intensity. **(I)** FSC vs. SSC on GFP-positive/DAPI-negative CaSki-GFP cells. **(J)** FSC vs. SSC plot on GFP-positive/DAPI-positive counting beads. Note: enriched cells were not stained with DAPI whereas the beads are positive when exited with the DAPI channel.

2.5 Real-time quantitative reverse-transcription polymerase chain reaction (qRT-PCR)

2.5.1 Reverse transcription

RNA was isolated by Trizol® extraction from the enriched cell pellet per the manufacturer's instructions. The RNA concentration and purity was determined spectrophotometrically based on absorbance at 260 nm and 280 nm. Equivalent amounts of RNA (≤1 μg) was reverse-transcribed into cDNA with Superscript® III First-Strand Synthesis SuperMix in a 20 μL reaction volume. The reaction mix composed of 10 μL of 2xRT reaction mix, two μL of reverse transcriptase enzyme, RNA (maximum 8 μL) and water free RNase to complete the volume to 20 μL. The mixture was then subjected to the following thermocyling protocol: 10 minutes at room temperature, 50°C for 30 minutes, and 85°C for 5 minutes, followed by chilling on ice. Hereafter 1 μL RNase H was added to the reaction mix and incubated at 37°C for 20 minutes. The cDNA was stored at -20°C until further analysis.

2.5.2 Multiplex real-time PCR reactions

Multiplex real-time PCR reactions for HPV16 E6 and E7, CK19, and $p16^{INK4A}$ were performed to detect CTCs. TaqMan® assays were used to assess E6, E7, CK19, and $p16^{INK4A}$ gene expression. 18S ribosomal RNA and/or TATA-box binding protein (TBP) were used as internal references. The Oligo Analyzer 3.1 and BLAST software (Basic Local Alignment Search Tool) were used to verify the specificity of primers and probes sequences listed in Table II-II. Primers and probes were purchased from Integrated DNA Technologies. Real time quantitative PCR reactions were performed using Platinum® Quantitative PCR SuperMix-UGD in a 15-μL reaction volume. Maximum 50 ng/μL of cDNA was used per reaction. The reaction mix composed of 3 μL of cDNA, 7.5 μL of master mix, 0.6 μL of $MgCl_2$; to a final concentration of 4.0 mM, 0.3 μL of probe; to a final concentration of 0.2 μM and 0.3 μL of each primer; to a final concentration of 0.2 μM. RNase free water was used to complete the volume to 15 μL. PCR reactions were run on a StepOnePlus™ Real time PCR instrument with initial incubations at 50°C for 2 minutes and 95°C for 10 minutes, followed by 40 cycles of 95°C for 15 seconds and 60°C for one minute. Reactions were performed in triplicates with positive, negative, and no template controls (NTC). Data was analyzed with StepOne™ Software by the comparative Ct method.

Table II-II. Sequence of primers and TaqMan probes.

Genes	Sequence (5'-3')	Location	Product size (Bp)
18s Forward Reverse Probe	 CGGCTACCACATCCAAGGAA CGCTATTGGAGCTGGAATTA TGCTGGCACCAGACTTGCCCTC	450-646	197
TBP Forward Reverse Probe	 ACAGGAGCCAAGAGTGAA AAACCCAACTTCTGTACAAC ACAGTCCAGACTGGCAGCAAGAAAATA	743-816	74
HPV16 E7 Forward Reverse Probe	 CAAGCAGAACCGGACAGA GTCTACGTGTGTGCTTTGTA CAAGTGTGACTCTACGCTTCGGTTGTG	691-786	96
HPV16 E6 Forward Reverse Probe	 AATGTTTCAGGACCCACAGG CTCACGTCGCAGTAACTGTTG AGCGACCCAGAAAGTTACCACAGTTATG	103-226	124
CK-19 Forward Reverse Probe	 TCGACAACGCCCGTCTG CCACGCTCATGCGCAG CCTGTTCCGTCTCAAACTTGGTTCGG	606-680	75
$P16^{INK4A}$ Forward Reverse Probe	 CTGCCCAACGCACCGAATA GCGCTGCCCATCATCATGA CTGGATCGGCCTCCGACCGTA	415-476	62

Relative expression of the target gene

The mean cycle threshold value (C_T) was determined for the target gene ($C_{T,\ target}$) and the endogenous control ($C_{T,\ ec}$), which represents the PCR cycle number at which the fluorescent signal is first detectable. Relative expression (ΔC_T) of the target gene was calculated by subtracting ($C_{T,\ ec}$) from ($C_{T,\ target}$). Relative fold expression was calculated by the following equation: $2^{-\Delta CT}$.

2.6 Uterine cervical cancer patients

All patient experiments were performed with the approval of the CHUM institutional review board. Blood was collected from HPV16-positive UCC patients at diagnosis in EDTA tubes and processed within 6 hours. PBMCs were non-magnetically enriched using ACK RBC lysis buffer with the exception of two patients enriched by Ficoll centrifugation. RNA was stored in TRIzol® at -80°C until further analysis. Then, RNA was isolated by TRIzol® extraction from the enriched cell pellet per the manufacturer's instructions. The RNA concentration and purity was determined spectrophotometrically based on absorbance at 260 nm and 280 nm. Multiplex qRT-PCR reactions for HPV16 E6 and E7, CK19, and $p16^{INK4A}$ were performed to detect CTCs. TBP was used as endogenous control. Normal PBMCs isolated from healthy females served as negative control.

CHAPTER III : RESULTS

3.1 Validation of Ficoll-Paque Enrichment

To optimize our enrichment procedures and define the source(s) of lost CTCs, we first wanted to determine the phases where CTCs localize. From our analysis, we found that an average of 50% of CTCs are located immediately above the Ficoll-Paque layer, whereas the remaining cells distributed in either the uppermost or bottommost phases or were lost during washing process.

Interestingly, cell lines derived from aggressive tumors exhibited a very low recovery rate (HeLa, U20S, and AT3-OVA) (Figure III-1).

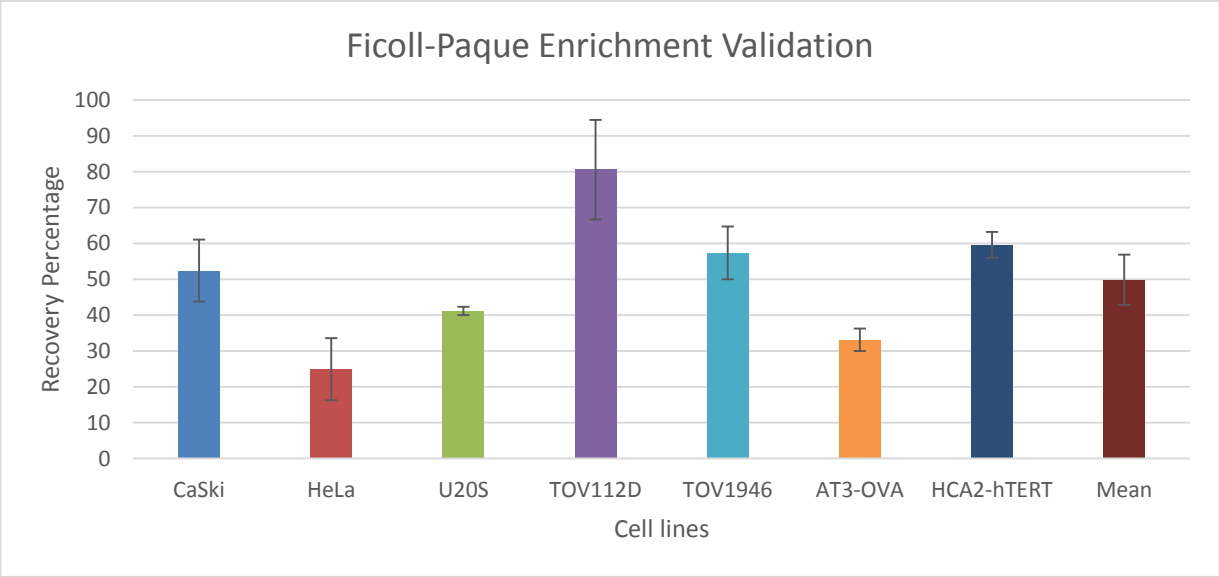

Figure III.1. Ficoll-Paque density gradient for cell separation. UCC cells localized in the layer immediately above the Ficoll-Paque phase. Recovery is plotted on the y-axes and varies greatly across cell lines with an average recovery of 50%. Values represent the mean ± standard error of the mean (SEM) for three independent experiments per cell line.

3.2 E6 and E7 oncogenes expression after enrichment using Ficoll-Paque density gradients

Figure III-2 demonstrates the detection of both markers from CaSki-GFP spiked at fixed concentrations in blood. We found that E7 detection was more sensitive than E6 from experiments performed in triplicate. Figure III-3 shows a lower detection limit of 10^3-10^4 cells/mL in blood for both markers, as determined by experiments performed at least in

duplicate. Below that threshold, we failed to observe a downward trend in the CT value that corresponds to the spiking scheme. In addition, the detection of E6 and E7 was not consistently reproducible below 1000 spiked cells/mL of blood, indicating the low sensitivity of Ficoll-Paque enrichment.

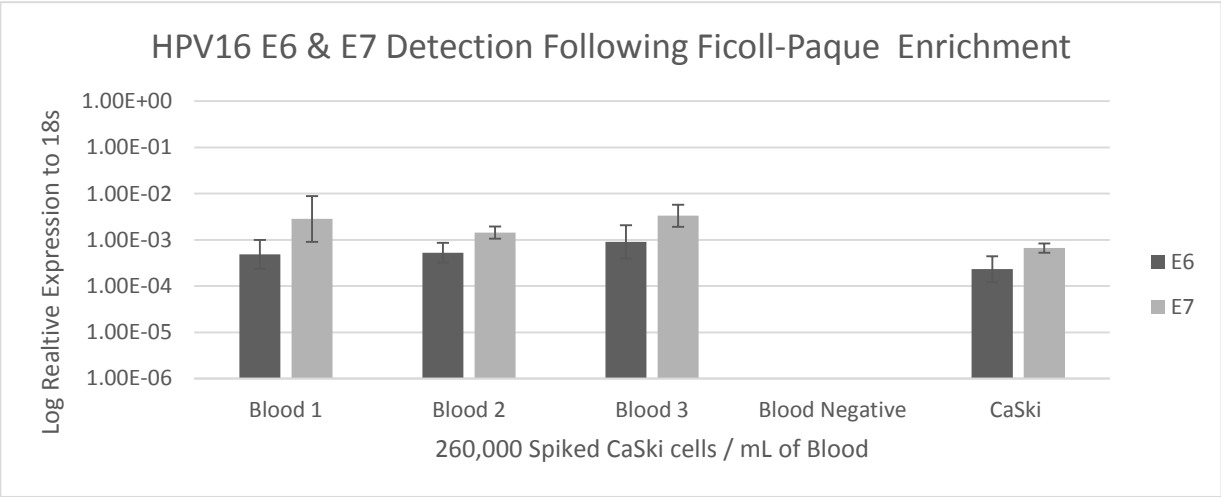

Figure III.2. Detection of HPV16 E6/E7 expression from CaSki UCC cells spiked into human blood following Ficoll-Paque density gradient enrichment. Blood spiked with 260,000 CaSki UCC cells was subjected to Ficoll-Paque enrichment for CTCs. RNA extracted from the enriched cells was subjected to qRT-PCR analysis for HPV16 E6 and E7 expression. Pure CaSki or PBMCs were used as positive and negative controls, respectively. Relative expression normalized to 18s ribosomal RNA is plotted on the y-axis.

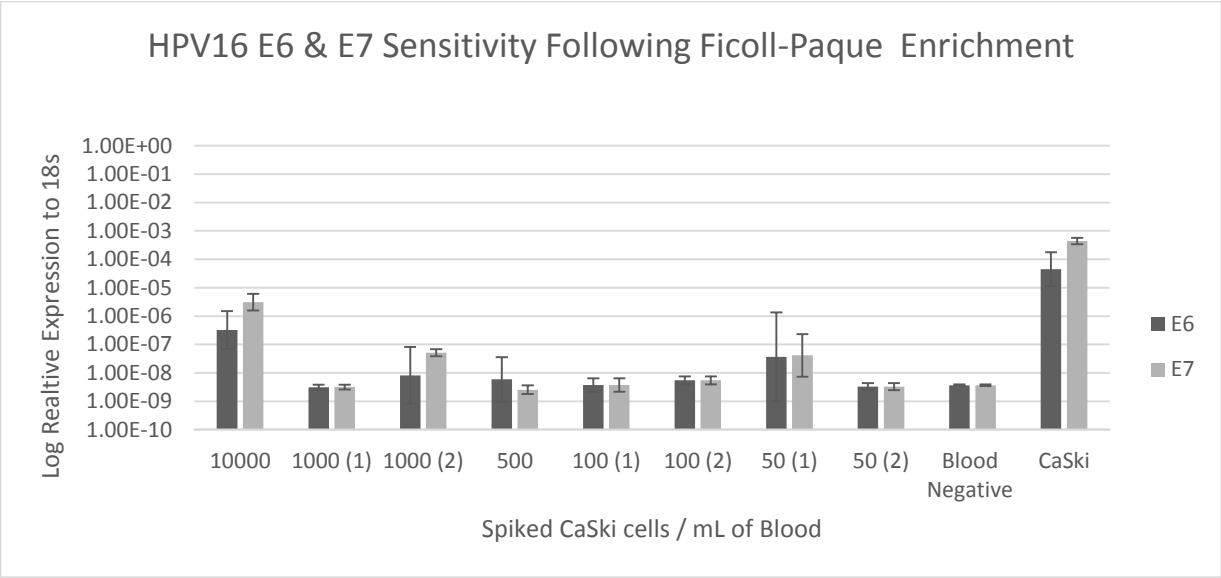

Figure III.3. HPV16 E6/E7 expression detection limits from CaSki cells spiked into human blood following Ficoll-Paque density gradient centrifugation. Blood samples were spiked with serial dilutions of CaSki cells and subjected to Ficoll-Paque enrichment. RNA extracted from the enriched cell pellet was analyzed for HPV16 E6/E7 expression by qRT-PCR. Relative expression normalized to 18s ribosomal RNA is plotted on the y-axis.

3.3 Detection of spiked cancer cells using flow cytometry following Ficoll-Paque enrichment

Ficoll-Paque enrichment demonstrated low recovery percentage and inter-sample variation (1.7-5.6%) (Table III-I), consistent with previous results from the qRT-PCR analysis. From this data, we concluded that the CTC detection threshold ranged between 1000-10,000 cells/mL of blood, below which we were unable to detect any cancer cells (Table III-II).

Table III-I. Flow cytometry cell count following enrichment by Ficoll-Paque.

Spiked cells per mL of blood	Recovered Cell counts/mL of Blood	Recovery %
Negative control	N/A	N/A
260,000	15144	5.6
260,000	4543	1.7
260,000	11246	4.2

Table III-II. Flow cytometry cell count following enrichment by Ficoll-Paque: Detection limit.

Spiked cells per mL of blood	Recovered Cell counts/mL of Blood	Recovery %
Negative control	N/A	N/A
10,000/mL	456	4.5
1000/mL	ND	ND
500/mL	ND	ND
100/mL	ND	ND
50/mL	ND	ND

3.4 Detection of spiked cancer cells by flow cytometry following RBC lysis enrichment

Enrichment by RBC lysis demonstrated a much higher recovery percentage, varying between 57-98.4 %, compared to Ficoll-Paque. Due to background activity, this single parameter method was reliable in isolating spiked cancer cells down to a threshold of 5,000 cancer cells/mL of blood (Table III-III). Below that threshold, the background activity is consistently higher than the number of spiked cells which account for higher percentage recovery (>100%).

Table III-III. Flow cytometry cell count following enrichment by RBC lysis

Spiked cells per mL of Blood	Recovered Cell counts/mL of Blood	Recovery %
Negative control	N/A	N/A
80000	51,100	63.9
40000	34300	85.8
20000	11800	59.0
10000	5712	57.1
5000	4920	98.4
2500	9030	361.2
1000	2392	239.2
500	1680	336.0
250	4740	1896.0

CHAPTER IV : ARTICLE

Detecting Uterine Cervical Cancer Cells Using Molecular Biomarkers: High Sensitivity of CK19-, p16INK4a- And HPVE6/E7-Mediated Detection in Parrafin Embededd tissues and Blood

Ahmed Mousa[1,2]*; Nawel Mechtouf[1]*; Guillaume B Cardin[1]; Vanessa Samouëlian[1,3]# and Francis Rodier[1,4]#

[1] CRCHUM et Institut du cancer de Montréal, Montreal, QC, Canada

[2] King Abdul Al-Aziz University, Faculty of Medicine, Department of obstetrics and gynecology, Jeddah, Saudi Arabia

[3] Université de Montréal, Département d'Obstétrique Gynécologie, Montreal, QC, Canada

[4] Université de Montréal, Département de Radiologie, Radio-Oncologie et Médicine Nucléaire, Montreal, QC, Canada

* These authors contributed equally

Running title: Detection of rare uterine cervical cancer cells using molecular biomarkers

RÉSUMÉ

Arrière-plan:

Le cancer du col de l'utérus (UCC) est le quatrième cancer de la femme en incidence dans le monde entier. L'essaimage des cellules cancéreuses (métastases) a un impact direct sur notre capacité à guérir le cancer. Pour le patientes atteintes de UCC, la présence de métastases ganglionnaires est un important facteur de risque indépendant associé à un mauvais pronostic. La détection de cellules tumorales circulantes (CTC) a également une valeur pronostique dans de nombreux cancers (sein, poumon, du côlon et de la prostate), mais cela n'est pas encore utilisé pour les UCC. Actuellement, le traitement du UCC est guidé par l'évaluation clinique et histologique. L'avancement dans les techniques moléculaires pour la détection de cellules cancéreuses disséminées rares pourrait améliorer considérablement la gestion de la maladie.

Objectif:

Utiliser des biomarqueurs moléculaires pour optimiser le processus d'enrichissement et de detection des cellules tumorales dans la circulation sanguine et les ganglions lymphatiques chez les patientes atteintes de UCC.

Matériel & Méthodes:

Nous avons lysé en Trizol une série de dilutions séquentielles d'une population mixte de cellules HeLa/CaSki et CaSki/HCA2-hTERT à l'aide de cellules fraîches et de cellules fixées à la formaline enrobées dans la paraffine, imitant les ganglions lymphatiques. Des cellules CaSki ont été ajoutées à des échantillons sanguins d'individus sains et nous avons comparé l'enrichissement positif ou négatif et l'absence d'enrichissement pour la collecte des cellules CaSki lors de la lyse des globules rouges. Les cellules cancéreuses ont été détectées par qRT-PCR sur les E6, E7, CK19 et $p16^{INK4a}$.

Résultat:

La limite de détection pour les E6 et E7 des VPH 16/18 est de 0.008% (1:12500 cellules) sur les échantillons frais et de 0.02% et 0.05% pour les HPV16 E6/E7 et HPV18 E6/E7 pour les

échantillons fixées en bloc de paraffine. La lyse des globules rouges seule ou couplée avec de l'enrichissement positif ou negative a une limite de detection de 50 cellules par mL de sang pour E6, E7, Ck19 et $p16^{INK4a}$. La sensibilité de la qPCR augmente avec l'enrichissement en réduisant le bruit de fond causé par les monocytes sanguins. Le gène $p16^{INK4a}$ est exprimé dans les individus normaux et peut être utilisé si la valeur d'expression médiane est déterminée.

Conclusion:

L'analyse par qRT-PCR des oncogènes du VPH est plus sensible pour détecter un ganglion lymphatique micrométastatique que l'examinen histologique. La détection par qRT-PCR des oncogènes du VPH, de CK19 et de $p16^{INK4a}$ dans les échantillons sanguins qRT-PCR montre une grande sensibilité.

Mots clés: diagnostic, carcinome cervical utérin, d'évaluation pré-thérapeutique, oncogènes viraux, des ganglions lymphatiques micrométastase, cellules circulant tumorales, qRT-PCR, E6 et E7 oncoprotéine, enrichissement immunomagnétique, détection moléculaire.

ABSTRACT

Background:

Uterine cervical cancer (UCC) is the fourth common cancer affecting women worldwide. In general, the dissemination of cancer cells (metastasis) directly impacts our ability to cure cancer. Lymph node metastasis is an important independent risk factor associated with poor prognosis. The detection of circulating tumor cells (CTCs) also has prognostic value in many other cancers (Breast, lung, colon and prostate), but this is not yet used for UCC. Currently, the treatment of UCC is guided by traditional clinical and pathological assessment. Advancement in molecular techniques for the detection of rare disseminated cancer cells could vastly improve disease management.

Objective:

To use molecular biomarkers to optimize the enrichment and the detection of tumor cells in the bloodstream and in lymph node (LN) for UCC patients.

Material & Methods:

Series of sequential dilution of mixed population of UCC HeLa/CaSki cells and non-cancerous HCA2-hTERT cells imitating micrometastatic LN were prepared fresh or embedded in paraffin blocks and subjected to RNA extraction. In CTCs spiking models, CaSki cells were serially diluted and spiked into human blood collected from healthy volunteers. Enrichment using red blood cells (RBC) lysis and RBC lysis combined with negative or positive magnetic enrichment were compared. E6, E7, CK19 and $p16^{INK4a}$ gene expression by Real-Time Quantitative Reverse Transcriptase polymerase chain reaction (qRT-PCR) were used to detect cancer cells.

Result:

HVP16/18 E6 & E7 mediated detection limits in fresh samples was 0.008% (1:12500 cells) compared to 0.02% and 0.05% (for HPV16 E6/E7 and HPV18 E6/E7 respectively) in paraffin blocks. In CTCs spiking model, qRT-PCR following RBC lysis alone or combined with negative or positive enrichment revealed detection limit of 50 cells per mL of blood for E6, E7, Ck19 and p16. The sensitivity of PCR increased with positive and negative enrichment by eliminating PBMC background.

Conclusion:

qRT-PCR of HPV oncogenes expression is more sensitive than pathological examination in detecting lymph node metastasis. qRT-PCR of HPV oncogenes, CK19, and p16 expression all demonstrated high sensitivity in detecting spiked cancer cell in paraffin blocks and in blood.

Key words: diagnostic, uterine cervical carcinoma, pretherapeutic evaluation, viral oncogenes, lymph node micrometastasis, circulating tumor cells, qRT-PCR, E6 and E7 oncoprotein, immunomagnetic enrichment, molecular detection.

INTRODUCTION

Uterine cervical cancer (UCC) is the fourth most common cancer affecting women worldwide and the fourth leading cause of cancer-related deaths in women [1]. Human papillomavirus (HPV) is the primary etiological risk factor for cervical cancer, and HPV is detected in 99.7% of cervical carcinomas [2]. The E6 and E7 oncoproteins encoded by high-risk HPV types are synergistically necessary and sufficient to induce cellular transformation and immortalization [3, 4]. E6 binds p53 and promotes ubiquitin-mediated degradation, while also inducing BAK (Bcl-2-homologous antagonist/killer) degradation and telomerase activation; whereas, E7 binds and inactivates retinoblastoma tumor suppressor protein (Rb), leading to the release of the E2F transcriptional activator, a loss of cyclin-dependent kinase (CDK) inhibition, and the indirect upregulation of the cellular tumor suppressor $p16^{INK4A}$. This process potentiates genomic instability, cellular immortalization, and malignant transformation [5-10]. Notably, abolishing E6 and E7 expression in cervical cancer cell lines lead to growth arrest, cellular senescence, and apoptosis highlighting the dependence of UCC cells for these viral oncogenes [11-16].

Early-stage therapy can consist of surgical or primary radiotherapy, which have comparable outcomes but different toxicity profiles [17]. Approximately 50% of patients require adjuvant radiotherapy for risk factors identified from primary surgery and pathological examination including pelvic lymph node metastasis, parametrial involvement, and positive resection margins; however, this combination of surgery and radiotherapy is associated with increased morbidity [17-19].

Pelvic lymph node metastasis is an independent prognostic factor associated with decrease disease-free interval and survival, and occurs in about 21% of patients with early-stage UCC [20]. Radiological assessment lacks the sensitivity to detect lymph node metastasis [21]. The sensitivity of PET/CT scan, MRI and CT to detect lymph node metastases ≥5 mm in diameter is 75%, 56% and 58% respectively, and those smaller falls below the detection limit of these technologies [22]. Approximately 15% of stage I-B UCC patients relapse, despite the absence of lymph node metastasis by routine histopathological examination and clear surgical margins [18]. A retrospective re-examination of surgically resected pelvic lymph nodes detected micrometastasis in 22.2% of cases and reported a range of 3.8-23.9% from a review of current literature [23, 24]. Micrometastases and isolated tumor cells (ITC) are defined as tumor clusters

between 0.2-2 mm and ≤0.2 mm in size, respectively; with the later found in 10-90% of lymph nodes deemed negative by routine histological examination [25, 26]. In cervical carcinoma, micrometastasis is an independent risk factor associated with lower overall survival [27, 28]. The advent of ultrastaging has improved detection rate of lymph node metastasis [29, 30]; however, the technique is cumbersome and requires the examination of several slides. Sentinel lymph node (SLN) mapping has emerged to improve detection rates and reduce complications associated with complete pelvic lymphadenectomy [30-32]. The SLN is the first lymph node in the lymphatic pathway draining a tumor and, if that lymph node is negative, then all others are assumed negative. However, the performance of SLN mapping depends on multiple factors including the technique used to identify the SLN [27, 33], surgical experience [34], tumor volume [35, 36], and pathological examination [27, 37]. A large multicenter retrospective study determined that SLN mapping and ultrastaging had a sensitivity and false negative rate for metastasis of 91% and 2.8%, respectively [38].

Cytokeratin 19 (CK19) expression is prevalent in epithelial tumor cells and has recently been investigated as a potential tumor marker. A previous study using CK19 qRT-PCR to detect lymph node micrometastasis in cervical cancer found expression in ~50% of lymph nodes. Moreover, 44% of histologically negative lymph nodes were positive for CK19, a result that correlated with clinicopathological features [39]. In breast carcinoma, a one-step nucleic acid amplification assay (OSNA) for CK19 has been used for the rapid intraoperative detection of lymph node metastasis with a sensitivity of 93.3% [40], whereas the analysis of frozen sections has a 58 % sensitivity for detecting nodal micrometastasis [41]. A similar result for the low performance of frozen section analysis has been reported for UCC [42-44], suggesting that CK19 OSNAs may be valuable for the management uterine cervical cancer.

Studies addressing the presence of circulating tumor cells (CTCs) in UCC are scarce. Pao et al. previously reported on the detection of CTCs in 92% patients with metastatic cervical cancer by HPV16 E6 RT-PCR [45]. In follow up by the same group, the HPV16 and/or 18 E6 oncogenes expression were detected in 51.4% of locally advanced UCC and was associated with a higher risk of recurrence, distant metastasis, and lower overall survival [46].

Overall, the development of sensitive molecular biomarkers could dramatically improve the diagnostic and treatment selection process for UCC patients. Herein, we describe the detection of lymph node micrometastases and CTCs in experimental models using fresh material,

paraffin-embedded blocks, and blood using qRT-PCR for the HPV E6/E7, CK19, and $p16^{INK4A}$ gene expression.

MATERIAL AND METHODS

Cell Culture

HeLa and HCA2-hTERT (obtained from ATCC) cell lines were cultured in Dulbecco's Modified Eagle Medium (DMEM) media and the CaSki cells (obtained from ATCC) in RPMI media. Media was supplemented with 8% FBS, 100 IU/mL penicillin, and 100 μg/mL streptomycin. The cells were grown at 37°C in a humidified atmosphere of 5% CO_2. Sub-confluent cells were passaged every two to three days using 0.05% trypsin supplemented with 0.53 mM EDTA.

CTC Enrichment

Blood from healthy volunteers were collected in EDTA-treated tubes and informed consent were obtained from the volunteers. CaSki cells were serially diluted and spiked into blood and enriched either using RBC lysis alone or in combination with negative or positive selection with αCD45 (leukocyte common antigen) or αEpCAM (epithelial cell adhesion molecule) antibodies, respectively. RBC lysis was performed with ACK lysis buffer as previously described [47]. Briefly, 10 mL buffer was added per mL of blood and incubated for 5 minutes at room temperature. Incubations were extended for an additional 5 minutes if lysis was incomplete. Cells then were collected by centrifugation at 400*g* for 5 minutes at 4°C and washed once with cold PBS before use in subsequent analyses or enrichment protocols. CD45-negative and EpCAM-positive selection was accomplished by magnetic separation with antibody-coated Dynabeads® following the manufacturer's protocol. Briefly, cells were incubated with the respective Dynabeads for 30 minutes at 2-8°C, and then exposed to magnet for 10 minutes to deplete CD45-positive mononuclear cells or isolate EpCAM-positive cancer cells. Supernatants from both separations were transferred to new tubes. All samples were washed once with cold PBS prior to use in subsequent procedures.

RNA Extraction

RNA was isolated from freshly harvested cells and enriched with TRIzol® reagent using the manufacturer's protocol, or extracted from formalin-fixed paraffin-embedded (FFPE) samples using the RecoverAll™ Total Nucleic Acid Isolation Kit (Ambion, Inc.) with minor changes to the manufacturer's protocol. Briefly, fifteen 10 μm paraffin sections for each sample were

subjected to proteinase digestion for one hour at 50°C, and left for additional 15 minute intervals until clear and fluid. The eluate was repurified with the RNeasy® MinutesElute™ Cleanup Kit (QIAGEN). The RNA quantity and purity was determined by A260/280 ratios as measured on a spectrophotometer. RNA was stored at -80°C until further analysis.

Real-time quantitative reverse-transcription polymerase chain reaction (qRT-PCR)

Superscript III First-strand Synthesis Supermix (Invitrogen) was used to synthesize cDNA per manufacturer's protocol. Reactions were performed with ≤1 μg RNA in a 20 μL reaction volume. Gene expression was measured using TaqMan® Assays. Oligo Analyzer 3.1 and BLAST software (Basic Local Alignment Search Tool) were used to verify the specificity of primers and probes sequences for E6, E7, CK19 and $p16^{INK4A}$ (Table IV-I). Probes and primers were purchased from Integrated DNA Technology. Expression of 18S ribosomal RNA and/or TATA-box binding protein (TBP) served as internal controls. Platinum® Quantitative PCR SuperMix-UGD was used for qRT-PCR reactions. cDNA (≤150 ng) was amplified in a 15μL reaction mixture with final concentrations of 4 mM $MgCl_2$, 0.2 μM probe, and 0.2 μM of each primer. Reactions were run on a StepOnePlus™ Real time PCR instrument with initial incubations at 50°C for 2 minutes and 95°C for 10 minutes, followed by 40 thermocycles of 95°C for 15 seconds and 60°C for one minute. Reactions were performed in triplicate with positive, negative, and no template controls (NTC). Data was analyzed with StepOne™ Software using the comparative Ct method.

Preparation of Formalin-Fixed Paraffin-Embedded (FFPE) Lymph Node models

Paraffin block containing 50/50 mixes of HeLa-HPV16/18+/CaSki-HPV16+ or CaSki-HPV16+/HCA2-hTERT-HPV- cells were made to test for HPV-18 and HPV-16 detection, respectively. Blocks of pure CaSki or HCA2-hTERT cells were made to serve as negative controls for HPV18 and HPV16, respectively. Of note, CaSki cell line contains an integrated HPV16 genome as well as sequences related to HPV18; however, HPV16 RNA is solely expressed [48, 49]. Mixtures of 10^6 total cells (5×10^5 per cell type) were vortexed and centrifuged at 1500 RPM for 10 minutes. Cell pellets were suspended in 500 μL 10% formalin, transferred tubes containing well-shaped solid histogel and centrifuged for 15 minutes at 2500 RPM. The resulting supernatant was aspirated and 2-5 mL of histogel was added to enclose the

pellet. The histogel was allowed to solidify for 20 minutes, followed by the addition of 1-2 mL 10% formalin. The blocks were incubated overnight at 4°C prior to paraffin embedding.

Correlation of the Mixed Cell Model to Lymph Node Metastasis

Macrometastasis, micrometastasis, and ITCs in lymph nodes are defined as tumor clusters >2 mm, 0.2-2 mm, and <0.2 mm, respectively [25, 26]. Knowing that the upper limit of normal pelvic lymph node size is one cm [50], we calculated the lymph node volume using the following formula: $4/3 \times 3.14 \times R^3$, where R is defined as the radius and equals half the diameter. We hypothesize that macrometastases, micrometastases, and ITCs occupy >0.8%, 0.008-0.8%, and less than 0.008% of lymph node volumes, respectively. Calculations are presented in Table IV-II.

RESULTS

Analysis of HPV16/18 E6/E7 oncogenes expression from a mix population of fresh cells

Serial dilutions of CaSki UCC cells in HCA2-hTERT and HeLa UCC cells in CaSki UCC cells were prepared in order to determine the lower detection limit of E6/E7 expression by qRT-PCR. All values were normalized to ribosomal 18s gene expression to eliminate variation in the RNA quantity between samples and the expression of both markers decreased with increased serial dilutions, indicating successful dilution schemes. We determined that for HPV16 E7 and HPV18 E6 and E7, the lower detection limit for HPV16 E7, HPV18 E6, and HPV18 E7 expression is 0.008%, which is significantly different from the HCA2-hTERT and CaSki negative controls, respectively (Figure IV-1) (Table IV-III). HPV18 E6 and E7 expression was undetectable in pure CaSki cells; however, weak basal non-specific HPV16 E6 and E7 expression was observed in HCA2-hTERT cells.

HPV 16/18 E6 and E7 oncogenes expression from FFPE cell mixtures

To further determine the ability to detect metastatic cancer cells in FFPE lymph nodes using molecular biomarker expression, we examined the E6/E7 qRT-PCR sensitivity threshold for RNA extracted from FFPE lymph node models. First, multiple reference genes were assessed to identify reliable constitutively expressed internal reference genes following FFPE-deparaffinization, resulting in the selection of 18s ribosomal RNA. In addition, we observed a 1000-fold lower signal from RNA extracted following FFPE-deparaffinization process when compared to that obtained from fresh material. We then serially diluted RNA extracted from

50/50 positive-negative cell population mixes into RNA extracted from negative cell populations and made cDNA for subsequent qRT-PCR analysis to detect E6 and E7 oncogenes expression. Notably, the expression of both markers diminished with progressive cell dilutions and was detectable down to a dilution factor of 0.02% for HVP16 E6/E7 (Figure IV-2; A-B) and 0.05% for HPV18 E6/E7 (Figure IV-2; C-D) (Table IV-IV).

CTCs detection using molecular biomarkers

We next defined the lower detection limits of the UCC molecular biomarkers E6, E7, CK19 and $p16^{INK4A}$ for identifying CTCs, and evaluated their dependency on various methods of CTCs enrichment. Figure IV-3;A-B show the relative detection of HPV16 E6 and E7 oncogenes expression normalized to TBP following enrichment using RBC lysis reagent. TBP was selected as an internal reference to avoid multiplex PCR saturation phenomenon associated with abundant levels of ribosomal 18s. A decrease in both expression markers correlated with the progressive dilutions of cancer cells down to 50 spiked cancer cells per mL of blood and a 1000-fold difference was observed between the 50 cells/mL positive sample and negative control, with an increased sensitivity for E7 oncogene expression compared to E6. Similarly, $p16^{INK4A}$ expression decreased with serial dilutions of cancer cells down to a level approximating 50 cells/mL of blood (Figure IV-3C). Due to its endogenous expression in normal cells, a low level of $p16^{INK4A}$ expression was detected in the negative blood control, but to a low level comparable to expectations for normal cellular physiology [51]. Significantly, a 1000-fold difference was observed between the 50 cells/mL positive sample and negative control. Finally, CK19 expression shown in Figure 3D reveal a sensitivity down to 50 cells/mL of blood and similarly a 1000-fold difference was observed between the 50 cells/mL positive sample and negative control

Following CTC negative enrichment, E6 and E7 oncogenes expression was analyzed in the enriched, CD45-negative and the resulting CD45-positive PBMC population and normalized to 18S ribosomal RNA expression (Because of very low amounts of starting material, E6 and E7 multiplex PCR detection were performed simultaneously and normalized to ribosomal 18S expression). Both markers correlated with the serial dilutions of cancer cells down to 50 spiked cells per mL of blood (Figure IV-4A). Non-normalized cycle threshold values were used as the variation of ribosomal 18s expression across samples caused by extremely low quantities of

recovered RNA prevented effective normalization. Similar pattern trended in the CD45-positive population, suggesting that a fraction of tumor cells either attached to CD45-postive cells or where non-specifically bound by the anti-CD45 antibodies (Figure IV-4B).

When comparing the positive versus negative isolation methods, we determined that both techniques were capable of detecting spiked cancer cells down to 50 cells/mL (Figure IV-5; A,C). However, we found that our positive enrichment method was able to recover more cells than the negative enrichment method. As for CD45-based negative enrichment, E6 and E7 oncogenes expression was also observed in the EpCAM-negative cell fraction isolates (Figure IV-5; D,E), suggesting that some tumor cells lacked EpCAM expression. Nevertheless, both enrichment techniques improved the qRT-PCR sensitivity by eliminating the PBMC background noise.

DISCUSSION AND CONCLUSIONS

UCC is the fourth most common cancer in woman worldwide. Surgery is the primary standard of care for early-stage UCC, and is supplemented with adjuvant radiotherapy based lymph node status, positive margins, and parametrial invasion as determined by histopathological assessment. Lymph node micrometastasis is an independent risk factor associated with reduced overall survival [24, 28]. Approximately 15% of stage IB patients relapse, despite negative LN and clear surgical margins [18]. Pathologists have an ~1% chance in detecting micrometastasis using conventional H&E staining [52]. SLN mapping and molecular ultrastaging has improved the detection rate of micrometastases, yet detection can still vary between 19-95% depending on methods used [29].

Advances in molecular biology techniques and applications have improved the detection of metastatic cancer in both sensitivity and specificity. Here, we describe a model to estimate the size of metastases harbored in a one cm^3 lymph node. Macrometastases is more than 2 mm in size and occupy more than 0.8% of one cm^3 lymph node; micrometastases is 0.2-2 mm in size and occupy 0.008-0.8% of one cm^3 lymph node and ITC is $\leq$ 0.2 mm in size and occupy $\leq$ 0.008% of one cm^3 lymph node (Table IV-III). Through our analyses, we purport that analysis of HPV E6/E7 oncogenes expression by qRT-PCR is sufficient to detect a mass of tumor cells in equivalent to macrometastases (> 0.8%) and micrometastases (0.008-0.8%), but not ITCs (< 0.008%), which fell below the detection limits.

FFPE tissues are widely used for histological diagnosis. The identification and validation of molecular markers using FFPE tissue is an area of intense research activity given the amount of tumor samples preserved in this manner, and any molecular methods successful at this type of analysis would allow the use of retrospectively banked pathology samples to clearly define the clinical impact rare cancer cells. The mRNA extracted from FFPE tissue is difficult to analyze, since formalin fixation results in protein/nucleic acid crosslinking and RNA degradation [53]. In our study, we observed lower sensitivity of qRT-PCR with RNA extracted from FFPE tissue compared to that extracted from fresh material. Notably, E6 and E7 oncogenes expression was 1000-fold less in FFPE cells compared to fresh isolates. RNA extracted from FFPE tissue had an A260/280 $\geq$ 1.9 and RNA disintegration was excluded by agarose gel electrophoresis, suggesting that RNA fragmentation may have occurred during the deparaffinization process. HPV16 and 18 E6/E7 oncogenes expression by qRT-PCR is sufficient to detect a mass of tumor cells in equivalent to 0.02% and 0.05% of a one cm^3 lymph node respectively. Because this detection limit is in the middle of the size of the micrometastasis category, the probability of detecting micrometastasis using the HVP16 and HVP18 oncogenes expression from FFPE tissue would be 98% and 95%, respectively, potentially missing the smaller micrometastasis and clearly falling short of ITC detection.

In this study, we also sought to determine the sensitivity and specificity of known cancer biomarkers for identifying UCC CTCs using qRT-PCR. The E6 and E7 oncogenes expression exhibited the highest specificity and sensitivity with the ability to detect 50 cells/mL of blood. Furthermore, a $\geq$1000-fold difference between the 50 cells/mL positive sample and negative control implies a greater sensitivity probably approaching 1 cell/mL of blood. Specifically, the X cycle threshold difference between the positive and the negative signals can be directly interpreted to a value of Y (log2 of Y) and used to be divided by 50 cells/mL to obtain a value of Z, which equal to one cell/mL. Both positive and negative enrichment methods improved the PCR sensitivity by eliminating PBMCs derived RNA background. However, positive enrichment recovered most cancer cells and provide the additional advantage of allowing the potential analysis of tumor gene expression on a highly pure isolate. It is important to note that EpCAM downregulation during EMT likely results in lower EpCAM expression and is a limitation of this technique since some cancer cells could be loss in the EpCAM negative fraction as observed in figure (5 B and D). In CD45-mediated negative enrichment, E6 and E7

oncogenes expression in the resultant cell population indicated that tumor cells attached or were engulfed by macrophages. The prognostic value of cells expressing both CD45 and tumor markers have not yet been determined [54]. Furthermore, $p16^{INK4A}$ was sufficient to detect UCC cancer cells down to lower than 50 cells/mL of blood and (potentially approaching 1 cell/mL of blood, see above); however, endogenous $p16^{INK4A}$ expression could make it difficult to distinguish CTCs from normal cells unless appropriate cutoff median expression values are established. Setting these values may be further complicated since $p16^{INK4A}$ expression varies depending on normal physiological activity and can increase with age and smoking [51]. CK19 had similar sensitivity to the E6 and E7 oncogenes expression; however, the marker is not specific to tumors and can be found in isolates from normal individuals [55]. We postulate that if an appropriate cutoff median expression value is established for a normal expression level, then this marker may be used for CTC detection. Using RT-PCR with established cutoff value to detect CK19 transcript in breast cancer patients, 2.2% of healthy females were positive compared to 31% and 40% of those with early and metastatic breast cancer, respectively. Moreover, the CK19 expression levels were significantly higher in breast cancer patient compared to those in the control group [56]. There are a limited number of studies addressing the detection of CTCs in UCC. Pao et al. used a Ficoll-Paque density gradient medium to enrich CTCs prior to HPV E6 oncogene expression analysis by RT-PCR, which was detected in 92% of stage IV-B UCC [45]. In follow up by the same group, HPV16/18 E6 expression was detected in 51.4% of locally advanced UCC cases and was associated with a higher risk of recurrence, distant metastasis, and lower overall survival [46]. In contrast, a study using Ficoll-Paque isolation followed by EpCAM-mediated positive selection was sufficient to detect ≥3.33 CTCs/mL with an average recovery was 50%. It was also capable of detecting CTCs in 23% patients with locally advanced UCC stage [57]. Digital-Direct-RT-PCR for HPV16/18 E6 expression imparted a sensitivity of one CTC per 500,000 normal cells and the ability to detect 5 CTCs/mL of blood [58]. In addition, the PCR sensitivity was inversely related to the background number of PBMCs. Finally, CK19 nested RT-PCR was shown to detect CTCs in 21.4% of stage IB-IIB patient; although, its expression did not correlate with any clinicopathological parameters [59].

In conclusion, qRT-PCR for E6 and E7 oncogenes expression is a sensitive and specific technique to detect CTCs and small lymph node metastases in UCC. Notably, we demonstrate

the ability to detect lymph node micrometastases equivalent to 0.2 mm in size and circulating tumor cells approaching 1 cell/mL of blood. The sensitivity of qRT-PCR in detecting HPV16/18 E6 and E7 is markedly affected by formalin fixation process as expected and is sufficient to detect a mass of tumor cells in equivalent to 0.02% and 0.05% of a one cm^3 lymph node potentially missing the smaller micrometastasis and clearly falling short of ITC detection. We also show that CK19 and $p16^{INK4A}$ can be used as adjuvant markers to verify CTCs detection, provided that appropriate cutoff median expression values are determined to differentiate between normal and malignant expression levels.

FIGURE AND TABLE LEGENDS:

Figure IV-1: E6/E7 oncogenes expression in a mix of cell populations containing HPV positive and/or negative cells.

RNA was extracted from freshly mixed cell populations containing UCC cancer cell lines. E6 and/or E7 oncogenes expression was then analyzed by qRT-PCR. **(A)** E6 oncogene expression in HPV16-negative CaSki UCC and HPV16-positive HCA2-hTERT immortalized fibroblast cells demonstrating detection limit at 0.008% ($p < 0.01$). **(B)** E6 and **(C)** E7 oncogenes expression in HPV18-negative CaSki and HPV18-positive HeLa cells demonstrating detection limit at 0.008% for both markers ($p < 0.05$). Values represent the mean ± SD for a minimum of two experimental replicates.

Figure IV-2: E6/E7 oncogenes expression from formalin-fixed, paraffin-embedded UCC mixtures.

Serial dilutions of RNA extracted from formalin-fixed, paraffin-embedded blocks comprised of a 50/50 mix of UCC cells and human fibroblasts were examined for E6 and E7 oncogenes expression by qRT-PCR. **(A)** E6 and **(B)** E7 expression from HPV16-positive CaSki UCC cells mixed with HCA2-hTERT fibroblasts demonstrating detection limit at 0.02% for both markers. **(C)** E6 and **(D)** E7 expression from HPV18-negative CaSki mixed with HPV18-positive HeLa cells demonstrating detection limit at 0.05% for both markers. Values represent the mean ± SD for a minimum of three experimental replicates.

Figure IV-3: Expression of E6/E7 pathway constituents from CaSki cells spiked into human blood following isolation by RBC lysis.

The expression of **(A)** E6, **(B)** E7, **(C)** p16, and (**D)** CK19 were analyzed by qRT-PCR from RNA extracted from CaSki cells isolated by RBC lysis enrichment. CaSki represents RNA extracted from pure cancer cells demonstrating detection limit at 50 cancer-cells/mL of blood% for all markers. Values represent the mean ± SD for a minimum of three experimental replicates.

Figure IV-4: E6/E7 expression in CaSki cells spiked into human blood following negative enrichment. E6 and E7 expression in was analyzed by qRT-PCR in **(A)** CD45-negative CaSki cells and **(B)** the depleted CD45-positive population.

Figure IV-5: Comparison E6/E7 expression detection from CaSki cells spiked into human blood following positive or negative enrichment. E6 and E7 expression were analyzed following positive or negative enrichment with αEpCAM or αCD45, respectively. **(A-B)** E6 and **(C-D)** expression in **(A, C)** EpCAM-positive and CD45-negative isolates, and **(B, D)** EpCAM-negative and CD45-positive isolates.

Table IV-I: Sequence of primers and TaqMan probes

Table IV-II: Calculation of micrometastatic focus volume in one cm lymph node.

Table IV-III: Detection limit of HVP oncogenes expression in fresh RNA.

Table IV -IV: Detection limit of HPV oncogenes expression in RNA extracted from FFPE cells block.

Figure IV.1

A

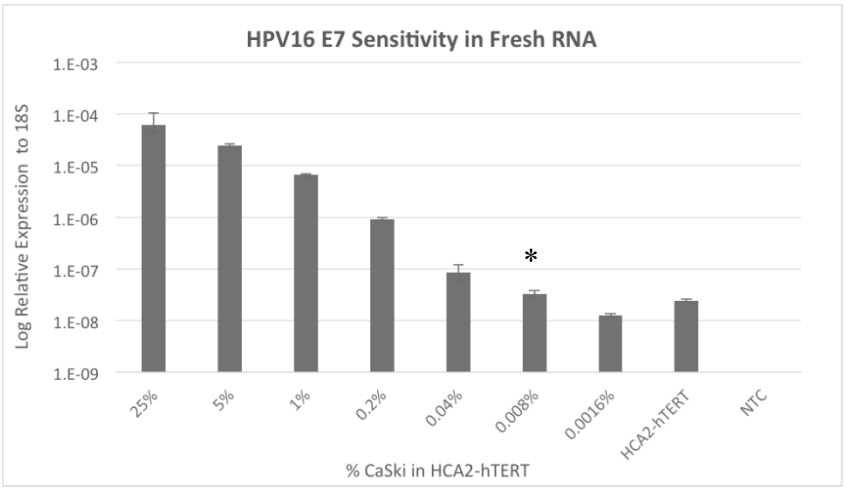

B

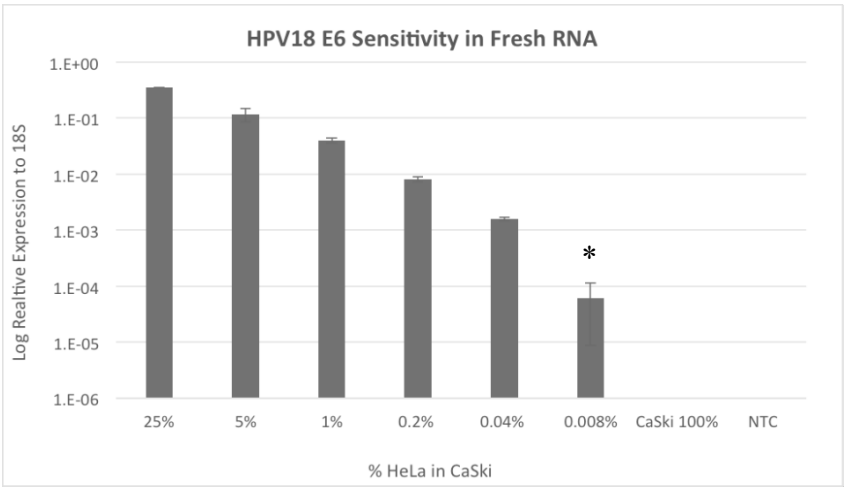

C

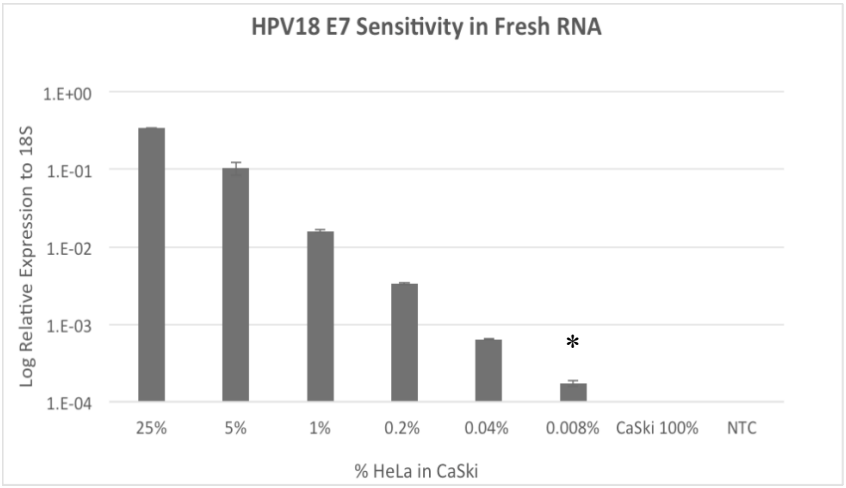

Figure IV.2

A

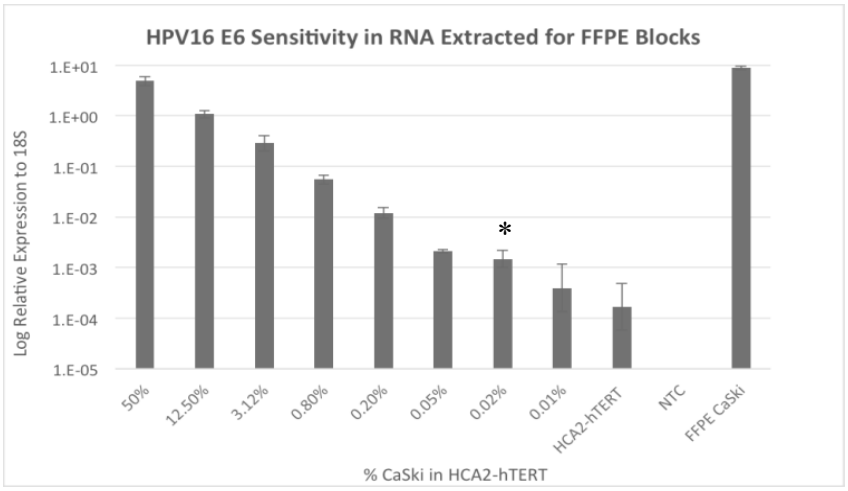

B

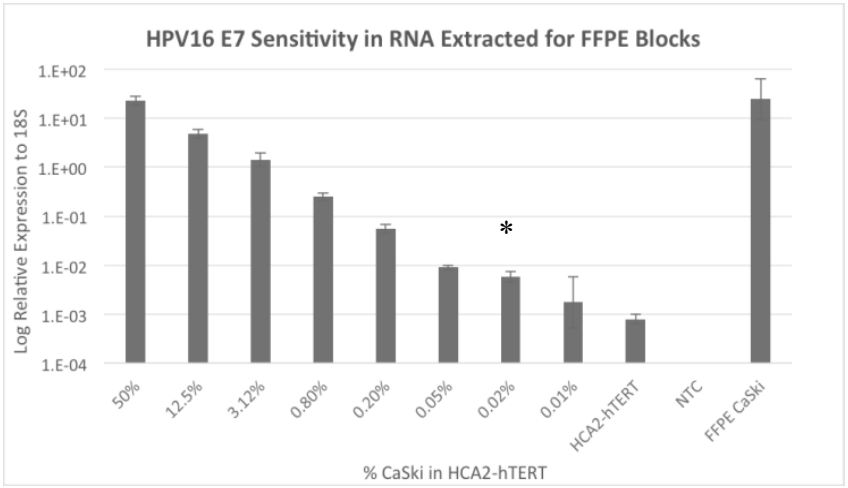

C

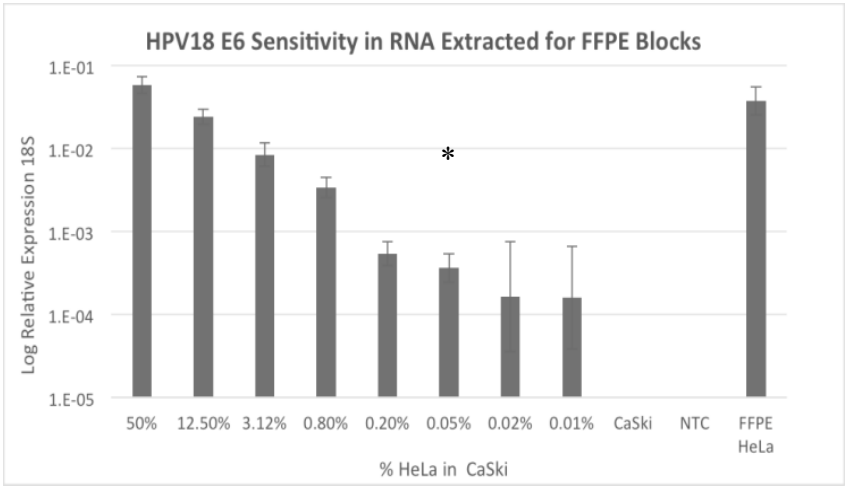

D

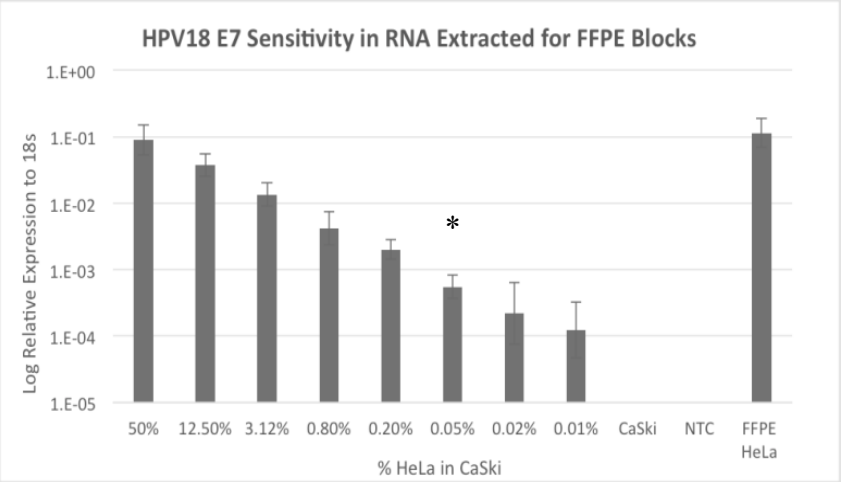

Figure IV.3

A

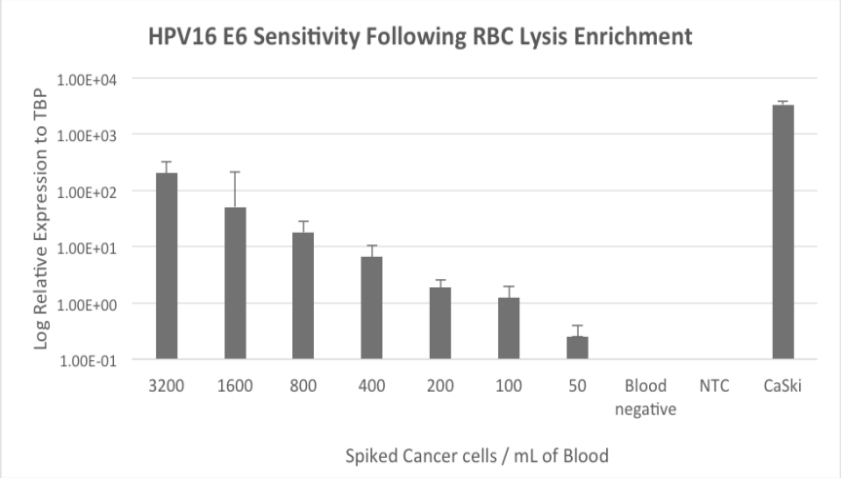

B

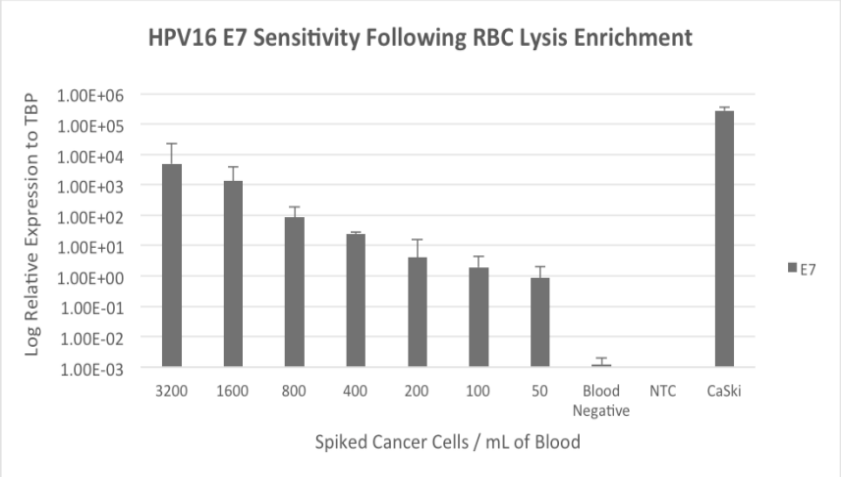

C

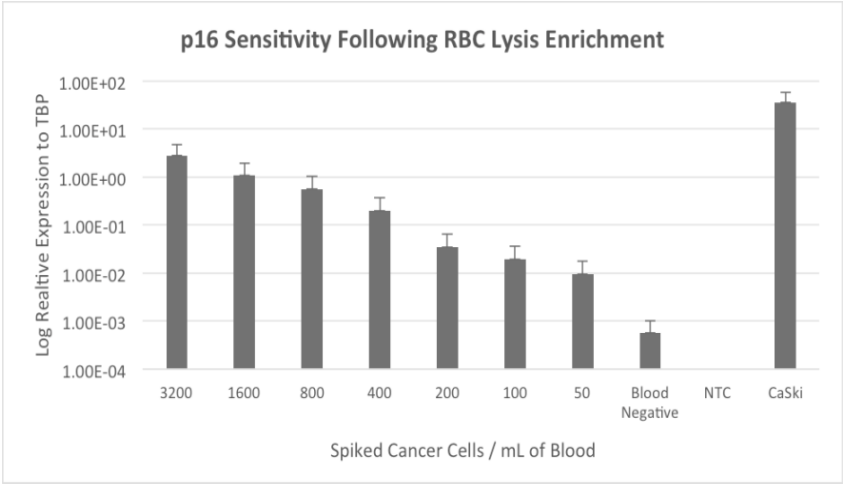

D

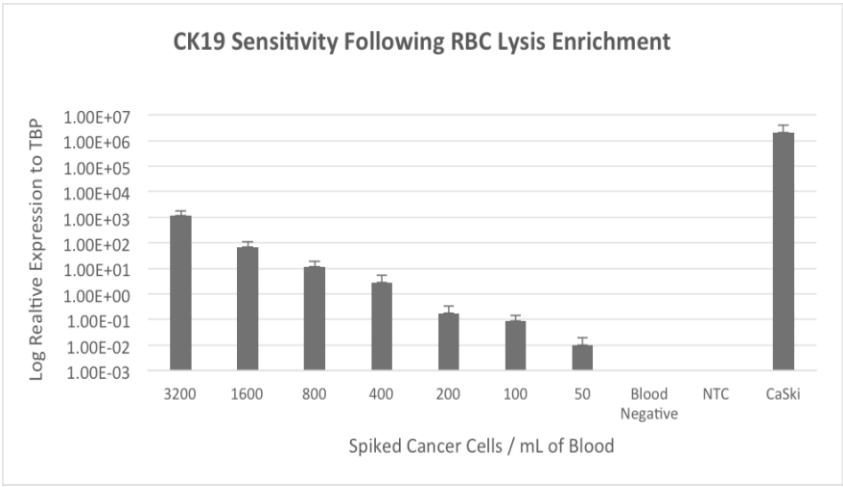

Figure IV.4

A

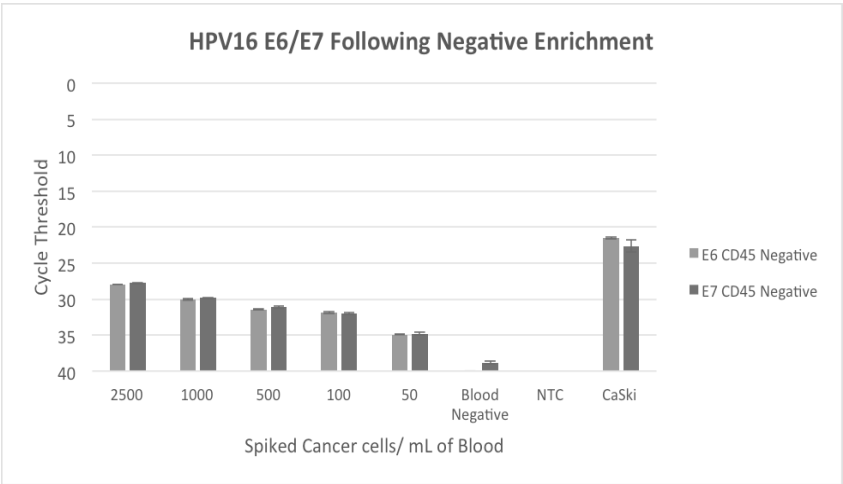

B

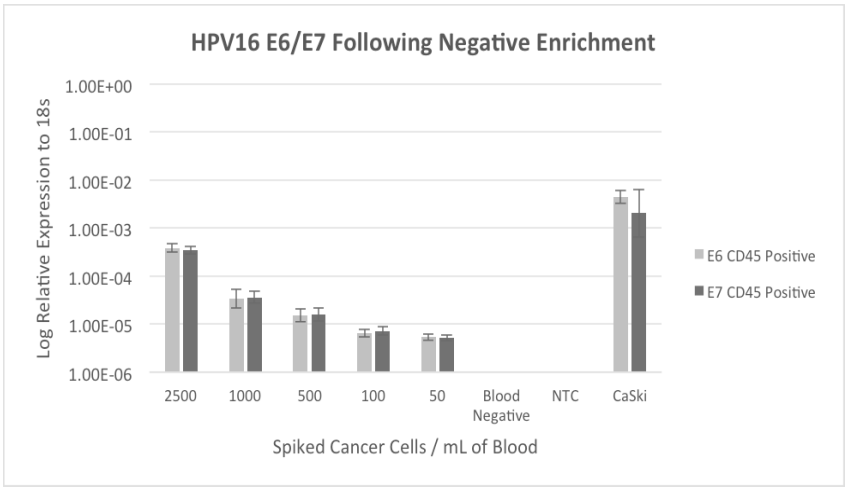

Figure IV.5

A

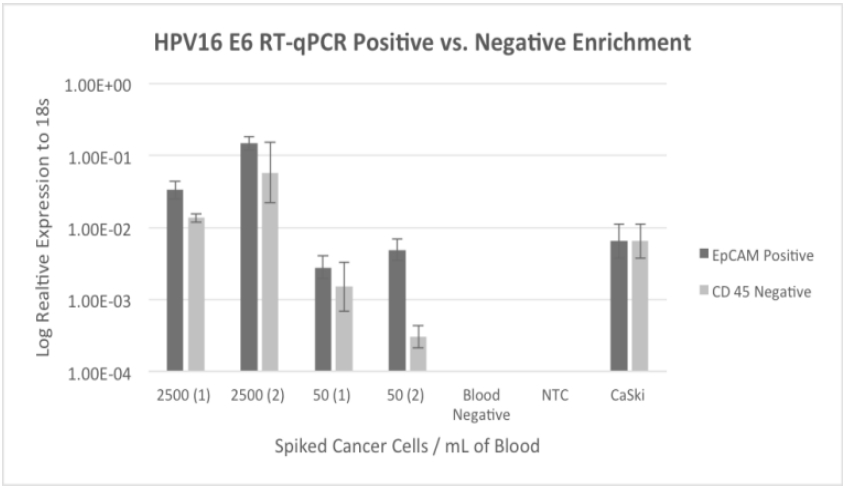

B

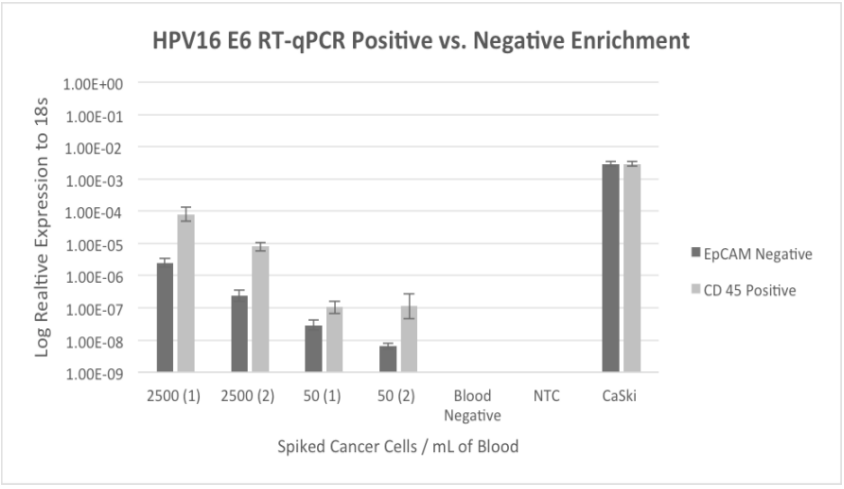

C

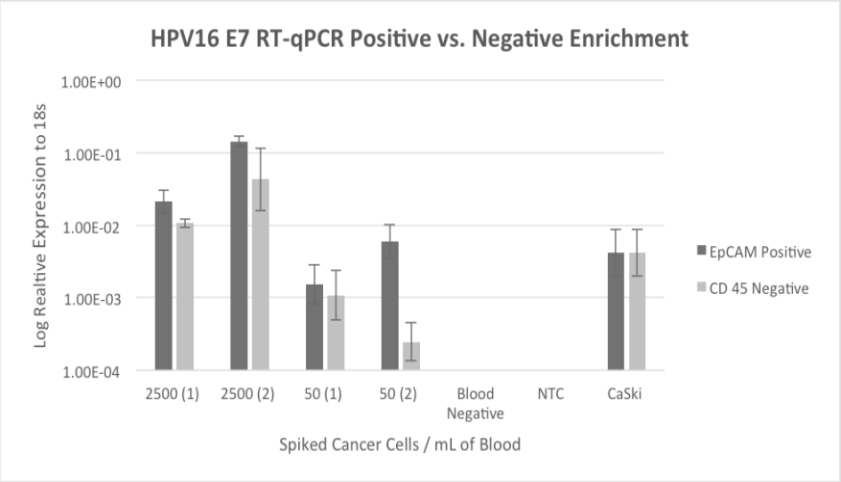
HPV16 E7 RT-qPCR Positive vs. Negative Enrichment
Log Realtive Expression to 18s
1.00E+00
1.00E-01
1.00E-02
1.00E-03
1.00E-04
2500 (1)
2500 (2)
50 (1)
50 (2)
Blood Negative
NTC
CaSki
Spiked Cancer Cells / mL of Blood
EpCAM Positive
CD 45 Negative

D

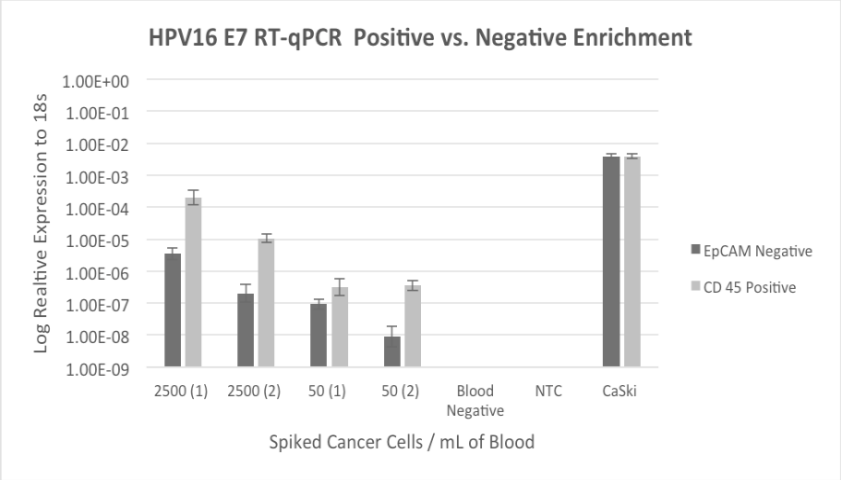
HPV16 E7 RT-qPCR Positive vs. Negative Enrichment
Log Realtive Expression to 18s
1.00E+00
1.00E-01
1.00E-02
1.00E-03
1.00E-04
1.00E-05
1.00E-06
1.00E-07
1.00E-08
1.00E-09
2500 (1)
2500 (2)
50 (1)
50 (2)
Blood Negative
NTC
CaSki
Spiked Cancer Cells / mL of Blood
EpCAM Negative
CD 45 Positive

Table IV-I

Genes	Sequence (5'-3')	Location	Product size (bp)
18s Forward Reverse Probe	 CGGCTACCACATCCAAGGAA CGCTATTGGAGCTGGAATTA TGCTGGCACCAGACTTGCCCTC	450-646	197
CK-19 Forward Reverse Probe	 TCGACAACGCCCGTCTG CCACGCTCATGCGCAG CCTGTTCCGTCTCAAACTTGGTTCGG	606-680	75
HPV16 E6 Forward Reverse Probe	 AATGTTTCAGGACCCACAGG CTCACGTCGCAGTAACTGTTG AGCGACCCAGAAAGTTACCACAGTTATG	103-226	124
HPV16 E7 Forward Reverse Probe	 CAAGCAGAACCGGACAGA GTCTACGTGTGTGCTTTGTA CAAGTGTGACTCTACGCTTCGGTTGTG	691-786	96
HPV18 E6 Forward Reverse Probe	 AACACGGCGACCCTACAA CTGTCTCTATACACCACAATAATC CGGAACTGAACACTTCACTGCAAGACATA	125-280	156
HPV18 E7 Forward Reverse Probe	 AGCGACTCAGAGGAAGAAA CGTCTGCTGAGCTTTCTACTAC CTCAATTCTGGCTTCACACTTACAACACA	683-833	151
P16 ^{INK4A} Forward Reverse Probe	 CTGCCCAACGCACCGAATA GCGCTGCCCATCATCATGA CTGGATCGGCCTCCGACCGTA	415-476	62
TBP Forward Reverse Probe	 ACAGGAGCCAAGAGTGAA AAACCCAACTTCTGTACAAC ACAGTCCAGACTGGCAGCAAGAAAATA	743-816	74

Table IV-II

	Size	Volume	Percentage of tumor occupying a 1 cm LN
Normal lymph Node	1 cm	523.6 mm^3	N/A
Macrometastasis	>2 mm	>4.2 mm^3	> 0.8%
Micrometastasis Upper limit Lower limit	 2 mm 0.2 mm	 4.2 mm^3 0.00418 mm^3	 0.8% 0.008%
ITC	≤ 0.2 mm	≤ 0.00418 mm^3	≤ 0.008%

Table IV-III

Detection limit in fresh tissue		
	E6	E7
HPV16	0.008%	0.008%
HPV18	0.008%	0.008%

Table IV-IV

Detection limit in FFPE		
	E6	E7
HPV16	0.02%	0.02%
HPV18	0.05%	0.05%

BIBLIOGRAPHY

1. Incidence/mortality data. Ferlay J, S.I., Ervik M, Dikshit R, Eser S, Mathers C, Rebelo M, Parkin DM, Forman D, Bray, F. GLOBOCAN 2012 v1.0, Cancer Incidence and Mortality Worldwide: IARC CancerBase No. 11 [Internet]. Lyon, France: International Agency for Research on Cancer; 2013. Available from: http://globocan.iarc.fr.
2. Walboomers, J.M., et al., *Human papillomavirus is a necessary cause of invasive cervical cancer worldwide.* J Pathol, 1999. **189**(1): p. 12-9.
3. Hawley-Nelson, P., et al., *HPV16 E6 and E7 proteins cooperate to immortalize human foreskin keratinocytes.* EMBO J, 1989. **8**(12): p. 3905-10.
4. Munger, K., et al., *The E6 and E7 genes of the human papillomavirus type 16 together are necessary and sufficient for transformation of primary human keratinocytes.* J Virol, 1989. **63**(10): p. 4417-21.
5. Munger, K. and P.M. Howley, *Human papillomavirus immortalization and transformation functions.* Virus Res, 2002. **89**(2): p. 213-28.
6. zur Hausen, H., *Papillomaviruses and cancer: from basic studies to clinical application.* Nat Rev Cancer, 2002. **2**(5): p. 342-50.
7. Khleif, S.N., et al., *Inhibition of cyclin D-CDK4/CDK6 activity is associated with an E2F-mediated induction of cyclin kinase inhibitor activity.* Proc Natl Acad Sci U S A, 1996. **93**(9): p. 4350-4.
8. Kiyono, T., et al., *Both Rb/p16INK4a inactivation and telomerase activity are required to immortalize human epithelial cells.* Nature, 1998. **396**(6706): p. 84-8.
9. Vande Pol, S.B. and A.J. Klingelhutz, *Papillomavirus E6 oncoproteins.* Virology, 2013. **445**(1-2): p. 115-37.
10. Roman, A. and K. Munger, *The papillomavirus E7 proteins.* Virology, 2013. **445**(1-2): p. 138-68.
11. Desaintes, C., et al., *Expression of the papillomavirus E2 protein in HeLa cells leads to apoptosis.* EMBO J, 1997. **16**(3): p. 504-14.
12. Hu, G., et al., *Suppression of tumorigenesis by transcription units expressing the antisense E6 and E7 messenger RNA (mRNA) for the transforming proteins of the human papilloma virus and the sense mRNA for the retinoblastoma gene in cervical carcinoma cells.* Cancer Gene Ther, 1995. **2**(1): p. 19-32.
13. Hwang, E.S., et al., *Inhibition of cervical carcinoma cell line proliferation by the introduction of a bovine papillomavirus regulatory gene.* J Virol, 1993. **67**(7): p. 3720-9.
14. Wells, S.I., et al., *Papillomavirus E2 induces senescence in HPV-positive cells via pRB- and p21(CIP)-dependent pathways.* EMBO J, 2000. **19**(21): p. 5762-71.
15. Wu, L., et al., *E2F-Rb complexes assemble and inhibit cdc25A transcription in cervical carcinoma cells following repression of human papillomavirus oncogene expression.* Mol Cell Biol, 2000. **20**(19): p. 7059-67.
16. von Knebel Doeberitz, M., et al., *Inhibition of tumorigenicity of cervical cancer cells in nude mice by HPV E6-E7 anti-sense RNA.* Int J Cancer, 1992. **51**(5): p. 831-4.
17. Landoni, F., et al., *Randomised study of radical surgery versus radiotherapy for stage Ib-IIa cervical cancer.* Lancet, 1997. **350**(9077): p. 535-40.
18. Delgado, G., et al., *Prospective surgical-pathological study of disease-free interval in patients with stage IB squamous cell carcinoma of the cervix: a Gynecologic Oncology Group study.* Gynecol Oncol, 1990. **38**(3): p. 352-7.
19. Yuan, C., et al., *Recurrence and survival analyses of 1,115 cervical cancer patients treated with radical hysterectomy.* Gynecol Obstet Invest, 1999. **47**(2): p. 127-32.

20. Benedetti-Panici, P., et al., *Lymphatic spread of cervical cancer: an anatomical and pathological study based on 225 radical hysterectomies with systematic pelvic and aortic lymphadenectomy.* Gynecol Oncol, 1996. **62**(1): p. 19-24.
21. Selman, T.J., et al., *Diagnostic accuracy of tests for lymph node status in primary cervical cancer: a systematic review and meta-analysis.* CMAJ, 2008. **178**(7): p. 855-62.
22. Sironi, S., et al., *Lymph node metastasis in patients with clinical early-stage cervical cancer: detection with integrated FDG PET/CT.* Radiology, 2006. **238**(1): p. 272-9.
23. Cote, R.J., et al., *Role of immunohistochemical detection of lymph-node metastases in management of breast cancer. International Breast Cancer Study Group.* Lancet, 1999. **354**(9182): p. 896-900.
24. Horn, L.C., et al., *Detection of micrometastases in pelvic lymph nodes in patients with carcinoma of the cervix uteri using step sectioning: Frequency, topographic distribution and prognostic impact.* Gynecol Oncol, 2008. **111**(2): p. 276-81.
25. Hermanek, P., et al., *International Union Against Cancer. Classification of isolated tumor cells and micrometastasis.* Cancer, 1999. **86**(12): p. 2668-73.
26. Schwartz, G.F., et al., *Proceeding of the consensus conference of the role of sentinel lymph node biopsy in carcinoma or the breast April 19-22, 2001, Philadelphia, PA, USA.* Breast J, 2002. **8**(3): p. 124-38.
27. Darai, E., et al., *Sentinel lymph node biopsy in gynaecological cancers: the importance of micrometastases in cervical cancer.* Surg Oncol, 2008. **17**(3): p. 227-35.
28. Cibula, D., et al., *Prognostic significance of low volume sentinel lymph node disease in early-stage cervical cancer.* Gynecol Oncol, 2012. **124**(3): p. 496-501.
29. Euscher, E.D., et al., *Ultrastaging improves detection of metastases in sentinel lymph nodes of uterine cervix squamous cell carcinoma.* Am J Surg Pathol, 2008. **32**(9): p. 1336-43.
30. Cormier, B., et al., *Establishing a sentinel lymph node mapping algorithm for the treatment of early cervical cancer.* Gynecol Oncol, 2011. **122**(2): p. 275-80.
31. Balega, J. and P.O. Van Trappen, *The sentinel node in gynaecological malignancies.* Cancer Imaging, 2006. **6**: p. 7-15.
32. Gortzak-Uzan, L., et al., *Sentinel lymph node biopsy vs. pelvic lymphadenectomy in early stage cervical cancer: is it time to change the gold standard?* Gynecol Oncol, 2010. **116**(1): p. 28-32.
33. Eiriksson, L.R. and A. Covens, *Sentinel lymph node mapping in cervical cancer: the future?* BJOG, 2012. **119**(2): p. 129-33.
34. Plante, M., et al., *Laparoscopic sentinel node mapping in early-stage cervical cancer.* Gynecol Oncol, 2003. **91**(3): p. 494-503.
35. Zarganis, P., et al., *The sentinel node in cervical cancer patients: role of tumor size and invasion of lymphatic vascular space.* In Vivo, 2009. **23**(3): p. 469-73.
36. Altgassen, C., et al., *Multicenter validation study of the sentinel lymph node concept in cervical cancer: AGO Study Group.* J Clin Oncol, 2008. **26**(18): p. 2943-51.
37. Diaz, J.P., et al., *Sentinel lymph node biopsy in the management of early-stage cervical carcinoma.* Gynecol Oncol, 2011. **120**(3): p. 347-52.
38. Cibula, D., et al., *Bilateral ultrastaging of sentinel lymph node in cervical cancer: Lowering the false-negative rate and improving the detection of micrometastasis.* Gynecol Oncol, 2012. **127**(3): p. 462-6.
39. Van Trappen, P.O., et al., *Molecular quantification and mapping of lymph-node micrometastases in cervical cancer.* Lancet, 2001. **357**(9249): p. 15-20.
40. Tsujimoto, M., et al., *One-step nucleic acid amplification for intraoperative detection of lymph node metastasis in breast cancer patients.* Clin Cancer Res, 2007. **13**(16): p. 4807-16.
41. Tanis, P.J., et al., *Frozen section investigation of the sentinel node in malignant melanoma and breast cancer.* Ann Surg Oncol, 2001. **8**(3): p. 222-6.

42. Slama, J., et al., *High false negative rate of frozen section examination of sentinel lymph nodes in patients with cervical cancer.* Gynecol Oncol, 2013. **129**(2): p. 384-8.
43. Fader, A.N., et al., *Sentinel lymph node biopsy in early-stage cervical cancer: utility of intraoperative versus postoperative assessment.* Gynecol Oncol, 2008. **111**(1): p. 13-7.
44. Bats, A.S., et al., *Diagnostic value of intraoperative examination of sentinel lymph node in early cervical cancer: a prospective, multicenter study.* Gynecol Oncol, 2011. **123**(2): p. 230-5.
45. Pao, C.C., et al., *Detection of human papillomavirus mRNA and cervical cancer cells in peripheral blood of cervical cancer patients with metastasis.* J Clin Oncol, 1997. **15**(3): p. 1008-12.
46. Tseng, C.J., et al., *Detection of human papillomavirus types 16 and 18 mRNA in peripheral blood of advanced cervical cancer patients and its association with prognosis.* J Clin Oncol, 1999. **17**(5): p. 1391-6.
47. Wentzensen, N., S. Vinokurova, and M.v.K. Doeberitz, *Systematic Review of Genomic Integration Sites of Human Papillomavirus Genomes in Epithelial Dysplasia and Invasive Cancer of the Female Lower Genital Tract.* Cancer Research, 2004. **64**(11): p. 3878-3884.
48. Pater, M.M. and A. Pater, *Human papillomavirus types 16 and 18 sequences in carcinoma cell lines of the cervix.* Virology, 1985. **145**(2): p. 313-8.
49. Yee, C., et al., *Presence and expression of human papillomavirus sequences in human cervical carcinoma cell lines.* Am J Pathol, 1985. **119**(3): p. 361-6.
50. Torabi, M., S.L. Aquino, and M.G. Harisinghani, *Current concepts in lymph node imaging.* J Nucl Med, 2004. **45**(9): p. 1509-18.
51. Liu, Y., et al., *Expression of p16(INK4a) in peripheral blood T-cells is a biomarker of human aging.* Aging Cell, 2009. **8**(4): p. 439-48.
52. Gusterson, B.A., et al., *Occult axillary lymph-node micrometastases in breast cancer.* The Lancet, 1990. **336**(8712): p. 434-435.
53. Srinivasan, M., D. Sedmak, and S. Jewell, *Effect of fixatives and tissue processing on the content and integrity of nucleic acids.* The American journal of pathology, 2002. **161**(6): p. 1961-1971.
54. van de Stolpe, A., et al., *Circulating tumor cell isolation and diagnostics: toward routine clinical use.* Cancer Res, 2011. **71**(18): p. 5955-60.
55. Burchill, S.A., et al., *Detection of epithelial cancer cells in peripheral blood by reverse transcriptase-polymerase chain reaction.* Br J Cancer, 1995. **71**(2): p. 278-81.
56. Stathopoulou, A., et al., *Real-Time Quantification of CK-19 mRNA-Positive Cells in Peripheral Blood of Breast Cancer Patients Using the Lightcycler System.* Clinical Cancer Research, 2003. **9**(14): p. 5145-5151.
57. Weismann, P., et al., *The detection of circulating tumor cells expressing E6/E7 HR-HPV oncogenes in peripheral blood in cervical cancer patients after radical hysterectomy.* Neoplasma, 2009. **56**(3): p. 230-8.
58. Pfitzner, C., et al., *Digital-Direct-RT-PCR: a sensitive and specific method for quantification of CTC in patients with cervical carcinoma.* Sci Rep, 2014. **4**: p. 3970.
59. Yuan, C.C., et al., *Detecting cytokeratin 19 mRNA in the peripheral blood cells of cervical cancer patients and its clinical-pathological correlation.* Gynecol Oncol, 2002. **85**(1): p. 148-53.

CHAPTER V : RESULTS FROM UTERINE CERVICAL CANCER PATIENTS

After we successfully demonstrated the ability of E6/E7, CK19 and $P16^{INK4A}$ in detecting spiked CaSki cell line and their detection limit using qRT-PCR, we sought to evaluate these molecular biomarkers to detect CTC in uterine cervical patients RNA extracted from non-magnetically enriched PBMC. Ten patients with HPV16-positive uterine cervical tumor were recruited. The median patient age was 52 years at diagnosis [range 31–72]. Nine patients had squamous cell carcinoma, whereas one had adenocarcinoma. Five patients were stage IB, four were stage II, and one patient was stage 1A-1. Co-infection with multiple HPV types was detected in 50% of the patients. HPV35, 39, 52 and 58 are oncogenic types, while the others were considered low risk HPV types (Table V-1). None of the patients was tested positive for HPV18.

Table V-I. Clinical characteristics of UCC patients.

Age	52 years (median)
Histology	
Squamous carcinoma	9
Adenocarcinoma	1
Stage	
1A1	1
1B	
IB1	2
IB 2	3
II	
IIA	2
IIB	2
HPV type	
HPV16	10
Multiple co-infection	5
Total number	10

None of the patients had detectable E6 and E7 oncogenes expression in their enriched PBMC (Figure V-1).

CK19 expression was undetectable in all control samples with the exception of CAm35 and was extremely low compared to the CaSki cell line. In comparison, substantial CK19 expression was detected in patients 5 and 27 all of which had stage II disease. CK19 transcripts were also detectable in patients 14 with stage IIA, patient 21 with stage IB-2 and patient 22 with stage IIA. However, these expression levels were similar to healthy volunteers. CK19 transcript was not detectable in patient ID 8, 35, 32, 33 and 37 (Figure V-2).

$P16^{INK4A}$ transcripts were detectable at similar level across patients and control samples except patient ID 37 that had significantly higher expression level. However, the endogenous control of patient ID 37 had cycle threshold at 33.2 compared to 29 for other samples that explain the higher relative expression compared to the control samples (Figure V-3).

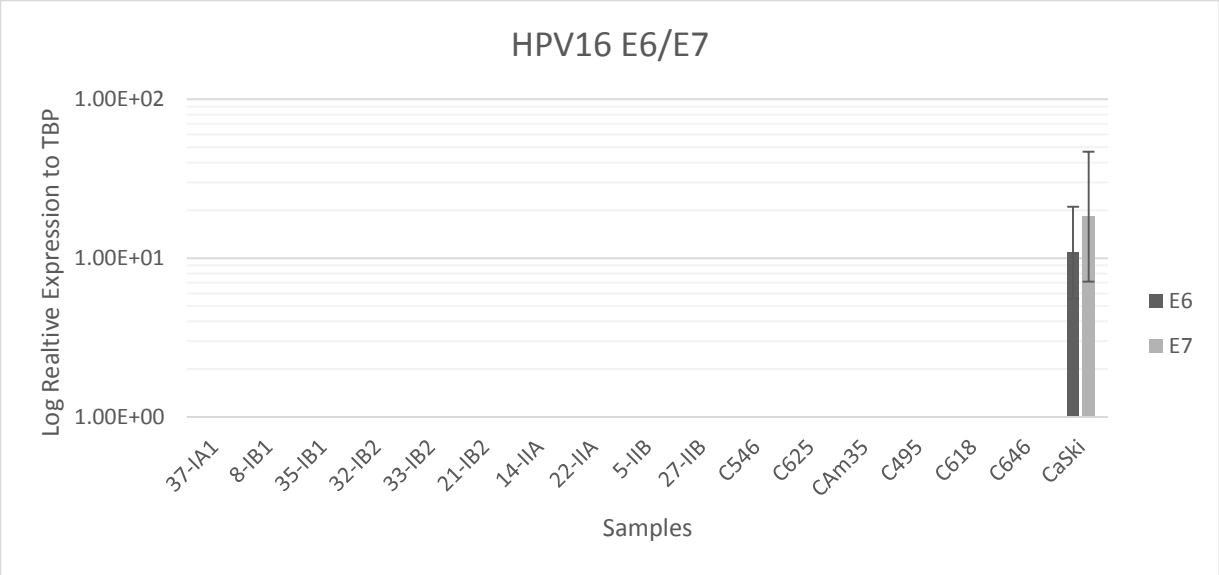

Figure V.1. qRT-PCR of HPV16 E6/E7 in PBMC enriched from UCC patients. Multiplex E6 and E7 qRT-PCR was performed in RNA extracted from non-magnetically enriched PBMC of uterine cervical patients by RBC lysis (except patient ID 8 and 5 in which Ficoll used to enrich PBMC). Sample IDs starting with the letter (C) collected from healthy female served as negative controls, while HPV16-positive CaSki cells served as a positive control. The y-axis denotes the log relative expression to TBP.

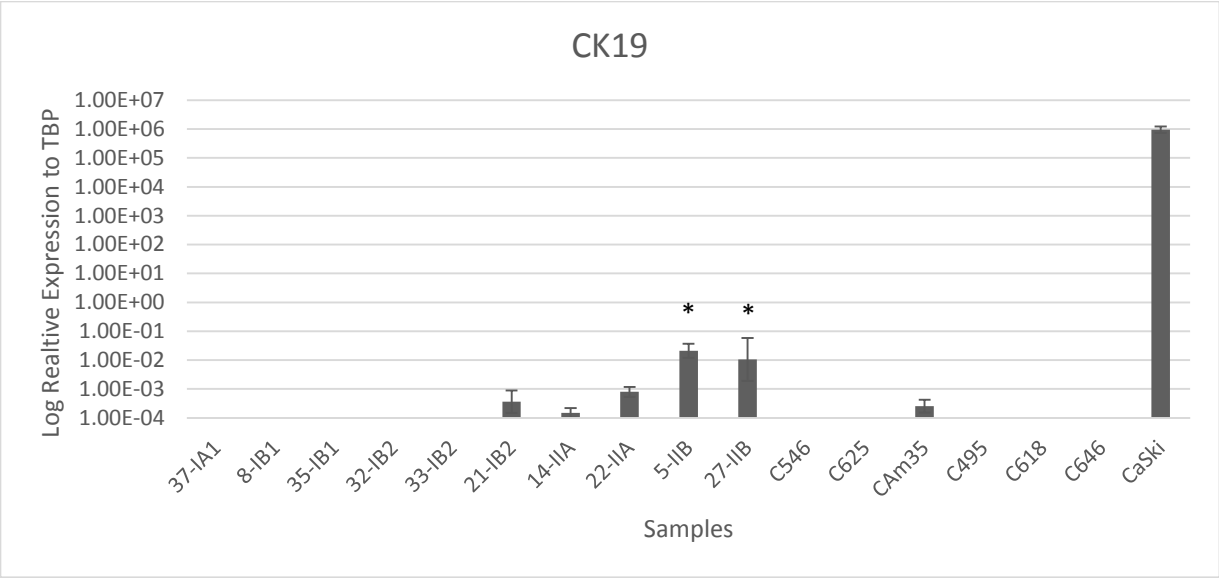

Figure V.2. qRT-PCR of CK19 in PBMC enriched from UCC patients. Multiplex CK19 qRT-PCR was performed in RNA extracted from non-magnetically enriched PBMC of uterine cervical patients by RBC lysis (except patient ID 8 and 5 in which Ficoll used to enrich PBMC). Sample IDs starting with the letter (C) collected from healthy female served as negative controls, while HPV16-positive CaSki cells served as a positive control. The y-axis denotes the log relative expression to TBP. ($p < 0.02$)

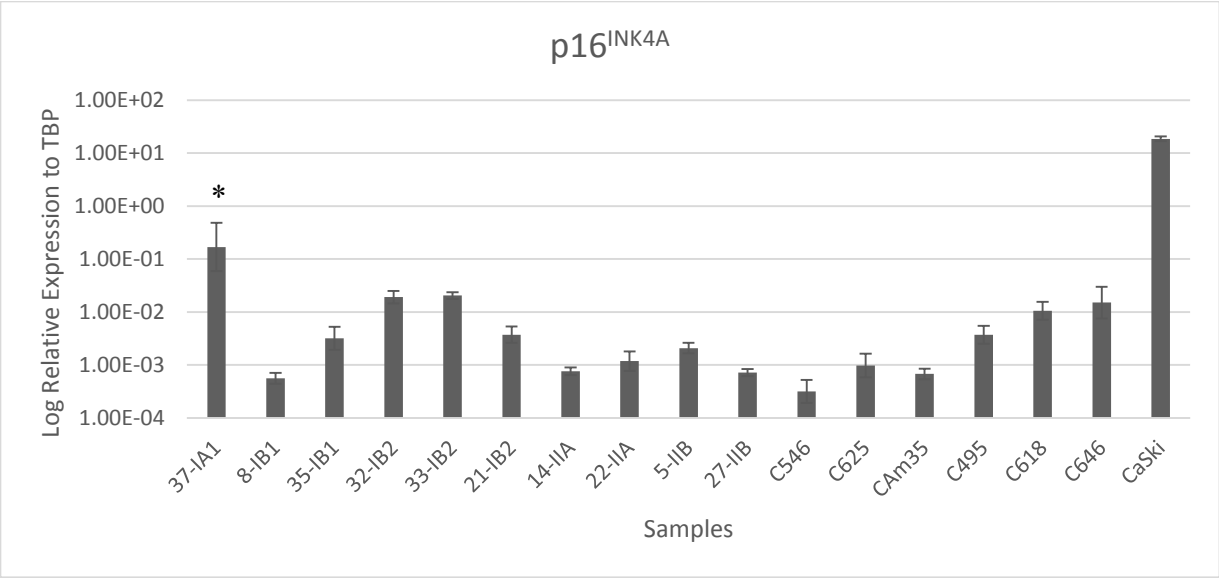

Figure V.3. p16^{INK4A} qRT-PCR analysis in PBMC enriched from UCC patients. Multiplexed qRT-PCR analysis for p16^{INK4A} was performed in RNA extracted from non-magnetically enriched PBMCs from UCC patients by RBC lysis (except patient ID 8 and 5 in which Ficoll used to enrich PBMC). Sample IDs starting with the letter (C) collected from healthy females and HPV16-positive CaSki cells served as negative and positive controls, respectively. The y-axis represents log relative expression to TBP endogenous control.

CHAPTER VI : DISCUSSION

CTCs enrichment techniques

1) Ficoll density enrichment

Several techniques are available to enrich CTCs, with density separation and RBC lysis being the most common. Ficoll-Paque density gradients are widely used to enrich CTCs based on cellular density. The technique has an average recovery of only 70% due to cell loss during the process [190]. Our results are consistent with those previously published: cell loss is attributed to multiple washes, attachment to granulocytes and RBCs, and the wide variation in tumor cell density [26]. The detection limit of Ficoll-Paque enrichment with consistent reproducibility was 1,000 cells/mL of blood with subsequent detection with qRT-PCR for HPV16 oncogenes expression, and exhibited an average recovery of 50%.

In comparison, OncoQuick is a density medium that uses a porous barrier to prevent the PBMC interphase from mixing with granulocytes and RBC after centrifugation, whereas the FDA-approved CellSearch system using αEpCAM-conjugated nanoparticles to detect CTCs. These technologies identified CTCs in 23% and 54% of patients, respectively, with CellSearch recovering a greater percentage of targeted cells [191].

2) RBC lysis

To improve sensitivity and increase the recovery rates for our analysis, we used RBC lysis buffer independently or in cooperation with other enrichment methods. ACK buffer specifically lyses RBCs and leaves nucleated cells intact. The recovery rate is greater than 90% with a minimal effect on cell viability and cell surface antibody interaction [190].

We found a detection limit of 50 CTCs/mL of blood following ACK lysis buffer enrichment. Isolated RNA had an A260/280 $\geq$ 1.8, demonstrating an adequate concentration and quality. Moreover, RNA integrity was verified by electrophoresis using Agilent Bioanalyzer and demonstrated intact 18S and 28S bands with no RNA disintegration. Furthermore, processing time and variation is minimized compared to Ficoll-Paque.

3) Positive and negative enrichment

To further enhance the sensitivity of the PCR and reduce the false positive rate as result of high background from PBMCs, we sought to determine the value of positive and negative enrichment.

Positive enrichment of cancer cells was based on EpCAM expression, an epithelial cell surface marker expressed by most cancers of epithelial cell origin [192]. The sensitivity of PCR in the detection of E6 and E7 improved when either positive or negative enrichment combined with RBC lysis as result of eliminating most of the PBMC-derived RNA.

Positive enrichment yielded a highly purified cell fraction providing for gene expression profiling and the elimination of false positives. Disadvantages of positive enrichment include the inability to detect cancer cells of non-epithelial origin and those that have lost EpCAM expression during the process of EMT [35, 41-46], the latter of which might explain the detection of E6 and E7 in the supernatant fraction.

Negative enrichment was based on the CD45-mediated depletion of macrophages, monocytes and lymphocytes. This technique isolated cancer cells regardless of their surface cell markers; however, we were able to detect E6 and E7 in the CD45-positive fraction. It has been demonstrated previously that most CTCs within the blood are either engulfed by macrophages or non-specific binding of anti-CD45 antibodies to Fc receptors, thus explaining the detection of HPV oncogenes expression in this fraction [27-30].

CTCs detection

1) Flow cytometry

Advances in flow cytometry have permitted the analysis of thousand particles in a short time and is currently used for cell sorting, counting, and biomarker detection [193]. Fluorescence-activated cell sorting (FACS) sorts cells based on their fluorescence following immunofluorescent labeling. For our studies, we used the CaSki cells tagged with GFP in order to differentiate them from normal PBMCs. The detection limit was 10^3-10^4 cells and 5,000 cells/mL of blood following enrichment with Ficoll and RBC lysis buffer, respectively, when analyzed by single parameter flow cytometry. However, GFP is not normally expressed in human cancer cells. The sensitivity of flow cytometry can be improved with the use of multi-parameter immunofluorescent labeling for multiple markers simultaneously. Hu et al. reported a sensitivity of one CTC per 100,000 normal cells in breast cancer [67].

However, this platform lacks the sensitivity to isolate rare cells, requires a lengthy time for staining, necessitates the removal of RBCs, and samples must be analyzed on expensive

equipment [68]. Moreover, the identification of unpurified viable CTCs is less conducive to further molecular and biological characterization [19].

2) Detection using molecular biomarkers in experimental spiking model

a) HPV viral oncogenes

The E6 and E7 oncogenes of HPV are constitutively expressed by most uterine cervical cancer cells to maintain malignant phenotype [118-123]. Moreover, these markers are not expressed by normal cell types, making them ideal markers for detecting CTCs in UCC.

In an experimental spiking model, the sensitivity of PCR in detecting spiked CaSki cells following RBC lysis was 50 cells/mL with the ability to detect 1 cell/mL of blood based on the difference between the relative expressions of the lowest spiked cells and the negative control samples. Specifically, the X cycle threshold difference between the positive and the negative signals can be directly interpreted to a value of Y (log2 of Y) and used to be divided by 50 cells/mL to obtain a value of Z, which equal to one cell/mL.

Using Ficoll density separation, the detection limit was 1,000 spiked cells/mL of blood. Below that level, detection was not consistently reproducible. None of the control subjects exhibited E6 and E7 expression.

The sensitivity of PCR in detecting circulating tumor cells based on E6 and E7 oncogenes expression is one cell in the background of 10^6 cells [159].

b) Cytokeratin 19

Cytokeratin (CK) is an intermediate filament protein that participates in the formation of the cellular cytoskeleton. It is expressed only by epithelial cell types and is usually maintained during malignant transformation [173, 174]. Detection of CK19 in either blood or lymph nodes provides indirect evidence for the presence of cancer cells.

In an experimental spiking model, the sensitivity of PCR for spiked CaSki cells following RBC lysis was 50 cells/mL with the ability to detect 1 cell/mL of blood based on the difference between the relative expressions of the lowest spiked cells and the control samples. Specifically, the X cycle threshold difference between the positive and the negative signals can be directly interpreted to a value of Y (log2 of Y) and used to be divided by 50 cells/mL to obtain a value of Z, which equal to one cell/mL. However, CK19 expression is not tumor-specific and was detectable in control subjects. It was previously determined that CK19

transcripts can be detected in ≤20% of normal healthy individuals and/or those with benign disease [26]. Moreover, CK19 pseudogenes have been identified and could result in false positives [194, 195]. The primers used in our CK19 analyses were constructed to avoid detection of these pseudogenes.

We postulate that if an appropriate cutoff median expression value is established for a normal expression level, then this marker may be used for CTC detection. Using RT-PCR with established cutoff value to detect CK19 transcript in breast cancer patients, 2.2% of healthy females were positive compared to 31% and 40% of those with early and metastatic breast cancer, respectively. Moreover, the CK19 expression levels were significantly higher in breast cancer patient compared to those in the control group [196].

The sensitivity of PCR in detecting CTCs based on CK19 is one cell in the background of 10^6 cells [163].

c) P16^{INK4A}

$P16^{INK4A}$ is cyclin dependent kinase (CDK) inhibitor that functions as tumor suppressor in the transition from G1/S phase. It binds CDKs and inhibits the phosphorylation of Rb to prevent the release of the E2F transcription factors [181, 182]. $P16^{INK4A}$ is indirectly overexpressed in cervical cancer as result of functional inactivation of Rb by the oncoprotein E7 and can be used as molecular biomarker for diagnosis [183].

In experimental spiking model, the sensitivity of PCR in detecting spiked CaSki cells following RBC lysis was 50 cells/mL with the ability to detect 1 cell/mL of blood based on the difference between the relative expressions at the lowest spiked sample and control samples. Specifically, the X cycle threshold difference between the positive and the negative signals can be directly interpreted to a value of Y (log2 of Y) and used to be divided by 50 cells/mL to obtain a value of Z, which equal to one cell/mL.

However, the marker is non-tumor specific and expression level increases in healthy individual with age and smoking [197-199]. The expression of $p16^{INK4A}$ is usually very low compared to cancer cell lines and, if appropriate cutoff median value is established, may be useful for the detection of CTCs.

3) Detection of CTCs in uterine cervical patients

UCC tumor bank has been developed during laboratory experimentation to optimize detection techniques. Ficoll-Paque was used to enrich PBMC from the first six patients. As we determined that RBC lysis buffer was more sensitive than Ficoll-Paque for enriching tumor cells, and was used to process blood samples collected from future patients. Those whose primary tumors tested positive for HPV16 at the time of the diagnosis were subjected to qRT-PCR to detect CTCs. No patients with advanced-stage UCC had been recruited at the time this study was conducted.

Six patients were at stage I and four patients had stage II disease. None of these patients tested positive for E6 or E7 transcripts in the blood. Those patients had early stage disease, which explain the negative result. Pao et al. used nested RT-PCR to detect E6 oncogene expression in the blood of 12/13 patients with metastatic UCC. In follow up by the same group, they were also able to detect HPV16/18 E6 transcript in 51% (18/35) of locally advanced stage disease. Fourteen patients were stage IIB and, of those, 42% were positive. However, one of the primers used in the first round of nested PCR and one in the second round could detect genomic HPV DNA. HPV DNA has been detected in the peripheral blood in 12-24% of patients with invasive UCC and 1.8% in patients with high-grade cervical lesions [200-203]. Detection of HPV DNA in the circulation can be result of shedding early apoptotic or necrotic tumor cells into the circulation and tumor cell engulfment by macrophages [204-206]. Using DD-RT-PCR with primers similar to those used in this experiment, 3/10 patients with recurrent disease were positive for E6 expression in their blood [162]. Two patients with distant metastasis had the highest CTC count. DD-RT-PCR demonstrated a sensitivity of 1 CTC for every 500,000 PBMCs, and a sensitivity of 5 CTCs/mL of blood. The number of PBMC background drastically affected the sensitivity of the PCR. In our study, PBMCs were enriched with RBC lysis and subjected to qRT-PCR. However, we did not take into consideration the number of PBMCs, which could explain our negative result. An experimental spiking compared RBC lysis, standard Ficoll centrifugation, and modified gradient Ficoll centrifugation combined with immunomagnetic positive enrichment targeting EpCAM in detecting E6 and E7 using nested RT-PCR. In contrast to our finding, the latter was found to be the most sensitive with ability to detect 3.33 cells/mL of blood with consistent reproducibility compared to 13.3 and 5.33 cells/mL for the former studies, respectively [161]. However, the addition of immunomagnetic

separation is factor that improved PCR sensitivity by eliminating the PBMC-derived RNA. The centrifugation force used to collect cells in RBC lysis protocol was 3000*g* compared to 1800*g* used in the other protocols, which could have resulted in cell membrane damage and RNA disintegration as result of RNase released from lysed RBCs. Moreover, the quantity of RNA used to synthesize the cDNA was based on volume rather than a known measured quantity. The sensitivity of PCR was inversely related to the amount of cDNA that was introduced into the reaction. Using the modified protocol combined with EpCAM positive enrichment, 3/13 patients with UCC were positive for E6/E7 expression. Two patients had stage IB and were positive for HPV16 E6/7 and the third patient had stage IIIA and was positive for HPV35 E6/E7. The remaining negative patients were of stage I disease and three of them had lymph node metastasis. The detection rate was 23% for the whole group, while for stage I disease only was 18.1%. Interestingly, all patients had HPV DNA detected in their blood.

Using CK19, we were able to detect CTCs in two patients who had clinical stage II disease. The level of CK19 expression was 2-3 log higher than the negative control samples. Three patients had CK19 expression level similar to the negative control, and were thus considered negative. The detection rate of CTC using CK19 was 20% in all tested patients whereas in stage II disease the detection rate was 50% (2/4 patients). Using nested RT-PCR to detect CTCs through CK19 transcript, 21.4% of stage IB-IIB patients were positive. None of the healthy female controls were positive, while only 5.7% with benign gynecological disease was positive [163]. Mitsuhashi et al. used RT-PCR of EGFR mRNA to detect CTCs and compared it to CK19 expression. Notably, EGFR was expressed in 98% of primary tumors and 6.3%, 31.3%, and 46.2% of stage I, II, and III/IV, respectively. None of the controls expressed EGFR. CK19 was detected in 77.8% of patients; however, 65% of the controls were positive as well [164]. Using qRT-PCR with established cutoff value to detect CK19 transcript in breast cancer patients, 2.2% of healthy female were positive while 31% and 40% patients with early and metastatic breast cancer were positive, respectively. Moreover, the level of CK19 expression was significantly higher in breast cancer patients compared to controls [196].

$P16^{INK4A}$ was expressed with similarly across control subjects and patients. No studies have been conducted to evaluate the usefulness of $p16^{INK4A}$ for the detection of CTCs in UCC. Other studies have used circulating tumor DNA in the detection of CTC $p16^{INK4A}$ and its aberrant methylation [207, 208]. We postulate if an appropriate cutoff median value is established, this

marker would be able to identify CTCs, as $p16^{INK4A}$ had a detection limit of 50 cells/mL in samples with the ability to detect to 1 cell/mL of blood.

In summary, we demonstrated the ability of HPV E6/E7, CK19 and $p16^{INK4A}$ to detect CTCs using qRT-PCR in experimental spiking model and their detection limit. The sensitivity of PCR improved with the addition of either negative or positive magnetic enrichment. E6/E7 are the most sensitive and specific markers to detect CTCs in experimental spiking model. CK19 and $P16^{INK4A}$ had basal expression in control subjects and appropriate cutoff median expression values have to be established to identify CTCs.

In UCC patients, CTCs were detected in 20% from all tested patients and 50% in stage II disease using CK19 gene expression. Those with negative result, six patients had stage I disease and two patients had stage II disease. This finding is in concordance with the reported literatures that range between 21-42% for stage 1B-II UCC patients. On the contrary, none of the tested patients had E6/E7 oncogenes expression. This group of patients had mainly stage one disease and low volume disease compared to other reported studies. However, two patients had CK19 gene expression detected while E6/E7 were negative. We postulate that CK19 gene expression is more abundant than E6/E7, which accounts for the contradictory finding. Specifically, there is 5-log difference between CK19 and E6/E7 genes expression in CaSki cell line. During the progression of oncogenic HPV-infected lesion, the number of viral genomes that integrates into to the host genome varies. For instance, CaSki cell line (HPV16-positive) has 60-600 estimated copies number of integrated HPV genome per cell; HeLa cell line (HPV18-positive) has 10-50 copies; and SiHa cell line (HPV16-positive) has 1-2 copies [209]. Additionally we did not account for the number of PBMC, which could be a factor that resulted in the contradictory finding. The average number of PBMC in one mL of blood is 5-7 millions. DD-RT-PCR demonstrated a sensitivity of 1 CTC for every 500,000 PBMCs and a sensitivity of 5 CTCs/mL of blood. The number of PBMC background drastically affected the sensitivity of the PCR and the detection of one cell in more than 500,000 PBMCs background was not possible using E6/E7 gene expression. Thus, negative or positive enrichment should be used to eliminate most of PBMC-derived RNA background to reduce the inhibitory effect on PCR reaction.

CONCLUSION

Detection of circulating tumor cells is dependent on multiple factors including the rarity of these cells within the blood, the enrichment process, cancer cell heterogeneity, and detection techniques. Ficoll-Paque, a widely used density medium to enrich tumor cells, has low sensitivity in enriching CTCs with detection limit of 1,000 cells/mL of blood using qRT-PCR for HPV E6/E7 oncogenes expression with an average recovery of 50%. We demonstrated low recovery rate, inter- and intra-variation in recovery rate among operators, and interestingly, aggressive tumor cell lines had the lowest recovery rate. RBC lysis demonstrated superiority with minimal cell loss with recovery of >90%. HPV16 E6/E7 expression evaluated by qRT-PCR is the most sensitive and specific marker to detect UCC cells at approximately 1 cell/mL of blood in an experimental spiking model. CK19 and $p16^{INK4A}$ had a similar detection limit to HPV oncogenes and can be used to verify the diagnosis provided a cutoff median expression value is determined for normal individuals. Both positive and negative enrichment using immunomagnetic improved PCR sensitivity by eliminating PBMC-derived background RNA. Positively enriched cells of high purity could be used to assess tumor genes expression; however, tumors of non-epithelial origin and those with low EpCAM expression resulting from EMT could not be detected. Negatively enriched tumor cells were less pure when compared to positive enrichment. Moreover, tumor cells that attached to and/or engulfed by macrophages were lost. In the early-stage UCC patients, CTCs were detected in 2/10 patients using CK19 gene expression. None of the patients had detectable HPV16 E6 and E7 expression. $P16^{INK4A}$ was expressed at a similar level across all samples. These finding suggest that CTCs are very rare in early UCC, in agreement with previous reports.

PERSPECTIVES

Uterine cervical cancer tumor bank at CHUM has been developed recently and currently includes over 70 patients. Ten patients were tested for CTCs and two of them were positive for CK19, all of which had stage II disease. Six patients with stage I and one patient with stage II disease were negative for CK19, E6/E7 and $p16^{INK4A}$. Our finding is compatible with the previously reported literature. To validate the ability of these markers to detect CTCs in UCC, metastatic UCC patients would be the best candidates to withdraw a definitive conclusion.

Here, we report that HPV16 E6/E7 oncogene expression is sufficient to detect CTCs in UCC. However, other HPV oncogenic types can be included as well. To further optimize the PCR sensitivity, future patients should be enriched with RBC lysis combined with negative enrichment to eliminate PBMC background that could affect the PCR sensitivity. If preliminary data in UCC patients is encouraging and demonstrates the ability to detect CTCs, patients will be followed up with serial CTC detection to determine its prognostic significance.

CHAPTER VII : BIBLIOGRAPHY

1. Talmadge, J.E. and I.J. Fidler, *AACR centennial series: the biology of cancer metastasis: historical perspective.* Cancer Res, 2010. **70**(14): p. 5649-69.
2. Fidler, I.J., *The pathogenesis of cancer metastasis: the 'seed and soil' hypothesis revisited.* Nat Rev Cancer, 2003. **3**(6): p. 453-8.
3. Hanahan, D. and R.A. Weinberg, *Hallmarks of cancer: the next generation.* Cell, 2011. **144**(5): p. 646-74.
4. Witsch, E., M. Sela, and Y. Yarden, *Roles for growth factors in cancer progression.* Physiology (Bethesda), 2010. **25**(2): p. 85-101.
5. Shaw, R.J. and L.C. Cantley, *Ras, PI(3)K and mTOR signalling controls tumour cell growth.* Nature, 2006. **441**(7092): p. 424-30.
6. Pouyssegur, J., F. Dayan, and N.M. Mazure, *Hypoxia signalling in cancer and approaches to enforce tumour regression.* Nature, 2006. **441**(7092): p. 437-43.
7. Carmeliet, P. and R.K. Jain, *Angiogenesis in cancer and other diseases.* Nature, 2000. **407**(6801): p. 249-57.
8. Baluk, P., H. Hashizume, and D.M. McDonald, *Cellular abnormalities of blood vessels as targets in cancer.* Curr Opin Genet Dev, 2005. **15**(1): p. 102-11.
9. Nagy, J.A., et al., *Heterogeneity of the tumor vasculature.* Semin Thromb Hemost, 2010. **36**(3): p. 321-31.
10. Kalluri, R. and R.A. Weinberg, *The basics of epithelial-mesenchymal transition.* J Clin Invest, 2009. **119**(6): p. 1420-8.
11. Scheel, C. and R.A. Weinberg, *Cancer stem cells and epithelial-mesenchymal transition: concepts and molecular links.* Semin Cancer Biol, 2012. **22**(5-6): p. 396-403.
12. Ksiazkiewicz, M., A. Markiewicz, and A.J. Zaczek, *Epithelial-mesenchymal transition: a hallmark in metastasis formation linking circulating tumor cells and cancer stem cells.* Pathobiology, 2012. **79**(4): p. 195-208.
13. Pantel, K. and R.H. Brakenhoff, *Dissecting the metastatic cascade.* Nat Rev Cancer, 2004. **4**(6): p. 448-56.
14. Rack, B., et al., *Circulating tumor cells predict survival in early average-to-high risk breast cancer patients.* J Natl Cancer Inst, 2014. **106**(5).
15. Wang, F.B., et al., *A higher number of circulating tumor cells (CTC) in peripheral blood indicates poor prognosis in prostate cancer patients--a meta-analysis.* Asian Pac J Cancer Prev, 2011. **12**(10): p. 2629-35.
16. Ma, X.L., et al., *Meta-analysis of circulating tumor cells as a prognostic marker in lung cancer.* Asian Pac J Cancer Prev, 2012. **13**(4): p. 1137-44.
17. Zhang, L., et al., *Meta-analysis of the prognostic value of circulating tumor cells in breast cancer.* Clin Cancer Res, 2012. **18**(20): p. 5701-10.
18. Groot Koerkamp, B., et al., *Circulating tumor cells and prognosis of patients with resectable colorectal liver metastases or widespread metastatic colorectal cancer: a meta-analysis.* Ann Surg Oncol, 2013. **20**(7): p. 2156-65.
19. Yu, M., et al., *Circulating tumor cells: approaches to isolation and characterization.* J Cell Biol, 2011. **192**(3): p. 373-82.
20. Reprinted from Cancer Letters, Paterlini-Brechot, P.Benali, N. L., Circulating tumor cells (CTC) detection: Clinical impact and future directions, 180-204, Copyright (2007), with permission from Elsevier.
21. Zeisberg, M. and E.G. Neilson, *Biomarkers for epithelial-mesenchymal transitions.* J Clin Invest, 2009. **119**(6): p. 1429-37.

22. Lamouille, S., J. Xu, and R. Derynck, *Molecular mechanisms of epithelial-mesenchymal transition.* Nat Rev Mol Cell Biol, 2014. **15**(3): p. 178-96.
23. Mani, S.A., et al., *The epithelial-mesenchymal transition generates cells with properties of stem cells.* Cell, 2008. **133**(4): p. 704-15.
24. Singh, A. and J. Settleman, *EMT, cancer stem cells and drug resistance: an emerging axis of evil in the war on cancer.* Oncogene, 2010. **29**(34): p. 4741-51.
25. Thiery, J.P. and J.P. Sleeman, *Complex networks orchestrate epithelial-mesenchymal transitions.* Nat Rev Mol Cell Biol, 2006. **7**(2): p. 131-42.
26. Paterlini-Brechot, P. and N.L. Benali, *Circulating tumor cells (CTC) detection: clinical impact and future directions.* Cancer Lett, 2007. **253**(2): p. 180-204.
27. Luzzi, K.J., et al., *Multistep nature of metastatic inefficiency: dormancy of solitary cells after successful extravasation and limited survival of early micrometastases.* Am J Pathol, 1998. **153**(3): p. 865-73.
28. Dunn, G.P., et al., *Cancer immunoediting: from immunosurveillance to tumor escape.* Nat Immunol, 2002. **3**(11): p. 991-8.
29. Uhr, J.W. and K. Pantel, *Controversies in clinical cancer dormancy.* Proc Natl Acad Sci U S A, 2011. **108**(30): p. 12396-400.
30. Paez, D., et al., *Cancer dormancy: a model of early dissemination and late cancer recurrence.* Clin Cancer Res, 2012. **18**(3): p. 645-53.
31. Bøyum, A., *[9] Separation of lymphocytes, granulocytes, and monocytes from human blood using iodinated density gradient media*, in *Methods in Enzymology*, J.J.L. Giovanni Di Sabato and V. Helen Van, Editors. 1984, Academic Press. p. 88-102.
32. Rosenberg, R., et al., *Comparison of two density gradient centrifugation systems for the enrichment of disseminated tumor cells in blood.* Cytometry, 2002. **49**(4): p. 150-8.
33. Naume, B., et al., *Detection of isolated tumor cells in peripheral blood and in BM: evaluation of a new enrichment method.* Cytotherapy, 2004. **6**(3): p. 244-52.
34. Lin, Z., et al., *In vivo antigen-driven plasmablast enrichment in combination with antigen-specific cell sorting to facilitate the isolation of rare monoclonal antibodies from human B cells.* Nat. Protocols, 2014. **9**(7): p. 1563-1577.
35. Allard, W.J., et al., *Tumor cells circulate in the peripheral blood of all major carcinomas but not in healthy subjects or patients with nonmalignant diseases.* Clin Cancer Res, 2004. **10**(20): p. 6897-904.
36. Vona, G., et al., *Isolation by size of epithelial tumor cells : a new method for the immunomorphological and molecular characterization of circulatingtumor cells.* Am J Pathol, 2000. **156**(1): p. 57-63.
37. Zheng, S., et al., *Membrane microfilter device for selective capture, electrolysis and genomic analysis of human circulating tumor cells.* J Chromatogr A, 2007. **1162**(2): p. 154-61.
38. Zheng, S., et al., *3D microfilter device for viable circulating tumor cell (CTC) enrichment from blood.* Biomed Microdevices, 2011. **13**(1): p. 203-13.
39. Litvinov, S.V., et al., *Ep-CAM: a human epithelial antigen is a homophilic cell-cell adhesion molecule.* J Cell Biol, 1994. **125**(2): p. 437-46.
40. Riethdorf, S., et al., *Detection of circulating tumor cells in peripheral blood of patients with metastatic breast cancer: a validation study of the CellSearch system.* Clin Cancer Res, 2007. **13**(3): p. 920-8.
41. Fehm, T., et al., *Cytogenetic evidence that circulating epithelial cells in patients with carcinoma are malignant.* Clin Cancer Res, 2002. **8**(7): p. 2073-84.
42. Willipinski-Stapelfeldt, B., et al., *Changes in cytoskeletal protein composition indicative of an epithelial-mesenchymal transition in human micrometastatic and primary breast carcinoma cells.* Clin Cancer Res, 2005. **11**(22): p. 8006-14.

43. Sieuwerts, A.M., et al., *Anti-epithelial cell adhesion molecule antibodies and the detection of circulating normal-like breast tumor cells.* J Natl Cancer Inst, 2009. **101**(1): p. 61-6.
44. Mikolajczyk, S.D., et al., *Detection of EpCAM-Negative and Cytokeratin-Negative Circulating Tumor Cells in Peripheral Blood.* J Oncol, 2011. **2011**: p. 252361.
45. Konigsberg, R., et al., *Detection of EpCAM positive and negative circulating tumor cells in metastatic breast cancer patients.* Acta Oncol, 2011. **50**(5): p. 700-10.
46. Aktas, B., et al., *Stem cell and epithelial-mesenchymal transition markers are frequently overexpressed in circulating tumor cells of metastatic breast cancer patients.* Breast Cancer Res, 2009. **11**(4): p. R46.
47. van de Stolpe, A., et al., *Circulating tumor cell isolation and diagnostics: toward routine clinical use.* Cancer Res, 2011. **71**(18): p. 5955-60.
48. Demel, U., et al., *Detection of tumour cells in the peripheral blood of patients with breast cancer. Development of a new sensitive and specific immunomolecular assay.* J Exp Clin Cancer Res, 2004. **23**(3): p. 465-8.
49. Zieglschmid, V., et al., *Combination of immunomagnetic enrichment with multiplex RT-PCR analysis for the detection of disseminated tumor cells.* Anticancer Res, 2005. **25**(3A): p. 1803-10.
50. Yang, L., et al., *Optimization of an enrichment process for circulating tumor cells from the blood of head and neck cancer patients through depletion of normal cells.* Biotechnol Bioeng, 2009. **102**(2): p. 521-34.
51. McCloskey, K.E., J.J. Chalmers, and M. Zborowski, *Magnetic cell separation: characterization of magnetophoretic mobility.* Anal Chem, 2003. **75**(24): p. 6868-74.
52. Haun, J.B., et al., *Bioorthogonal chemistry amplifies nanoparticle binding and enhances the sensitivity of cell detection.* Nat Nanotechnol, 2010. **5**(9): p. 660-5.
53. Lustberg, M., et al., *Emerging technologies for CTC detection based on depletion of normal cells.* Recent Results Cancer Res, 2012. **195**: p. 97-110.
54. Whitesides, G.M., *The origins and the future of microfluidics.* Nature, 2006. **442**(7101): p. 368-73.
55. Nagrath, S., et al., *Isolation of rare circulating tumour cells in cancer patients by microchip technology.* Nature, 2007. **450**(7173): p. 1235-9.
56. Maheswaran, S., et al., *Detection of mutations in EGFR in circulating lung-cancer cells.* N Engl J Med, 2008. **359**(4): p. 366-77.
57. Stott, S.L., et al., *Isolation of circulating tumor cells using a microvortex-generating herringbone-chip.* Proc Natl Acad Sci U S A, 2010. **107**(43): p. 18392-7.
58. Nora Dickson, M., et al., *Efficient capture of circulating tumor cells with a novel immunocytochemical microfluidic device.* Biomicrofluidics, 2011. **5**(3): p. 34119-3411915.
59. Gleghorn, J.P., et al., *Capture of circulating tumor cells from whole blood of prostate cancer patients using geometrically enhanced differential immunocapture (GEDI) and a prostate-specific antibody.* Lab Chip, 2010. **10**(1): p. 27-9.
60. Myung, J.H., et al., *Enhanced tumor cell isolation by a biomimetic combination of E-selectin and anti-EpCAM: implications for the effective separation of circulating tumor cells (CTCs).* Langmuir, 2010. **26**(11): p. 8589-96.
61. Sequist, L.V., et al., *The CTC-Chip: An Exciting New Tool to Detect Circulating Tumor Cells in Lung Cancer Patients.* Journal of Thoracic Oncology, 2009. **4**(3): p. 281-283 10.1097/JTO.0b013e3181989565.
62. Kang, J.H., et al., *A combined micromagnetic-microfluidic device for rapid capture and culture of rare circulating tumor cells.* Lab Chip, 2012. **12**(12): p. 2175-81.
63. Hoshino, K., et al., *Microchip-based immunomagnetic detection of circulating tumor cells.* Lab Chip, 2011. **11**(20): p. 3449-57.

64. Chen, C.L., et al., *Separation and detection of rare cells in a microfluidic disk via negative selection.* Lab Chip, 2011. **11**(3): p. 474-83.
65. Kuo, J.S., et al., *Deformability considerations in filtration of biological cells.* Lab Chip, 2010. **10**(7): p. 837-42.
66. Cruz, I., et al., *Evaluation of multiparameter flow cytometry for the detection of breast cancer tumor cells in blood samples.* Am J Clin Pathol, 2005. **123**(1): p. 66-74.
67. Hu, Y., et al., *Detection of circulating tumor cells in breast cancer patients utilizing multiparameter flow cytometry and assessment of the prognosis of patients in different CTCs levels.* Cytometry A, 2010. **77**(3): p. 213-9.
68. Dharmasiri, U., et al., *Microsystems for the capture of low-abundance cells.* Annu Rev Anal Chem (Palo Alto Calif), 2010. **3**: p. 409-31.
69. Krivacic, R.T., et al., *A rare-cell detector for cancer.* Proc Natl Acad Sci U S A, 2004. **101**(29): p. 10501-4.
70. Alix-Panabieres, C., *EPISPOT assay: detection of viable DTCs/CTCs in solid tumor patients.* Recent Results Cancer Res, 2012. **195**: p. 69-76.
71. Alix-Panabieres, C., et al., *Characterization and enumeration of cells secreting tumor markers in the peripheral blood of breast cancer patients.* J Immunol Methods, 2005. **299**(1-2): p. 177-88.
72. Alix-Panabieres, C., et al., *Full-length cytokeratin-19 is released by human tumor cells: a potential role in metastatic progression of breast cancer.* Breast Cancer Res, 2009. **11**(3): p. R39.
73. Voldman, J., *Electrical forces for microscale cell manipulation.* Annu Rev Biomed Eng, 2006. **8**: p. 425-54.
74. Chen, J., J. Li, and Y. Sun, *Microfluidic approaches for cancer cell detection, characterization, and separation.* Lab Chip, 2012. **12**(10): p. 1753-67.
75. Becker, F.F., et al., *Separation of human breast cancer cells from blood by differential dielectric affinity.* Proceedings of the National Academy of Sciences, 1995. **92**(3): p. 860-864.
76. Yang, J., et al., *Cell Separation on Microfabricated Electrodes Using Dielectrophoretic/Gravitational Field-Flow Fractionation.* Analytical Chemistry, 1999. **71**(5): p. 911-918.
77. Gascoyne, P.R.C., et al., *Dielectrophoretic separation of cancer cells from blood.* Industry Applications, IEEE Transactions on, 1997. **33**(3): p. 670-678.
78. Gascoyne, P.R., et al., *Isolation of rare cells from cell mixtures by dielectrophoresis.* Electrophoresis, 2009. **30**(8): p. 1388-98.
79. Moon, H.S., et al., *Continuous separation of breast cancer cells from blood samples using multi-orifice flow fractionation (MOFF) and dielectrophoresis (DEP).* Lab Chip, 2011. **11**(6): p. 1118-25.
80. Gupta, V., et al., *ApoStream™, a new dielectrophoretic device for antibody independent isolation and recovery of viable cancer cells from blood.* Biomicrofluidics, 2012. **6**(2): p. -.
81. Shim, S., et al., *Dynamic physical properties of dissociated tumor cells revealed by dielectrophoretic field-flow fractionation.* Integr Biol (Camb), 2011. **3**(8): p. 850-62.
82. Gascoyne, P.R. and S. Shim, *Isolation of circulating tumor cells by dielectrophoresis.* Cancers (Basel), 2014. **6**(1): p. 545-79.
83. Cristofanilli, M., et al., *Circulating tumor cells, disease progression, and survival in metastatic breast cancer.* N Engl J Med, 2004. **351**(8): p. 781-91.
84. Hayes, D.F., et al., *Circulating tumor cells at each follow-up time point during therapy of metastatic breast cancer patients predict progression-free and overall survival.* Clin Cancer Res, 2006. **12**(14 Pt 1): p. 4218-24.

85. Tewes, M., et al., *Molecular profiling and predictive value of circulating tumor cells in patients with metastatic breast cancer: an option for monitoring response to breast cancer related therapies.* Breast Cancer Res Treat, 2009. **115**(3): p. 581-90.
86. Bidard, F.-C., et al., *Clinical application of circulating tumor cells in breast cancer: overview of the current interventional trials.* Cancer and Metastasis Reviews, 2013. **32**(1-2): p. 179-188.
87. Lu, C.Y., et al., *Molecular detection of persistent postoperative circulating tumour cells in stages II and III colon cancer patients via multiple blood sampling: prognostic significance of detection for early relapse.* Br J Cancer, 2011. **104**(7): p. 1178-84.
88. Iinuma, H., et al., *Clinical significance of circulating tumor cells, including cancer stem-like cells, in peripheral blood for recurrence and prognosis in patients with Dukes' stage B and C colorectal cancer.* J Clin Oncol, 2011. **29**(12): p. 1547-55.
89. Danila, D.C., et al., *Circulating tumor cell number and prognosis in progressive castration-resistant prostate cancer.* Clin Cancer Res, 2007. **13**(23): p. 7053-8.
90. de Bono, J.S., et al., *Circulating tumor cells predict survival benefit from treatment in metastatic castration-resistant prostate cancer.* Clin Cancer Res, 2008. **14**(19): p. 6302-9.
91. Scher, H.I., et al., *Circulating tumour cells as prognostic markers in progressive, castration-resistant prostate cancer: a reanalysis of IMMC38 trial data.* Lancet Oncol, 2009. **10**(3): p. 233-9.
92. Scher, H.I.e.a., *Evaluation of circulating tumor cell (CTC) enumeration as an efficacy response biomarker of overall survival (OS) in metastatic castration-resistant prostate cancer (mCRPC): planned final analysis (FA) of COU-AA-301, a randomized, double-blind, placebo-controlled, phase III study of abiraterone acetate (AA) plus low-dose prednisone (P) post docetaxel [abstract]*. J. Clin. Oncol, 2011: LBA4517. **Vol 29, No 18_suppl (June 20 Supplement)**.
93. Pearl, M.L., et al., *Prognostic analysis of invasive circulating tumor cells (iCTCs) in epithelial ovarian cancer.* Gynecol Oncol, 2014. **134**(3): p. 581-90.
94. Morris, K.L., et al., *Circulating biomarkers in hepatocellular carcinoma.* Cancer Chemother Pharmacol, 2014. **74**(2): p. 323-32.
95. Qi, F., et al., *Quantitation of rare circulating tumor cells by folate receptor alpha ligand-targeted PCR in bladder transitional cell carcinoma and its potential diagnostic significance.* Tumour Biol, 2014. **35**(7): p. 7217-23.
96. Ignatiadis, M. and S.-J. Dawson, *Circulating tumor cells and circulating tumor DNA for precision medicine: dream or reality?* Annals of Oncology, 2014. **25**(12): p. 2304-2313.
97. Kallergi, G., et al., *Phosphorylated EGFR and PI3K/Akt signaling kinases are expressed in circulating tumor cells of breast cancer patients.* Breast Cancer Res, 2008. **10**(5): p. R80.
98. Errico, A., *Breast cancer: CTCs - a predictive approach for targeted cancer therapy.* Nat Rev Clin Oncol, 2014. **11**(9): p. 501.
99. Fehm, T., et al., *HER2 status of circulating tumor cells in patients with metastatic breast cancer: a prospective, multicenter trial.* Breast Cancer Res Treat, 2010. **124**(2): p. 403-12.
100. Bernard, H.U., et al., *Classification of papillomaviruses (PVs) based on 189 PV types and proposal of taxonomic amendments.* Virology, 2010. **401**(1): p. 70-9.
101. de Villiers, E.M., et al., *Classification of papillomaviruses.* Virology, 2004. **324**(1): p. 17-27.
102. Munoz, N., et al., *Epidemiologic classification of human papillomavirus types associated with cervical cancer.* N Engl J Med, 2003. **348**(6): p. 518-27.
103. Smith, J.S., et al., *Human papillomavirus type distribution in invasive cervical cancer and high-grade cervical lesions: a meta-analysis update.* Int J Cancer, 2007. **121**(3): p. 621-32.
104. Munoz, N., et al., *Chapter 1: HPV in the etiology of human cancer.* Vaccine, 2006. **24 Suppl 3**: p. S3/1-10.
105. Danos, O., M. Katinka, and M. Yaniv, *Human papillomavirus 1a complete DNA sequence: a novel type of genome organization among papovaviridae.* EMBO J, 1982. **1**(2): p. 231-6.

106. Stubenrauch, F., et al., *The E8E2C protein, a negative regulator of viral transcription and replication, is required for extrachromosomal maintenance of human papillomavirus type 31 in keratinocytes.* J Virol, 2000. **74**(3): p. 1178-86.
107. Stubenrauch, F., T. Zobel, and T. Iftner, *The E8 domain confers a novel long-distance transcriptional repression activity on the E8E2C protein of high-risk human papillomavirus type 31.* J Virol, 2001. **75**(9): p. 4139-49.
108. DiMaio, D. and L.M. Petti, *The E5 proteins.* Virology, 2013. **445**(1-2): p. 99-114.
109. Roman, A. and K. Munger, *The papillomavirus E7 proteins.* Virology, 2013. **445**(1-2): p. 138-68.
110. Vande Pol, S.B. and A.J. Klingelhutz, *Papillomavirus E6 oncoproteins.* Virology, 2013. **445**(1-2): p. 115-37.
111. Hawley-Nelson, P., et al., *HPV16 E6 and E7 proteins cooperate to immortalize human foreskin keratinocytes.* EMBO J, 1989. **8**(12): p. 3905-10.
112. Munger, K., et al., *The E6 and E7 genes of the human papillomavirus type 16 together are necessary and sufficient for transformation of primary human keratinocytes.* J Virol, 1989. **63**(10): p. 4417-21.
113. Wentzensen, N., S. Vinokurova, and M.v.K. Doeberitz, *Systematic Review of Genomic Integration Sites of Human Papillomavirus Genomes in Epithelial Dysplasia and Invasive Cancer of the Female Lower Genital Tract.* Cancer Research, 2004. **64**(11): p. 3878-3884.
114. Munger, K. and P.M. Howley, *Human papillomavirus immortalization and transformation functions.* Virus Res, 2002. **89**(2): p. 213-28.
115. zur Hausen, H., *Papillomaviruses and cancer: from basic studies to clinical application.* Nat Rev Cancer, 2002. **2**(5): p. 342-50.
116. Khleif, S.N., et al., *Inhibition of cyclin D-CDK4/CDK6 activity is associated with an E2F-mediated induction of cyclin kinase inhibitor activity.* Proc Natl Acad Sci U S A, 1996. **93**(9): p. 4350-4.
117. Kiyono, T., et al., *Both Rb/p16INK4a inactivation and telomerase activity are required to immortalize human epithelial cells.* Nature, 1998. **396**(6706): p. 84-8.
118. Desaintes, C., et al., *Expression of the papillomavirus E2 protein in HeLa cells leads to apoptosis.* EMBO J, 1997. **16**(3): p. 504-14.
119. Hu, G., et al., *Suppression of tumorigenesis by transcription units expressing the antisense E6 and E7 messenger RNA (mRNA) for the transforming proteins of the human papilloma virus and the sense mRNA for the retinoblastoma gene in cervical carcinoma cells.* Cancer Gene Ther, 1995. **2**(1): p. 19-32.
120. Hwang, E.S., et al., *Inhibition of cervical carcinoma cell line proliferation by the introduction of a bovine papillomavirus regulatory gene.* J Virol, 1993. **67**(7): p. 3720-9.
121. Wells, S.I., et al., *Papillomavirus E2 induces senescence in HPV-positive cells via pRB- and p21(CIP)-dependent pathways.* EMBO J, 2000. **19**(21): p. 5762-71.
122. Wu, L., et al., *E2F-Rb complexes assemble and inhibit cdc25A transcription in cervical carcinoma cells following repression of human papillomavirus oncogene expression.* Mol Cell Biol, 2000. **20**(19): p. 7059-67.
123. von Knebel Doeberitz, M., et al., *Inhibition of tumorigenicity of cervical cancer cells in nude mice by HPV E6-E7 anti-sense RNA.* Int J Cancer, 1992. **51**(5): p. 831-4.
124. Doorbar, J., *The papillomavirus life cycle.* Journal of Clinical Virology, 2005. **32, Supplement**(0): p. 7-15.
125. Stanley, M.A., *Epithelial cell responses to infection with human papillomavirus.* Clin Microbiol Rev, 2012. **25**(2): p. 215-22.
126. Chung, C.H. and M.L. Gillison, *Human papillomavirus in head and neck cancer: its role in pathogenesis and clinical implications.* Clin Cancer Res, 2009. **15**(22): p. 6758-62.

127. Incidence/mortality data. Ferlay J, S.I., Ervik M, Dikshit R, Eser S, Mathers C, Rebelo M, Parkin DM, Forman D, Bray, F. GLOBOCAN 2012 v1.0, Cancer Incidence and Mortality Worldwide: IARC CancerBase No. 11 [Internet]. Lyon, France: International Agency for Research on Cancer; 2013. Available from: http://globocan.iarc.fr.
128. Walboomers, J.M., et al., *Human papillomavirus is a necessary cause of invasive cervical cancer worldwide.* J Pathol, 1999. **189**(1): p. 12-9.
129. Centers for Disease Control and Prevention. Incidence, P., and Cost of Sexually Transmitted Infection in the United States-CDC Fact Sheet., 2013.
130. Syrjanen, K., et al., *Prevalence, incidence, and estimated life-time risk of cervical human papillomavirus infections in a nonselected Finnish female population.* Sex Transm Dis, 1990. **17**(1): p. 15-9.
131. Li, N., et al., *Human papillomavirus type distribution in 30,848 invasive cervical cancers worldwide: Variation by geographical region, histological type and year of publication.* Int J Cancer, 2011. **128**(4): p. 927-35.
132. Pecorelli, S., *Revised FIGO staging for carcinoma of the vulva, cervix, and endometrium.* Int J Gynaecol Obstet, 2009. **105**(2): p. 103-4.
133. Benedet, J.L., et al., *FIGO staging classifications and clinical practice guidelines in the management of gynecologic cancers. FIGO Committee on Gynecologic Oncology.* Int J Gynaecol Obstet, 2000. **70**(2): p. 209-62.
134. Gold, M.A., et al., *Surgical versus radiographic determination of para-aortic lymph node metastases before chemoradiation for locally advanced cervical carcinoma: a Gynecologic Oncology Group Study.* Cancer, 2008. **112**(9): p. 1954-63.
135. Patel, S., et al., *Imaging of endometrial and cervical cancer.* Insights Imaging, 2010. **1**(5-6): p. 309-328.
136. Amit, A., et al., *PET/CT in gynecologic cancer: present applications and future prospects--a clinician's perspective.* Obstet Gynecol Clin North Am, 2011. **38**(1): p. 1-21, vii.
137. Landoni, F., et al., *Randomised study of radical surgery versus radiotherapy for stage Ib-IIa cervical cancer.* Lancet, 1997. **350**(9077): p. 535-40.
138. Delgado, G., et al., *Prospective surgical-pathological study of disease-free interval in patients with stage IB squamous cell carcinoma of the cervix: a Gynecologic Oncology Group study.* Gynecol Oncol, 1990. **38**(3): p. 352-7.
139. Yuan, C., et al., *Recurrence and survival analyses of 1,115 cervical cancer patients treated with radical hysterectomy.* Gynecol Obstet Invest, 1999. **47**(2): p. 127-32.
140. Benedetti-Panici, P., et al., *Lymphatic spread of cervical cancer: an anatomical and pathological study based on 225 radical hysterectomies with systematic pelvic and aortic lymphadenectomy.* Gynecol Oncol, 1996. **62**(1): p. 19-24.
141. Selman, T.J., et al., *Diagnostic accuracy of tests for lymph node status in primary cervical cancer: a systematic review and meta-analysis.* CMAJ, 2008. **178**(7): p. 855-62.
142. Sironi, S., et al., *Lymph node metastasis in patients with clinical early-stage cervical cancer: detection with integrated FDG PET/CT.* Radiology, 2006. **238**(1): p. 272-9.
143. Horn, L.C., et al., *Detection of micrometastases in pelvic lymph nodes in patients with carcinoma of the cervix uteri using step sectioning: Frequency, topographic distribution and prognostic impact.* Gynecol Oncol, 2008. **111**(2): p. 276-81.
144. Cote, R.J., et al., *Role of immunohistochemical detection of lymph-node metastases in management of breast cancer. International Breast Cancer Study Group.* Lancet, 1999. **354**(9182): p. 896-900.
145. Hermanek, P., et al., *International Union Against Cancer. Classification of isolated tumor cells and micrometastasis.* Cancer, 1999. **86**(12): p. 2668-73.

146. Schwartz, G.F., et al., *Proceeding of the consensus conference of the role of sentinel lymph node biopsy in carcinoma or the breast April 19-22, 2001, Philadelphia, PA, USA.* Breast J, 2002. **8**(3): p. 124-38.
147. Darai, E., et al., *Sentinel lymph node biopsy in gynaecological cancers: the importance of micrometastases in cervical cancer.* Surg Oncol, 2008. **17**(3): p. 227-35.
148. Cibula, D., et al., *Prognostic significance of low volume sentinel lymph node disease in early-stage cervical cancer.* Gynecol Oncol, 2012. **124**(3): p. 496-501.
149. Euscher, E.D., et al., *Ultrastaging improves detection of metastases in sentinel lymph nodes of uterine cervix squamous cell carcinoma.* Am J Surg Pathol, 2008. **32**(9): p. 1336-43.
150. Cormier, B., et al., *Establishing a sentinel lymph node mapping algorithm for the treatment of early cervical cancer.* Gynecol Oncol, 2011. **122**(2): p. 275-80.
151. Balega, J. and P.O. Van Trappen, *The sentinel node in gynaecological malignancies.* Cancer Imaging, 2006. **6**: p. 7-15.
152. Gortzak-Uzan, L., et al., *Sentinel lymph node biopsy vs. pelvic lymphadenectomy in early stage cervical cancer: is it time to change the gold standard?* Gynecol Oncol, 2010. **116**(1): p. 28-32.
153. Eiriksson, L.R. and A. Covens, *Sentinel lymph node mapping in cervical cancer: the future?* BJOG, 2012. **119**(2): p. 129-33.
154. Plante, M., et al., *Laparoscopic sentinel node mapping in early-stage cervical cancer.* Gynecol Oncol, 2003. **91**(3): p. 494-503.
155. Zarganis, P., et al., *The sentinel node in cervical cancer patients: role of tumor size and invasion of lymphatic vascular space.* In Vivo, 2009. **23**(3): p. 469-73.
156. Altgassen, C., et al., *Multicenter validation study of the sentinel lymph node concept in cervical cancer: AGO Study Group.* J Clin Oncol, 2008. **26**(18): p. 2943-51.
157. Diaz, J.P., et al., *Sentinel lymph node biopsy in the management of early-stage cervical carcinoma.* Gynecol Oncol, 2011. **120**(3): p. 347-52.
158. Cibula, D., et al., *Bilateral ultrastaging of sentinel lymph node in cervical cancer: Lowering the false-negative rate and improving the detection of micrometastasis.* Gynecol Oncol, 2012. **127**(3): p. 462-6.
159. Pao, C.C., et al., *Detection of human papillomavirus mRNA and cervical cancer cells in peripheral blood of cervical cancer patients with metastasis.* J Clin Oncol, 1997. **15**(3): p. 1008-12.
160. Tseng, C.J., et al., *Detection of human papillomavirus types 16 and 18 mRNA in peripheral blood of advanced cervical cancer patients and its association with prognosis.* J Clin Oncol, 1999. **17**(5): p. 1391-6.
161. Weismann, P., et al., *The detection of circulating tumor cells expressing E6/E7 HR-HPV oncogenes in peripheral blood in cervical cancer patients after radical hysterectomy.* Neoplasma, 2009. **56**(3): p. 230-8.
162. Pfitzner, C., et al., *Digital-Direct-RT-PCR: a sensitive and specific method for quantification of CTC in patients with cervical carcinoma.* Sci Rep, 2014. **4**: p. 3970.
163. Yuan, C.C., et al., *Detecting cytokeratin 19 mRNA in the peripheral blood cells of cervical cancer patients and its clinical-pathological correlation.* Gynecol Oncol, 2002. **85**(1): p. 148-53.
164. Mitsuhashi, A., et al., *Detection of epidermal growth factor receptor mRNA in peripheral blood of cervical cancer patients.* Gynecol Oncol, 2003. **89**(3): p. 480-5.
165. Duffy, M.J., *Clinical uses of tumor markers: a critical review.* Crit Rev Clin Lab Sci, 2001. **38**(3): p. 225-62.
166. Duffy, M.J., et al., *CA125 in ovarian cancer: European Group on Tumor Markers guidelines for clinical use.* Int J Gynecol Cancer, 2005. **15**(5): p. 679-91.
167. Bustin, S.A. and R. Mueller, *Real-time reverse transcription PCR (qRT-PCR) and its potential use in clinical diagnosis.* Clin Sci (Lond), 2005. **109**(4): p. 365-79.

168. Mocellin, S., et al., *Quantitative real-time PCR: a powerful ally in cancer research.* Trends in molecular medicine, 2003. **9**(5): p. 189-195.
169. Papadopoulou, E., et al., *Cell-free DNA and RNA in plasma as a new molecular marker for prostate and breast cancer.* Ann N Y Acad Sci, 2006. **1075**: p. 235-43.
170. de Cremoux, P., et al., *Detection of MUC1-expressing mammary carcinoma cells in the peripheral blood of breast cancer patients by real-time polymerase chain reaction.* Clin Cancer Res, 2000. **6**(8): p. 3117-22.
171. Mejean, A., et al., *Detection of circulating prostate derived cells in patients with prostate adenocarcinoma is an independent risk factor for tumor recurrence.* J Urol, 2000. **163**(6): p. 2022-9.
172. Xi, L., et al., *Optimal markers for real-time quantitative reverse transcription PCR detection of circulating tumor cells from melanoma, breast, colon, esophageal, head and neck, and lung cancers.* Clin Chem, 2007. **53**(7): p. 1206-15.
173. Barak, V., et al., *Clinical utility of cytokeratins as tumor markers.* Clin Biochem, 2004. **37**(7): p. 529-40.
174. Moll, R., et al., *The catalog of human cytokeratins: patterns of expression in normal epithelia, tumors and cultured cells.* Cell, 1982. **31**(1): p. 11-24.
175. Van Trappen, P.O., et al., *Molecular quantification and mapping of lymph-node micrometastases in cervical cancer.* Lancet, 2001. **357**(9249): p. 15-20.
176. Tsujimoto, M., et al., *One-step nucleic acid amplification for intraoperative detection of lymph node metastasis in breast cancer patients.* Clin Cancer Res, 2007. **13**(16): p. 4807-16.
177. Tanis, P.J., et al., *Frozen section investigation of the sentinel node in malignant melanoma and breast cancer.* Ann Surg Oncol, 2001. **8**(3): p. 222-6.
178. Slama, J., et al., *High false negative rate of frozen section examination of sentinel lymph nodes in patients with cervical cancer.* Gynecol Oncol, 2013. **129**(2): p. 384-8.
179. Fader, A.N., et al., *Sentinel lymph node biopsy in early-stage cervical cancer: utility of intraoperative versus postoperative assessment.* Gynecol Oncol, 2008. **111**(1): p. 13-7.
180. Bats, A.S., et al., *Diagnostic value of intraoperative examination of sentinel lymph node in early cervical cancer: a prospective, multicenter study.* Gynecol Oncol, 2011. **123**(2): p. 230-5.
181. Lukas, J., et al., *Retinoblastoma-protein-dependent cell-cycle inhibition by the tumour suppressor p16.* Nature, 1995. **375**(6531): p. 503-6.
182. Weinberg, R.A., *The retinoblastoma protein and cell cycle control.* Cell, 1995. **81**(3): p. 323-330.
183. Santin, A.D., et al., *Gene expression profiles of primary HPV16- and HPV18-infected early stage cervical cancers and normal cervical epithelium: identification of novel candidate molecular markers for cervical cancer diagnosis and therapy.* Virology, 2005. **331**(2): p. 269-91.
184. Rodier, F., et al., *Persistent DNA damage signalling triggers senescence-associated inflammatory cytokine secretion.* Nat Cell Biol, 2009. **11**(8): p. 973-979.
185. Chouinard, G., et al., *Cell cycle-dependent localization of CHK2 at centrosomes during mitosis.* Cell Division, 2013. **8**(1): p. 7.
186. Loi, S., et al., *CD73 promotes anthracycline resistance and poor prognosis in triple negative breast cancer.* Proceedings of the National Academy of Sciences, 2013. **110**(27): p. 11091-11096.
187. Yee, C., et al., *Presence and expression of human papillomavirus sequences in human cervical carcinoma cell lines.* Am J Pathol, 1985. **119**(3): p. 361-6.
188. Ouellet, V., et al., *Characterization of three new serous epithelial ovarian cancer cell lines.* BMC Cancer, 2008. **8**(1): p. 152.
189. Provencher, D.M., et al., *Characterization of four novel epithelial ovarian cancer cell lines.* In Vitro Cellular & Developmental Biology - Animal, 2000. **36**(6): p. 357-361.

190. Lara, O., et al., *Enrichment of rare cancer cells through depletion of normal cells using density and flow-through, immunomagnetic cell separation.* Exp Hematol, 2004. **32**(10): p. 891-904.
191. Balic, M., et al., *Comparison of two methods for enumerating circulating tumor cells in carcinoma patients.* Cytometry B Clin Cytom, 2005. **68**(1): p. 25-30.
192. Went, P.T., et al., *Frequent EpCam protein expression in human carcinomas.* Hum Pathol, 2004. **35**(1): p. 122-8.
193. Shapiro, H.M., *Practical flow cytometry*. 2005: John Wiley & Sons.
194. Ruud, P., O. Fodstad, and E. Hovig, *Identification of a novel cytokeratin 19 pseudogene that may interfere with reverse transcriptase-polymerase chain reaction assays used to detect micrometastatic tumor cells.* Int J Cancer, 1999. **80**(1): p. 119-25.
195. Savtchenko, E.S., et al., *Embryonic expression of the human 40-kD keratin: evidence from a processed pseudogene sequence.* Am J Hum Genet, 1988. **43**(5): p. 630-7.
196. Stathopoulou, A., et al., *Real-Time Quantification of CK-19 mRNA-Positive Cells in Peripheral Blood of Breast Cancer Patients Using the Lightcycler System.* Clinical Cancer Research, 2003. **9**(14): p. 5145-5151.
197. Liu, Y., et al., *Expression of p16(INK4a) in peripheral blood T-cells is a biomarker of human aging.* Aging Cell, 2009. **8**(4): p. 439-48.
198. Cioffi-Lavina, M., et al., *P16 expression in squamous cell carcinomas of cervix and bladder.* Appl Immunohistochem Mol Morphol, 2010. **18**(4): p. 344-7.
199. Balgkouranidou, I., T. Liloglou, and E.S. Lianidou, *Lung cancer epigenetics: emerging biomarkers.* Biomark Med, 2013. **7**(1): p. 49-58.
200. Pornthanakasem, W., et al., *Human papillomavirus DNA in plasma of patients with cervical cancer.* BMC Cancer, 2001. **1**(1): p. 2.
201. Dong, S.M., et al., *Detection and quantitation of human papillomavirus DNA in the plasma of patients with cervical carcinoma.* Cancer Epidemiol Biomarkers Prev, 2002. **11**(1): p. 3-6.
202. Hsu, K.F., et al., *Clinical significance of serum human papillomavirus DNA in cervical carcinoma.* Obstet Gynecol, 2003. **102**(6): p. 1344-51.
203. Tsai, H.J., et al., *An association between human papillomavirus 16/18 deoxyribonucleic acid in peripheral blood with p16 protein expression in neoplastic cervical lesions.* Cancer Detect Prev, 2005. **29**(6): p. 537-43.
204. Gormally, E., et al., *Circulating free DNA in plasma or serum as biomarker of carcinogenesis: practical aspects and biological significance.* Mutat Res, 2007. **635**(2-3): p. 105-17.
205. Fleischhacker, M. and B. Schmidt, *Circulating nucleic acids (CNAs) and cancer--a survey.* Biochim Biophys Acta, 2007. **1775**(1): p. 181-232.
206. Jahr, S., et al., *DNA Fragments in the Blood Plasma of Cancer Patients: Quantitations and Evidence for Their Origin from Apoptotic and Necrotic Cells.* Cancer Research, 2001. **61**(4): p. 1659-1665.
207. Schwarzenbach, H., et al., *Cell-free Tumor DNA in Blood Plasma As a Marker for Circulating Tumor Cells in Prostate Cancer.* Clinical Cancer Research, 2009. **15**(3): p. 1032-1038.
208. Wong, I.H.N., et al., *Detection of Aberrant p16 Methylation in the Plasma and Serum of Liver Cancer Patients.* Cancer Research, 1999. **59**(1): p. 71-73.
209. Meissner, J.D., *Nucleotide sequences and further characterization of human papillomavirus DNA present in the CaSki, SiHa and HeLa cervical carcinoma cell lines.* J Gen Virol, 1999. **80 (Pt 7)**: p. 1725-33.